UNIVERSIDADE DE LISBOA

FACULDADE DE CIÊNCIAS

DEPARTAMENTO DE QUÍMICA E BIOQUÍMICA

Anoctamins – Novel members of ion channels family with extended functions and significance in disease

MESTRADO EM BIOQUÍMICA

Especialização em Bioquímica Médica

Madalena do Carmo Fragoso Pinto

Dissertação orientadora por:

Professora Doutora Margarida D. Amaral

2015

Table of contents

Acknowledgments/Agradecimentos

Ao concluir este trabalho não posso deixar de agradecer a todos os que, de alguma forma, me acompanharam e contribuíram para a sua realização.

Em primeiro lugar queria agradecer à Professora Margarida Amaral, não só por me ter dado a oportunidade de desenvolver o meu trabalho no seu laboratório (e grupo de investigação), como também por toda a orientação, acompanhamento e, principalmente, confiança depositada.

Agradeço à Professora Rita Zilhão, por todo o tempo que despendeu com o meu trabalho, e cuja ajuda foi absolutamente fundamental para conseguir cumprir os meus primeiros objetivos. Agradeço também à Professora Mariana Santa-Marta, que, mesmo sem nenhuma associação ao grupo de investigação, não mostrou qualquer hesitação em ajudar.

Agradeço a todos os meus colegas de laboratório, porque todos me ajudaram à sua maneira. Primeiramente queria agradecer à Verónica, que me introduziu no mundo da genética e me fez gostar puramente disto (mesmo quando nada parece fazer sentido...); à Sara Afonso que, não estando já presente no grupo, me ensinou grande parte do que sei sobre anoctaminas e me levou a dar os primeiros passos na investigação; à Joana, que me acompanhou ao longo do meu trabalho, e teve sempre paciência para as minhas "loucuras", até quando nada parecia funcionar; ao Hugo e ao Luís Marques cuja paciência infinita (mesmo com prazos e pressões) foram essenciais para o desenvolvimento deste trabalho e o tornaram definitivamente mais "bonito"; and I also really need to thank Nikhil, for all his help, for all the things he taught me about physiology and mainly for all the days "lost" because of my experiments. Obrigada igualmente ao Simão, e ao seu número mágico das mutagéneses – 53; ao João, e ao nosso grande Benfica!; ao Luís; ao Zé, que me motiva a não esquecer e a praticar o meu espanhol; e à Sara, e à sua constante energia e companhia – no 78 ou por vezes no ginásio. Agradeço ainda à Susana pelas lições, pela ajuda e motivação, pela boa disposição (em português, inglês e espanhol), pelos doces e frutas, e principalmente por tornar o laboratório num lugar mais divertido (e com boa música!). I also want to thank Ines, for all the conversations, advices, patience, support, company, fun and motivation. Danke shön! Por fim, não posso deixar de agradecer à Margarida e ao Coelho, que, para além da grande amizade fora do trabalho, sempre me acompanharam e apoiaram nos bons e maus momentos. E que continue a ser assim: "não se muda a equipa vencedora".

Agradeço aos meus "migos falsos" por toda a companhia e motivação e porque, sem vocês, a minha vida não tinha metade da diversão. Particularmente agradeço às melhores amigas que algum dia poderia pedir, Ana, Inês, Leonor, Margarida e Sílvia, por todos os momentos que passámos e por esta amizade que, no que depender de mim, será eterna.

Obrigada à minha amiga de sempre e para sempre, Babi, por todo o apoio incondicional, pela amizade e pela companhia constante.

Obrigada às FOX, por todos os momentos de dança, de convívio e de diversão, porque sei que estão sempre presentes e, apesar de me acharem "maluca" (excepto a "mana" Ana, que sabe o quão divertido é ser Bioquímica), nunca deixaram de mostrar o vosso apoio. Obrigada

especialmente à Vera, que mais do que uma “prima” é, desde há muitos anos, uma grande amiga.

Obrigada ao João, por me conhecer, por estar lá sem ter de pedir. Por tudo.

Não posso deixar de fazer um agradecimento personalizado à Margarida, que mais do que uma colega de curso, de ginásio, de festas, de viagens, de loucura por animais (e de vídeos de gatinhos), parceira de bancada do laboratório, boleia, companheira, e “gémea”, é parte da família que escolhi e a mais verdadeira definição de AMIGA.

A toda a minha família, um muito obrigada por todo o apoio e confiança. Em particular ao meu tio e aos meus primos Beatriz, Bernardo, Inês e João, que mais do que primos são meus irmãos e amigos.

Obrigada ao meu irmão Diogo que, apesar de ainda estar a aprender que a investigação também é um trabalho (“curiosidades”), nunca deixou de me apoiar. Obrigada à minha irmã Marta, que sempre mostrou o orgulho que tem em mim e que, ao fazer de mim o seu “modelo”, me torna uma pessoa melhor a cada dia que passa.

À Whitney e à Miu.

Por fim agradeço aos meus pais, porque sem vocês nada disto teria sido possível.

Obrigada a todos! Thank you everyone!

Abstract

Cystic Fibrosis (CF) is the most common lethal autosomal recessive disorder in the Caucasian population, affecting 1 in 2500-6000 new-borns. CF is caused by mutations in the Cystic Fibrosis Transmembrane Conductance Regulator (*CFTR*) gene, which encodes a cAMP-regulated chloride (Cl^-) and bicarbonate (HCO_3^-) channel expressed at the apical membrane of a variety of epithelial cells. The most common mutation in CF patients is F508del, a three base pair deletion that causes a single amino acid deletion from CFTR and disrupts its traffic and function, due to protein misfolding.

Obstructive lung disease is the primary cause of morbidity in CF patients. Other symptoms of CF include elevated concentrations of sodium chloride (Cl^-) in the sweat, pancreatic insufficiency, and male infertility, among others.

Besides its function as a Cl^- channel, CFTR also controls a number of other ion channels and transporters, being crucial to the ionic flow on epithelia. Among these other channels is the epithelial sodium (Na^+) channel (ENaC) and members of the anoctamin family, some of which have been shown to function as Cl^- channels.

The latter constitutes a class of proteins that is only expressed in eukaryotic organisms. In mammals the family contains ten members (Ano1 to Ano10), with high sequence conservation, particularly around the putative channel pore forming region. Since the identification of Ano1 as a Ca^{2+}-activated Cl^- channel (CaCCs), in 2008, anoctamins have raised high interest as possible alternative Cl^- channels to compensate for the loss of functional CFTR in CF. However, little is known about the regulation of their biogenesis, traffic or whether their channel function can be activated by other means, other than Ca^{2+} signalling. Such knowledge is, nevertheless, essential for their possible therapeutic use as alternative Cl^- channels for CFTR.

Anoctamins are involved in a variety of functions that besides ion transport, include phospholipid scrambling and regulation of other membrane proteins. Several lines of evidence suggest that anoctamins form homodimers, but the possibility of heterodimer formation has not been excluded. Also, some family members are reported to interact with each other.

Despite some knowledge on this protein family, the structure and functions of all family members are not completely defined. The first two members of the family (Ano1 and Ano2) function as Ca^{2+}-activated Cl^- channels (CaCCs), while Ano6 was described as scramblase and also as a main component of the outwardly rectifying Cl^- channels (ORCCs). Other members of the anoctamin family, such as Ano3, 4, 7, and 9, may work as phospholipid scramblases and/or ion channels, being their functions still poorly understood.

Mutations in anoctamin genes (*ANO3*, *ANO5*, *ANO6*, and *ANO10*) cause various genetic disorders, suggesting the involvement of anoctamins in a variety of cellular functions.

The core objective of this project was to identify novel regulators of Ano6 and also Ano9 and 10 and their interaction with other anoctamin family members and CFTR. To accomplish this goal three main tasks were proposed, namely, *i*) To generate novel cell lines stably expressing double-tagged Ano6, Ano9 and Ano10 constructs; *ii*) To use these constructs to develop robust cell-based traffic assays to be used in fluorescence high-throughput microscopy; *iii*) To use siRNA microscopy screens to identify novel genes involved in regulating the traffic of Ano6, Ano9 and Ano10 as potential drug targets for CF.

The first task was completed for Ano6 and Ano9, while the second one was only accomplished for Ano6, and the third just started also for this protein. In summary, in this MSc project, double-tagged constructs of Ano6, 9 and 10 were created. The constructs of Ano6 and Ano9 were cloned into lentiviral vectors, and several cell lines expressing the double-tagged anoctamins under an inducible (Tet-On) promoter were generated. CFBE Ano6/Ano9 3-HA GFP cells were characterized by immunostaining (with polarized and non-polarized cells) and Western Blot techniques. Additionally, functional analysis of these proteins was assessed by both the iodide efflux technique and analysis in perfused micro-Ussing chamber on open circuit mode. Finally, a pilot screen of a small siRNA library targeting 231 genes (previously tested for CFTR traffic) was performed for CFBE Ano6 3-HA GFP cells.

Overall the results showed that:

- The double-tagged construct of Ano6 is functional as a channel when overexpressed either in HEK 293T cells or in CFBE cells;
- The double-tagged construct of Ano9 seems to increase I^- efflux in HEK 293T but shows no effect on ion currents on CFBE cells;
- Overexpressed Ano6 is located at the plasma membrane (and also at the cytoplasm);
- Overexpressed Ano9 is mostly intracellularly located but when at the cell membrane possibly forms dimers;
- CFBE cells stably expressing the inducible (Tet-On) Ano6 3-HA GFP construct constitute a robust cellular model for siRNA screens by automated high-content microscopy (HCM);
- Results from a pilot siRNA screen suggest that Ano6 traffic to the plasma membrane is affected by genes involved in several biological processes like G-protein coupled receptor signalling, ion transport, protein phosphorylation, and regulation of apoptosis, among others.

Additional studies and further validation of these results could potentially constitute a new attractive approach for CF therapy involving alternative Cl^- channels. Indeed, the regulation of anoctamins' traffic is largely unknown and its better understanding will allow the exploration of this pathway to compensate for CFTR deficiency, making possible the development of new therapies for CF.

Key words: Cystic Fibrosis, CFTR, Anoctamins.

Resumo

A Fibrose Quística (FQ) é a doença autossómica recessiva letal mais comum na população caucasiana, com uma prevalência de 1 em cada 2500-6000 nascimentos. Esta doença é causada por mutações no gene *Cystic Fibrosis Transmembrane Conductance Regulator* (*CFTR*). Este gene, localizado no braço longo do cromossoma 7, codifica para uma glicoproteína com 1480 resíduos de aminoácidos localizada na membrana apical de uma grande variedade de células epiteliais, onde transporta cloreto (Cl^-) e bicarbonato (HCO_3^-).

Entre as mais de 2000 mutações conhecidas no gene *CFTR*, a mais comum consiste na deleção de três pares de bases, que resulta na remoção de uma fenilalanina na posição 508 (F508del) da proteína. Esta mutação está presente em aproximadamente 85% dos pacientes com FQ e afeta o processamento da proteína que, devido a um *folding* incorreto, fica retida intracelularmente ao nível do retículo endoplasmático (RE). Neste organelo é rapidamente enviada para degradação proteassomal, não chegando assim à membrana plasmática.

Para além do seu papel como canal de aniões, a CFTR também funciona como reguladora de outros canais, tendo um efeito inibitório crítico na absorção de sódio (Na^+) pela proteína ENaC (*epithelial Na^+ channel*). Assim, os pacientes com FQ apresentam uma secreção de aniões diminuída, acompanhada por um aumento na absorção de Na^+, o que leva à desidratação do líquido que reveste as vias respiratórias, *airway surface liquid* (ASL), e ao aumento da viscosidade e espessura do muco. Estas características causam uma eliminação ineficiente de agentes patogénicos pulmonares, resultando em infecções bacterianas recorrentes e, consequentemente, em inflamação crónica. Esta inflamação, dominada por neutrófilos, exacerba os processos de remodelação do tecido pulmonar e acaba por culminar na fibrose dos tecidos e perda da sua função. A doença pulmonar obstrutiva é a causa de morte mais comum em pacientes com FQ, sendo responsável por aproximadamente 80% da mortalidade.

Para além deste fenótipo, outras manifestações da doença incluem a elevada concentração de NaCl no suor (sendo a base dos testes de diagnóstico mais comuns), insuficiência pancreática, infertilidade masculina, e ainda outras manifestações menos comuns como diabetes, ileus meconial, e obstrução intestinal e hepática.

Como referido anteriormente, a CFTR tem um papel importante na regulação de outros canais e transportadores, sendo fundamental no transporte iónico no epitélio. Para além da ENaC já evidenciada, outros canais que possivelmente interatuam com a CFTR são os canais de cloreto ativados por cálcio (CaCC) e os canais de cloreto *outwardly rectifying* (ORCC), entre outros.

Os CaCCs funcionam como transportadores iónicos transepiteliais em células secretoras e são caracterizados por apresentarem uma ativação dependente do aumento dos níveis de Ca^{2+} intracelular. Por sua vez, os ORCC demonstram uma relação I/V *outwardly rectifying* e são ativados por despolarização celular e via PKA e UTP extracelular.

Vários estudos mostram que a CFTR inibe a produção endógena de corrente pelos CaCCs, estando esta aumentada nas vias respiratórias de pacientes com FQ. No entanto, a ativação dos ORCC pela PKA encontra-se diminuída no epitélio pulmonar de pacientes.

As anoctaminas, proteínas que pertencem a uma família de 10 membros (Ano1 a Ano10) com elevada semelhança estrutural, foram associadas aos canais já referidos como regulados pela CFTR. A anoctamina 1 (Ano1) foi identificada como CaCC, sendo a sua função inibida com a activação da CFTR, enquanto a função de transporte por parte da CFTR é diminuída com a sobreexpressão da Ano1. Para além disso, a Ano6 foi identificada como componente principal dos ORCC. Assim, na presença de CFTR não mutada, é observada uma ativação paralela da CFTR e da Ano6, enquanto a Ano1 é inibida. Pelo contrário, em células com a CFTR mutada, a função da Ano6 é atenuada e a função da Ano1 aparenta estar aumentada.

O interesse no estudo das anoctaminas aumentou fortemente desde a identificação da Ano1 como CaCC em 2008. Tal interesse deve-se maioritariamente ao facto destas poderem ser consideradas possíveis canais de Cl^- alternativos para compensar a falta de CFTR funcional na FQ. Não obstante, o conhecimento sobre a sua biogénese, tráfego e ativação, é ainda muito reduzido. Tal conhecimento é, no entanto, essencial para o seu possível uso terapêutico como canais de Cl^- alternativos para a CFTR.

As anoctaminas estão envolvidas numa variedade de funções que, para além da função como transportadoras de iões já referida, ainda incluem *scrambling* de fosfolípidos e regulação de outras proteínas membranares. Vários estudos sugerem que as anoctaminas formam homodímeros, sendo ainda possível a formação de heterodímeros. Estes estudos são corroborados pela descoberta de interação entre alguns membros da família. Entre estes encontram-se a Ano1 e a Ano9, uma vez que estudos mostram que a sobreexpressão da Ano9 origina uma forte inibição das correntes produzidas pela Ano1.

Apesar das características já conhecidas das anoctaminas, a estrutura e as funções de todos os membros da família ainda não estão completamente definidas. Enquanto os dois primeiros membros da família (Ano1 e Ano2) funcionam como CaCCs, a Ano6 foi descrita como principal componente dos ORCC e como *scramblase*. Outros membros da família, tais como Ano3, 4, 7 e 9, podem ter funções de *scramblases* e/ou canais de iões, estando ainda as suas funções concretas por desvendar.

Mutações nos genes das anoctaminas (nomeadamente *ANO3, ANO5, ANO6 e ANO10*) causam diferentes doenças genéticas, sugerindo o envolvimento destas proteínas numa variedade de funções celulares.

O objetivo do presente projeto foi a identificação de novos reguladores da Ano6, e ainda possivelmente da Ano9 e 10, e a interação das mesmas com outros membros da família de proteínas e com a CFTR. Para atingir este objetivo foram propostas três tarefas principais, nomeadamente, *i*) Criar linhas celulares que sobreexpressam de forma estável os construtos da Ano6, Ano9 e Ano10 com dois *tags*, *ii*) Usar estes construtos para desenvolver ensaios de tráfego robustos para serem utilizados em microscopia de fluorescência *high-throughput*, *iii*) Usar *screens* com bibliotecas de siRNAs para identificar novos genes envolvidos na regulação do tráfego da Ano6, Ano9 e Ano10, que possam ainda vir a ser utilizados como potenciais fármacos para a FQ.

O primeiro passo foi concluído, tendo o segundo sido apenas realizado para a Ano6 e o último começado para a mesma. Resumindo, neste projecto de mestrado foram criados construtos da Ano6, Ano9 e Ano10 com dois *tags*. Os construtos da Ano6 e Ano9 foram clonados em vetores lentivirais, e foram criadas várias linhas celulares que expressam estas anoctaminas

sob o efeito de um promotor indutível *Tet-On*. As células CFBE Ano6/Ano9 3-HA GFP foram caraterizadas por imunofluorescência (tanto em células polarizadas como não polarizadas) e por *Western Blot*. Adicionalmente a função destas proteínas foi testada em ensaios funcionais (efluxo de iodeto e *micro-Ussing chamber*). Por fim, para as células CFBE Ano6 3-HA GFP, foi feito um *screen* preliminar de uma pequena biblioteca de siRNAs que afetam 231 genes (previamente testados para o tráfego da CFTR).

Os resultados obtidos ao longo deste trabalho sugerem que:

- O construto com dois *tags* da Ano6 é funcional como canal quando sobreexpresso tanto em células HEK 293T como em CFBE;
- O construto com dois tags da Ano9 parece aumentar o efluxo de iodeto em células HEK 293T mas não apresenta nenhum efeito no transporte de iões quando sobreexpresso em células CFBE;
- A Ano6 sobreexpressa está localizada na membrana plasmática (e também no citoplasma);
- A Ano9 sobreexpressa está principalmente localizada no citoplasma, mas quando se localiza na membrana plasmática forma possivelmente dímeros;
- As células CFBE que expressam de forma estável o contruto Ano6 3-HA GFP constituem um modelo celular robusto para realizar *screens* com siRNAs por Microscopia Automatizada (Análise de Alto Conteúdo);
- Os resultados de um *screen* de siRNA preliminar sugerem que o tráfego da Ano6 para a membrana plasmática é afetado por genes envolvidos em vários processos biológicos, tais como na sinalização de recetores acoplados a proteínas G, transporte de iões, fosforilação de proteínas e regulação da apoptose, entre outros.

Estudos adicionais e posterior validação destes resultados podem potencialmente resultar numa nova estratégia apelativa para desenvolver terapias para a FQ envolvendo canais de Cl^- alternativos. A regulação do tráfego das anoctaminas é ainda desconhecida e o seu estudo aprofundado irá permitir a exploração destas vias para compensar o defeito da CFTR, tornando possível o desenvolvimento de novas terapias para a FQ.

Palavras-chave: Fibrose Quística, CFTR, Anoctaminas.

Abbreviations

ABC	ATP-binding cassette
Ano1-10	Anoctamin 1-10 (TMEM16A-H, J and K)
ASL	Airway surface liquid
ATP	Adenosine triphosphate
BSA	Bovine serum albumin
C-terminal	Carboxyl terminal
CaCC	Calcium activated chloride channel
cAMP	Cyclic adenosine monophosphate
cDNA	Complementary DNA
CF	Cystic fibrosis
CFBE41o- /CFBE	Cystic Fibrosis Bronchial Epithelial (cell line)
CFTR	Cystic Fibrosis Transmembrane Conductance Regulator
CO_2	Carbon dioxide
DAG	Diacylglycerol
DMEM	Dulbecco's Modified Eagle Medium
DMSO	Dimethylsulfoxide
Dox	Doxycycline
ECL	Extracellular loop
EMEM	Eagle’s minimum essential medium
ENaC	Epithelial sodium channel
ER	Endoplasmic reticulum
ERQC	Endoplasmic reticulum quality control
FBS	Foetal bovine serum
F508del	Deletion of phenylalanine (F) residue at position 508
GFP	Green fluorescent protein
HEK	Human embryonic kidney (cell line)
HeLa	Human cervical carcinoma (Henrietta Lacks) (cell line)
IP_3	Inositol 1,4,5-trisphosphate
kDa	KiloDalton
MCC	Mucociliary clearance
$MgCl_2$	Magnesium Chloride
MSD	Membrane-spanning domain
NaCl	Sodium Chloride

NBD	Nucleotide binding domain
N-terminal	Amino-terminal
ORCC	Outwardly rectifying chloride channel
PAGE	Polyacrylamide gel electrophoresis
PBS	Phosphate buffer saline
PBS-T	Phosphate buffer saline with tween
PCR	Polymerase chain reaction
PDZ	PSD-95, Disc-large, and ZO-1
PenStrep	Penicillin streptomycin solution
PIP_2	Phosphatidylinositol 4,5-bisphosphate
PKA	Protein kinase A
PKC	Protein kinase C
PLC	Phospholipase C
PM	Plasma membrane
PVDF	Polyvinylidene Fluoride
R domain	Regulatory domain
RNA	Ribonucleic acid
SDS	Sodium dodecyl sulphate
siRNA	Small interfering RNA
TMEM16	Transmembrane protein 16 – Anoctamins
Tris	Tris(hydroxymethyl)aminomethane
UV	Ultraviolet
wt	Wild type

1. Introduction

1.1) Cystic Fibrosis and deficient CFTR-mediated anion secretion

1.1.1) Cystic Fibrosis

Cystic Fibrosis (CF) is the most common lethal autosomal recessive disorder in the Caucasian population[1]. CF has an incidence of one in 2500-6000 new-borns and a carrier frequency of 1 in 25 to 40 individuals[2]. The frequency of CF varies among different ethnic groups, the highest being in individuals of Northern European heritage[3, 4].

After being first described in 1938 as a digestive disorder[5], it was only in 1989, through chromosome walking and jumping gene cloning techniques, that the gene responsible for CF was identified and named Cystic Fibrosis Transmembrane Conductance Regulator (CFTR)[6]. This gene encodes a cAMP-regulated chloride (Cl^-) and bicarbonate (HCO_3^-) channel expressed at the apical membrane of a variety of epithelial cells[7], and it was found to harbour mutations in all CF patients analysed[8]. The basic defect of the disease has been associated with decreased anion conductance across the apical membrane of epithelial cells[6]. The most common mutation in CF patients is F508del, a three base pair deletion that causes a single amino acid deletion from CFTR and disrupts its traffic and function, due to protein misfolding[4].

In addition to functioning as an anion channel, CFTR also regulates other channels, having a critical inhibitory effect on sodium (Na^+) absorption through the epithelial Na^+ channel (ENaC)[9, 10]. Consequently, CF is characterized by defective epithelial anion secretion and enhanced Na^+ absorption. These features lead to dehydration of the airway surface liquid layer (ASL), resulting in enhanced mucus viscosity and in impaired mucociliary clearance (MCC) which causes the accumulation of purulent secretions. As MCC is an important defence mechanism against pathogens and dust particles[11], its reduction in CF patients leads to recurring bacterial infections, especially by *Pseudomonas aeruginosa*[12]. The treatment of these infections is particularly hard, since *P. aeruginosa* adapts specifically to the pulmonary microenvironment in CF patients through the formation of biofilms and the production of a capsular polysaccharide that inhibits penetration by antimicrobial agents[13]. Thus, the patients' lungs develop chronic neutrophil-dominated inflammation from a very early age, exacerbating tissue remodelling processes, scarring and fibrosis[14]. Obstructive lung disease is currently the primary cause of morbidity in CF patients and is responsible for approximately 80% of mortality[15].

Elevated concentrations of Cl^- in the sweat is another characteristic of CF patients, being the basis for one of the most common diagnostic tests for CF: measurement of the sweat Cl^- levels[16].

The gastrointestinal tract is also affected in most patients, with approximately 85% showing pancreatic insufficiency (PI) as a result of the obstruction of the pancreatic ducts[17] and subsequent scarring and destruction of exocrine function. Pancreatic disease is believed to result from a reduced volume of pancreatic secretions characterized by low concentrations of HCO_3^-. Impaired HCO_3^- secretion results in poor clearance of the digestive enzymes, and their premature activation causes the destruction and fibrosis of the pancreas[7, 18]. In addition, the CF phenotype may include less common complications such as meconium ileus, distal intestinal obstruction syndrome (DIOS), pancreatitis, liver disease or diabetes, among others[16].

Finally, infertility is a general condition in males with CF, as a consequence of congenital bilateral absence of the vas deferens (CBAVD)[16]. Women are usually fertile but can also show a lower fertility rate possibly due to the obstruction the thick mucus imposes upon sperm entering the cervical canal[19].

The classical management of CF includes multisystem symptomatic treatments including chest percussion and mucolytics to improve clearance of thick secretions, administration of antibiotics to treat bacterial lung infections, anti-inflammatory agents for handling the chronic neutrophil-dominated airway inflammation, pancreatic enzyme replacement to compensate for the absence of their physiological secretion, and a vigorous hypercaloric diet to maintain a good nutritional status[4, 20].

With these symptomatic therapies and all the progress in the study of the disease, the median predicted age of survival in the US has increased from 33.4 years in 2003 to 40.7 years in 2013[21]. Despite such improvement, the burden of CF therapeutics is still very high and quality of life and life expectancy of most CF patients are still limited[22]. Therefore, the disease must be treated beyond its symptoms in order to effectively halt the cascade of effects downstream of CFTR dysfunction[2]. Regarding this goal, attention has turned to the development of treatments addressing the basic defect of the disease, associated with *CFTR* gene mutations.

The concept of treating patients through gene therapy, i.e., by inserting a correct copy of the CF gene into the patients' cells so that they would produce a functional protein, was a promising idea that could provide positive results regardless the class of the patients' mutations[23]. However, gene therapy trials with adenovirus vectors proved to be impractical because of the viral immunogenicity and low efficiency of vectors to insert DNA into epithelial cells. Recently, other potential vectors were considered, like adeno-associated viruses and liposomes[4, 24]. Indeed, latest studies showed that monthly lung delivery of plasmid DNA encoding the *CFTR* gene complexed with a cationic liposome was associated with a significant, albeit modest, increase in stabilisation of lung function[25].

As an alternative to classical or gene therapies, novel pharmacological approaches based on rescuing intracellular production, trafficking, or activation of CFTR started to appear as possible innovative treatments. Thus, novel compounds have emerged as promising drugs treating the basic defect of CF, namely correctors (agents that correct the localization of the F508del-CFTR protein from the endoplasmic reticulum – ER – to the cell membrane) and potentiators (drugs that increase function of CFTR located at the cell membrane) of CFTR[22]. Nevertheless, only some mutations can be circumvented by these approaches. Therefore, treatments to read-through premature stop mutations and manipulate other ion transport pathways which compensate for CFTR absence (bypass therapies), also have a major importance in the treatment of CF[26, 27].

1.1.2) CFTR – Gene and mutations

The *CFTR* gene is located on the long arm of chromosome 7 (region q31-q32) and consists of a highly complex TATA-less promoter and 27 exons spanning about 190 kb of genomic sequence[28].

About 2,000 CF-causing mutations have been reported in the *CFTR* gene, being grouped in 7 different functional classes, according to the molecular/cellular defect they confer (Fig.1): Class I mutations abolish protein production (often being nonsense mutations – with premature stop codons); Class II mutations result in defective protein processing and trafficking, due to protein misfolding; Class III mutations lead to proteins that have no function due to impaired channel gating; Class IV mutations cause a defective ion conductance; Class V mutations result in decreased protein synthesis; and Class VI mutations diminish retention/anchoring at the cell surface, often related with decreased protein stability at the plasma membrane[16, 29]. A novel class was recently proposed as those which result from deletions, insertions and hence are considered to be "unrescuable" by pharmacological agents[30].

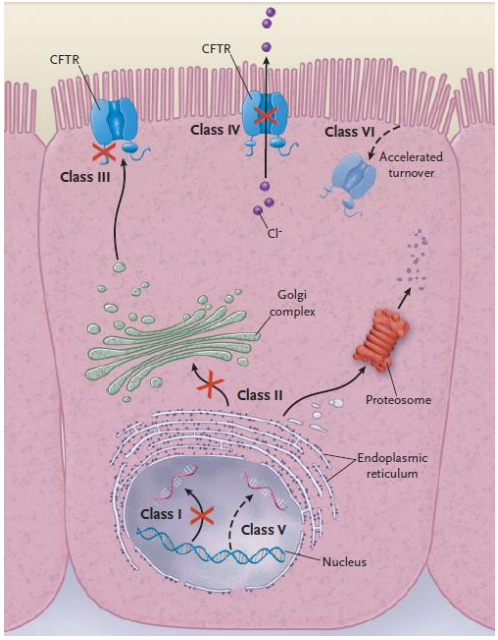

Figure 1 - **Categories of CFTR mutations[13].**

The ~2000 mutations found in the *CFTR* gene are thus distributed in these classes[31]. As already referred, the deletion of phenylalanine 508 in the first nucleotide binding domain (NBD1) of CFTR (F508del-CFTR) is the most common mutation[4]. This mutation belongs to the class II (no traffic) and it is present in approximately 85% of CF patients in at least one allele, being associated with a severe phenotype[21]. Evidence indicates that F508del-CFTR adopts an abnormal protein conformation which is recognized and retained by the endoplasmic reticulum quality control (ERQC), which rapidly targets it for proteasomal degradation. Consequently, only a small amount or no F508del-CFTR, depending on the cell type, reaches the plasma membrane[32].

1.1.3) CFTR – Protein structure and function

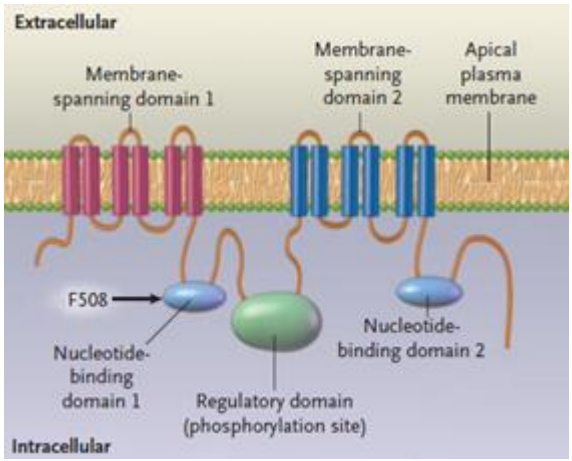

Figure 2 - **Hypothesized structure of CFTR. Adapted from [13].**

CFTR is a transmembrane protein expressed in the apical membrane of epithelial cells in the airways, intestine, reproductive tissues, and exocrine glands (such as sweat glands, exocrine pancreas, and salivary glands)[33]. CFTR is a symmetrical, polytopic protein with 1480 amino acid residues[6] that belongs to the superfamily of the ATP-binding cassette (ABC) transporters.

CFTR is composed of five domains: two regions that anchor the protein in the membrane known as membrane-spanning domains (MSD1 and MSD2), each containing six alpha helical segments; two cytosolic nucleotide-binding domains (NBD1 and NBD2) that bind ATP; and a central, highly charged

regulatory domain (RD) with multiple phosphorylation consensus sites[13]. The MSDs contribute to the formation of the selective pore, the NBDs bind and hydrolyse (NBD2) ATP to regulate channel gating and RD undergoes phosphorylation by protein kinase A (PKA) to control channel activity[34]. Both the amino (N) and carboxyl (C) terminal tails of CFTR are cytoplasmically oriented and mediate the interaction between CFTR and a variety of binding proteins[33]. The C-terminus of CFTR has a consensus sequence recognized by PDZ domains, to which several PDZ-domain proteins, notably NHERF1, have been shown to bind[35].

Like other proteins undergoing the secretory pathway, CFTR assembly starts with synthesis and folding in the ER, where it is glycosylated. Once checked for correct folding by the ERQC, this immature form of CFTR migrates to the Golgi complex, where it undergoes glycoside maturation[36].

CFTR functions mainly as a cAMP-regulated anion (Cl^- and HCO_3^-) channel at the apical membranes of epithelial cells, where it provides a pathway for anion movement across epithelia and regulates their flow[8, 32]. Additionally, CFTR has been associated with other processes like glutathione transport[37], regulation of other ion channels[38-40], regulation of intracellular vesicle transport, acidification of intracellular organelles[4], transepithelial electroneutral NaCl transport, control of osmotic water permeability, and apoptosis[16, 32]. Accordingly, CFTR appears to be truly a conductance regulator.

1.1.4) CFTR as a major regulator of other epithelial ion channels

As previously outlined, in the lung and in other epithelial tissues of CF patients, there is a hyper absorption of Na^+ mediated by ENaC. The functional relationship between CFTR and ENaC dictates the ability to clear bacteria and other harmful agents from the lungs by regulating water levels and composition of ASL. Data suggest that a direct physical interaction occurs between CFTR and ENaC[11]. Enhanced Na^+ conductance in CF is caused by a lack of downregulation of ENaC by non-functional CFTR. Co-expression of CFTR inverts PKA mediated regulation of ENaC by interfering with the gating mechanism of the channel, thus turning activation of ENaC by PKA into channel inhibition[41].

Apart from the well examined effects of CFTR on epithelial Na^+ conductance, CFTR also controls other ion channels and transporters, having a crucial effect on the ionic flow on epithelia. Among these channels are calcium (Ca^{2+})-activated Cl^- channels (CaCC)[41], outwardly rectifying Cl^- channel (ORCC)[42], K_{ATP} channels (such as ROMK2 and Kir 6.1), water channels and the volume-regulated anion channel (VRAC)[38].

It has been reported that CFTR inhibits endogenous CaCC currents in *Xenopus* oocytes, bovine pulmonary artery endothelium, and isolated parotid acinar cells[38, 43, 44]. Also, CaCC currents are enhanced in cultured CF airway epithelial cells as well as in freshly excised nasal tissues from CF patients[45, 46]. The ORCC regulation by PKA was found to be defective in CF human airway epithelia when compared to that of normal epithelia[44], while VRAC is inhibited by expression of CFTR[38].

The anoctamin protein family was found to be closely associated with these channels regulated by CFTR. Anoctamin 1 (Ano1) was identified as CaCC[47, 48], with its Ca^{2+}-activated Cl^- channel function being inhibited during the activation of CFTR, while CFTR currents are

attenuated by overexpression of Ano1 and both proteins could be co-immunoprecipitated[40]. Also, Ano6 was identified as the main component of ORCC[49]. Furthermore, anoctamins are shown to regulate the cellular volume possibly by operating as VRAC, by regulating intracellular Ca^{2+} signalling, or by acting as accessory proteins for the recently identified volume-regulated channel LRRC8A[48].

With these data it is clear that anoctamins might play a significant role in epithelial ion transport in CF. Therefore, the relationship between anoctamins and CFTR deserves further investigation to find a possible alternative way to conduct Cl^- across epithelia and thus compensate for the severe symptoms caused by lack of functional CFTR in CF.

1.2) Anoctamins

1.2.1) CaCCs and anoctamins

Ca^{2+}-activated Cl^- channels (CaCCs) were first described in the 1980s in *Xenopus* oocytes[51] and salamander photoreceptor inner segments[52]. CaCCs are ubiquitous and play key physiological cellular roles, such as transepithelial transport of salt and fluids[53], regulation of electrical membrane excitability in cardiac muscle and neurons[54], olfactory transduction[55], regulation of vascular tone[56], photoreception[57], maintenance of ionic homeostasis and pH, and cell-volume regulation[58].

CaCCs are activated by elevation of cytosolic cAMP or Ca^{2+}, cell swelling, extracellular acidification, membrane potential changes, or interaction with extracellular ligands. Depending on the cell type, Ca^{2+} activates CaCCs either by direct binding to the channel, indirectly through Ca^{2+}-binding proteins or via phosphorylation through Ca^{2+}/calmodulin-dependent protein kinase II (CaMKII)[59].

A frequently described property of CaCCs is the sensitivity to membrane potential, which modulates the response to Ca^{2+}. CaCCs are thus characterized by their voltage- and time-dependence at sub-saturating Ca^{2+} concentrations (<1 µM). At these low physiological Ca^{2+} levels, CaCCs are activated and deactivated by positive and negative membrane potentials, respectively. At micromolar Ca^{2+} levels, CaCCs are fully activated at all membrane potentials. Accordingly, the steady-state current-voltage relationship changes from outwardly rectifying to almost linear as the intracellular free Ca^{2+} concentration increases. However, this behaviour does not apply to all CaCCs, as in some cells CaCCs are voltage independent at all Ca^{2+} concentrations[59, 60].

Another feature that characterizes CaCCs is their poor anion selectivity, hardly discriminating between anions with a selectivity sequence similar to that of Eisenman type I ($SCN^- > I^- > Br^- > Cl^- > F^-$)[61].

Several attempts were made in the past to identify the proteins forming CaCCs, but the ubiquitous expression of CaCCs and the lack of specific inhibitors, turned it into a difficult task. The proteins that have been proposed as main constituents of CaCCs include members of the Cl^- channel, Ca^{2+}-activated (CLCA) family[62], CLC-3[63], and bestrophins[64].

CLCA proteins are unlikely candidates because the membrane currents elicited by their expression did not resemble CaCCs in terms of voltage-dependence, Ca^{2+} affinity, and sensitivity to pharmacological modulators. Also, CLCAs were excluded as membrane proteins, being defined as cell adhesion molecules which may be also secreted into the extracellular medium[65].

CLC-3 gene expression also causes the appearance of Cl^- currents that lack the typical voltage dependence of CaCCs[66]. Furthermore, salivary gland cells of CLC-3 knockout mice have normal CaCC activity.

In addition, bestrophins were proposed as Cl^- channels different from CaCCs, particularly in the small dependence of gating on membrane potential. Similarly, bestrophin-1 knockout mice have normal CaCC currents in cells from the retinal pigment epithelium[59], thus excluding these proteins as possible CaCCs.

Finally, in 2008, Ano1 (also TMEM16A) was identified as being a CaCC by three independent groups using different approaches. Yang and colleagues used a bioinformatics approach to identify Ano1, confirming its CaCC function by expression cloning in HEK 293 cells and using small interfering RNA (siRNA) knockdown in mouse salivary glands[47]. Caputo *et al.*, knowing that interleukin-4 stimulation of airway epithelial cells resulted in increased CaCC activity, were able to identify Ano1 by microarray analysis. They also demonstrated that Ano1 displays an ion channel activation, inhibition, and anion selectivity profile consistent with native airway CaCCs[48]. Lastly, Schroeder and colleagues used an expression cloning approach to identify the *Xenopus* orthologue of Ano1 and characterize its function and expression[67]. These authors also found that Ano2, a close paralog of Ano1, generates Ca^{2+}-activated Cl^- currents.

Thus, the anoctamin family (Ano, also known as TMEM16) exhibits similar characteristics to those expected for the classical CaCC. Moreover, anoctamins tissue expression has a big overlay with CaCCs, being found in sensory receptors, different types of smooth muscles, heart, endothelium, neuronal tissues, and epithelial organs[68].

The anoctamin family constitutes a class of proteins that is only expressed in eukaryotic organisms, including mammals, flies, worms, plants, protozoa and yeast[69]. In mammals the family contains ten members (TMEM16A-H, J and K, respectively renamed Ano1-10), with high sequence conservation, particularly around the putative pore forming region[70]. In spite of their close relationship, the proteins of this family combine different functions: some members were defined as CaCCs while others were defined as Ca^{2+}-activated scramblases, which catalyse the shuffling of lipids between the inner and outer leaflets of the membrane bilayer[71], or both.

Anoctamins have no apparent similarity to other ion channels. Moreover, multiple alternative splice variants exist in different cell types, suggesting that these proteins are the product of complex regulatory mechanisms still unknown[72, 73].

1.2.2) Anoctamins – Structure and Function

Structure

The term anoctamin was created due to the anion selectivity of the protein, while the prefix “oct” stood for its assumed eight transmembrane domains predicted from hydropathy profile analysis[47, 69]. However, recent crystallographic studies of the TMEM16 protein from the

fungus *Nectria haematococca* (nhTMEM16) suggest that these proteins have ten, and not eight, transmembrane domains[74]. Nevertheless, the name anoctamin or Ano is the official HUGO nomenclature and has replaced TMEM16 in Genbank[75].

The anoctamins' structure is still not completely understood. The best structure was determined with nhTMEM16, which shares a high degree of homology with mammalian anoctamins[74]. nhTMEM16 is a homodimer, in which both subunits are related by two-fold symmetry and show very similar conformations. Both N- and C-termini are located on the cytoplasmic side of the plasma membrane (Fig.3).

The structure harbours two regions that are presumably in contact with the membrane: the dimer cavity, at the dimer interface, which is predominantly composed of hydrophobic and aromatic residues conserved within the protein family; and the subunit cavity, a hydrophilic membrane-spanning crevice contained within each subunit[74].

It is currently not yet clear whether the dimer cavity plays a critical role on protein function. However, the subunit cavity is linked to Ca^{2+} activation and probably also to catalytic properties of the protein. In Ano1, 2, and 6, the subunit cavity may constitute the ion conduction pore, as suggested by the influence of point mutations of residues facing the subunit cavity on ion selectivity and conductance[76].

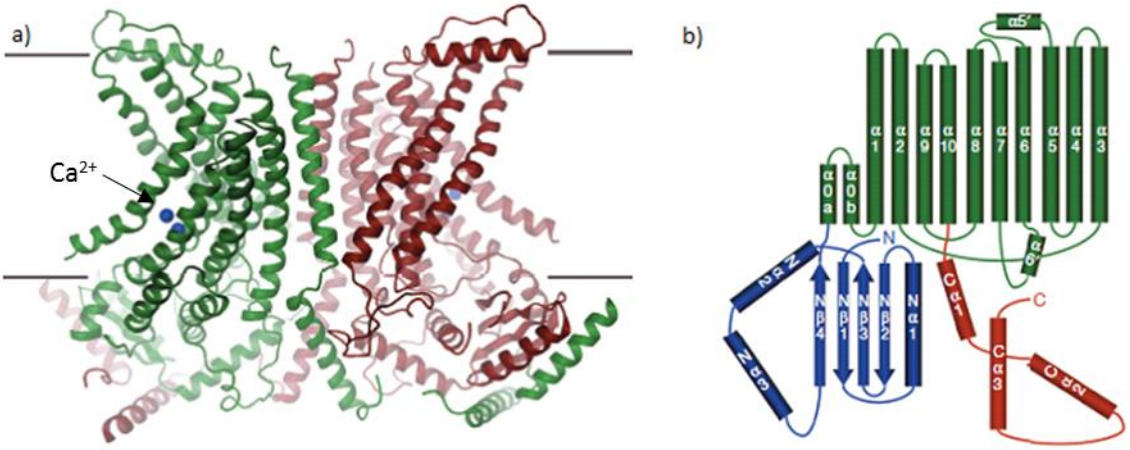

Figure 3 – **a) Ribbon representation of the nhTMEM16 dimer. The view is from within the membrane and bound Ca^{2+} ions are shown as blue spheres (black arrow). b) Topology of the nhTMEM16 subunit. The transmembrane domain is shown in green and the N- and C-terminal domains in blue and red, respectively. Adapted from [74].**

Studies performed with mouse anoctamins are in agreement with the results obtained with nhTMEM16, showing that Ano1 forms a stable homodimer[77, 78]. Ano1 subunits associate before being trafficked to the plasma membrane and the oligomeric state is independent of changes in intracellular Ca^{2+} concentration, suggesting that the homodimeric structure of Ano1 is not a determinant of channel gating[73].

Moreover, Ano1 was shown to co-immunoprecipitate with the more closely related homolog Ano2. The ability for close homologs to interact extends across species, as *Xenopus* Ano1 was co-immunoprecipitated by both mouse Ano1 and Ano2[68].

These results indicate that anoctamins are dimeric proteins, and the interactions responsible for channel assembly seem to be well-conserved. The N-terminal domain appears

to be essential and sufficient for dimerization, but there are probably other inter-subunit contact interfaces present in the dimer[79].

Cellular localization and Functions

Proteins of the anoctamin family are widely expressed, namely in epithelia[80, 81]. Ano6, 8 and 10 are broadly expressed in mouse and human tissues. Ano9 is mostly expressed in epithelial tissues and Ano1 is expressed in almost every kind of secretory epithelium like salivary gland, pancreas, gut, mammary gland, prostate tissue, and airway epithelium[73]. Ano2, 3, and 4 are preferentially expressed in sensory receptor cells and neuronal tissues[80]. Ano5 is expressed in skeletal muscle and thyroid gland and Ano7 seems specifically expressed in prostate[60]. Therefore, epithelial tissues express Ano1, 5, 6, 7, 8, 9, and 10.

Subcellular localization of the family members is not completely defined, although membrane expression is most obvious for Ano1 and Ano2[80]. Studies with HEK 293 overexpressing anoctamins showed that Ano1, 2, 4, 6 and 7 are well expressed in the plasma membrane while Ano8, 9 and 10 traffic poorly to membrane and are mostly localized in the cytoplasm[82].

Although the functions of some family members are still inconsistent, it is now clear that Ano1 and Ano2 produce Ca^{2+}-activated Cl^- currents[47, 83].

Ano1 is the most well studied member of the anoctamin family, and it contributes to Ca^{2+}-activated epithelial Cl^- secretion in a broad range of tissues[84, 85]. Ano1 is strictly membrane localized and requires cytoskeletal interactions to be fully activated. This protein is activated by a rise in intracellular Ca^{2+} [48], and the Ca^{2+}-binding protein calmodulin seems essential for its activation[81, 86].

Ano2 is the main component of the CaCCs involved in olfactory sensory neurons and in the photoreceptor synaptic terminals in retina[87, 88].

Ano3 was found to co-localize and directly interact with Slack, the protein forming the Na^+-activated K^+ channel. When expressed in HEK 293 cells, Ano3 did not form ion channels by itself but increased the activity of Slack when both proteins were expressed together[71, 89].

Finding the correct functions of Ano6 has been a real challenge. Ano6 was shown to act as a Ca^{2+} activated non-selective cation channel[76], possibly also as CaCC[90] and it was identified as a major component of the ORCC[49]. These channels are known to be activated upon excision of the cell membrane from the intact cell and after strong depolarization[49, 91] and are also activated by cAMP and PKA. Ano6 has a role in lipid scrambling by facilitating the exchange of phosphatidylserine from the inner to the outer leaflet of the bilayer[92], a process that is essential for membrane biogenesis in the ER[93], blood coagulation[76, 94], and apoptosis[49], among other cellular processes. Ca^{2+}-dependent scrambling activity was also detected in Ano3, Ano4, Ano7 and Ano9, although with different preference to lipid substrates[95].

Additionally, Ano1, Ano6 and Ano10 have been found to contribute to cellular volume regulation[48, 96, 97].

Ano9 and Ano10 have intriguing functions, as both were shown to reduce baseline Cl^- conductance as well as ATP-induced anion currents[81]. Also co-expression of Ano9 with Ano1 led to the inhibition of Ano1 activity, and it is conceivable that it may also regulate other family members[82]. These data suggest that some anoctamins influence each other, which could be explained by a heterodimeric architecture[80].

Another level of complexity in anoctamins arises from their alternative splicing. For instance, it was revealed for Ano6 the existence of four isoforms. Since all isoforms shared similar ion selectivity, the existence of isoforms cannot explain the discrepant results obtained so far. Therefore, it is possible that phospholipid scrambling is the main function of Ano6 whereas ion transport is a secondary activity that is activated at less physiological conditions[98, 99].

Besides all the different cellular functions already described, Ano1 and Ano6 were also associated with cell migration[100], suggesting that anoctamins can also be considered as a novel family of regulators of cell proliferation and apoptosis, which may be of particular relevance during development, activation of immune cells[101], and cancer[102].

1.2.3) Anoctamin related diseases

Anoctamins attracted the interest of cancer biologists for several years before their identification as ion channels because of their potential role in cell volume regulation and cancer malignancy[103]. Although these proteins are up-regulated in tumours, mutations in anoctamins genes are not linked to carcinogenesis[104]. Nevertheless, anoctamins may participate in cell proliferation and/or tumour progression.

As previously stated, some anoctamins, such as Ano1 and Ano6, are associated with cell volume regulation and migration, so their up-regulation could provide a growth or metastatic advantage to cancer cells[105]. Accordingly, splicing variants of Ano6 are associated with metastatic ability of mammary cancers in mice and are also correlated with poor prognosis of patients with breast cancer[106]. Additionally, *ANO1* gene is located within the 11q13 amplicon, a chromosomal *locus* that is frequently amplified in a number of different human cancers, such as gastrointestinal stromal tumour (GIST)[107], urinary bladder cancer, breast cancer[108] and head and neck squamous cell carcinoma[109, 110]. Ano7 has also been associated with cancer, being up-regulated in prostate cancer[111].

Anoctamins are also related with several other diseases. Among the members of the anoctamin family, Ano5 was the first to be associated with human diseases. Gnathodiaphyseal dysplasia, a rare dominant skeletal syndrome, is caused by mutations in the *ANO5* gene[112, 113]. *ANO3* gene mutations cause an autosomal dominant form of craniocervical dystonia[114] and mutations in the *ANO10* gene are linked to autosomal recessive spinocerebellar ataxia and atrophy[115].

Beyond its role in cancer, Ano1 dysfunction causes multiple defects in epithelial organs. Ano1 knockout mice die early during postnatal phase and exhibit severe tracheomalacia (tracheal cartilage malformation)[116]. Moreover, there is also accumulation of mucus in the lumen of tracheas of Ano1-KO mice, which shows the importance of Ano1 in MCC in mouse airways[84].

Also, mutations at a splice-acceptor site of the *ANO6* gene, that cause the premature termination of the protein, lead to Scott syndrome. This is a bleeding disorder which results from a defect in phospholipid scrambling activity of the outer membrane leaflet of platelets[117].

These findings point out the relevance of the study of anoctamins to use these proteins as therapeutic targets.

1.2.4) CFTR and anoctamins

It has been suggested that there is a crosstalk between cAMP and Ca^{2+} dependent Cl^- secretion (CFTR and anoctamins, respectively). It is known that purinergic receptors such as $P2Y_2$ or $P2Y_6$ couple to both cAMP and Ca^{2+} [118] and that intracellular Ca^{2+} controls enzymes such as adenylate cyclase and phosphodiesterases that determine intracellular cAMP levels[119]. Also, other messengers like the IP_3 receptor binding protein IRBIT may link IP_3/Ca^{2+} signalling by binding to CFTR[120].

Indeed, as previously discussed, CFTR is a major regulator of ion channels and it can interact with several proteins, including anoctamins.

CFTR inhibits endogenous Ca^{2+} activated Cl^- conductance in *Xenopus* oocytes, bovine pulmonary artery endothelium and parotid acinar cells[38, 44, 46]. Also, Ano1 knockout mice were shown to display symptoms that resemble those of CF, like low Cl^- secretion and accumulation of mucus in the airways[84, 121]. Additionally, Ano1 is present in apical membrane of airway epithelial cells[84], and it was reported that CaCC function of Ano1 is enhanced in CF epithelial cells and inhibited during activation of CFTR. Inversely, CFTR currents were attenuated by overexpression of Ano1, which again suggests that both Cl^- channels are related[40]. Moreover, since the expression of F508del-CFTR does not influence CaCC, it is likely that the CFTR–Ano1 interaction occurs at the plasma membrane[38].

Among the remaining members of the anoctamin family, Ano6 also seems to interact with CFTR, being activated through stimulation of CFTR or during apoptosis. The ORCC regulation by PKA was found to be defective in CF airway epithelia but it was corrected once complemented with the wt-*CFTR* gene[42, 122]. It has been reported that the NBD1 and the RD of CFTR are essential for CFTR's ability to interact with ORCC[38]. Indeed, CFTR is thought to regulate the ORCC by facilitating cellular release of ATP. Once released, ATP stimulates the channel through a purinergic receptor ($P2Y_2$)[17].

It is possible that CFTR and Ano1/6 interact directly or through scaffold proteins. Studies demonstrating that CFTR translocates G_q-coupled receptors to the plasma membrane of *Xenopus* oocytes allowing for Ca^{2+} increase and activation of Ano1[123] support the hypothesis of CFTR/Anoctamins interaction through PDZ binding proteins. Nevertheless, more studies need to be performed to solve this question and deepen the knowledge on these interactions.

In summary, in the presence of wt-CFTR, parallel activation of CFTR and Ano6 (ORCC) is observed, while Ano1 (CaCC) is inhibited. In contrast, in CF cells, the ORCC is attenuated while CaCC currents appear upregulated.

Thus, these discoveries suggest that anoctamins may partially mimic and overcome the defects caused by CFTR loss, improving CF therapies[124]. However, although CaCC appears

enhanced in CF, it may not be able to compensate for defective CFTR. This can be explained by the small contribution of CaCCs to airway Cl^- secretion and by the fact that activation of CaCC is largely transient, in contrast to the permanent CFTR-dependent Cl^- secretion[40]. Yet, activation of latent CaCCs could compensate for CFTR loss of function in CF patients[47].

Nevertheless, since these alternative ion channels are not expressed in the other affected organs in patients with CF[125], potential benefits of therapeutic targeting are likely limited to the lungs. Despite this limitation, these strategies can result in an effective treatment of lung disease in CF patients regardless of their genotype. Importantly, these therapies may also be beneficial for patients with chronic obstructive pulmonary disease (COPD), or asthma[125].

The evidence of CFTR/anoctamins interaction create possible alternative pharmacological targets for CF that could lead to a more sustained Cl^- secretion in the patients, thus correcting the basic defect of the disease. However, to that end a deeper knowledge on CaCC/anoctamin function, activation, traffic, regulation and mechanism of interaction with CFTR is essential.

1.3) Objectives of the present work

The main goals of the present work were to identify novel regulators of anoctamin 6, 9 and 10 and to study their interaction with other anoctamin family members as well as with CFTR. In order to accomplish this goal, several milestones were established, namely:

1. To generate double-tagged constructs of Ano6, Ano9 and Ano10 to allow quantification of both their total levels as well as the fraction at the plasma membrane (PM) by fluorescent microscopy (Fig.4 and 5);
2. To clone the double-tagged constructs of Ano6, Ano9 and Ano10 into an inducible (Tet-On) lentiviral vector (pLVX-TRE3G);
3. To generate stable cell lines expressing the inducible double-tagged anoctamin constructs through lentiviral transduction;
4. To perform siRNA microscopy screens to identify genes involved in regulating the traffic of Ano6, Ano9 and Ano10 as potential drug targets for CF;
5. To perform functional characterization of the stable cell lines overexpressing the double-tagged anoctamin constructs;
6. To look for physical and functional interactions among anoctamin family members.

Identification of the roles of these proteins and their functional interactions will shed light into the understanding of their physiological functions. Moreover, this knowledge will allow the comprehension of the pathogenic role of this protein family in diseases, and will possibly suggest novel therapeutic approaches to CF.

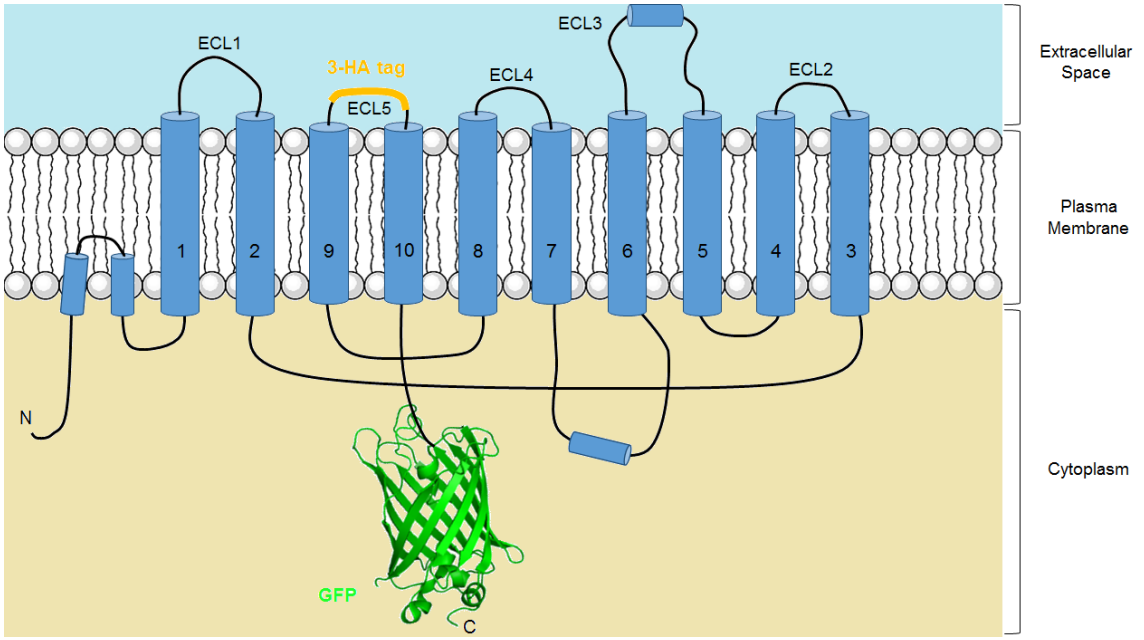

Figure 4 – **Schematic representation of the Ano6/Ano10 traffic reporter construct, based on the structure predicted in [74]. Topology of the Ano6/Ano10 molecule: GFP was fused to the C-terminus of Ano6 and Ano10, and the 3-HA tag was introduced in their 5th extracellular loop (ECL5).**

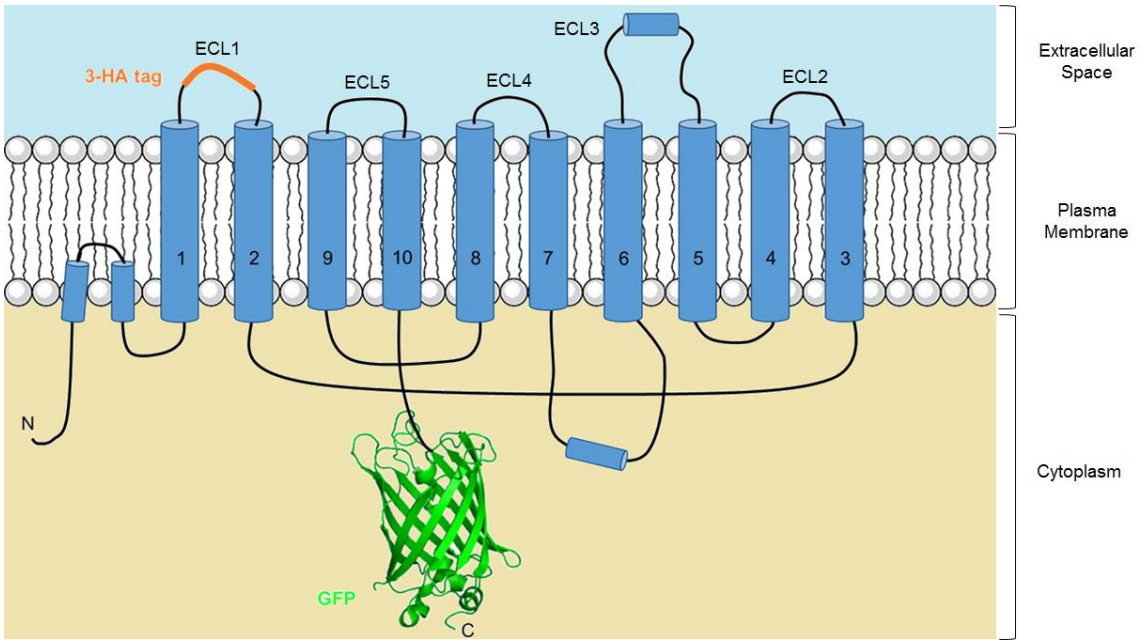

Figure 5 - **Schematic representation of the Ano9 traffic reporter construct, based on the structure predicted in [74]. Topology of the Ano9 molecule: GFP was fused to the C-terminus of Ano9 and the 3-HA tag was introduced in its 1st extracellular loop (ECL1).**

2. Materials and Methods

2.1) Generation of cell lines overexpressing anoctamin 6, 9 and 10

2.1.1) Plasmids and cDNAs

cDNAs of human anoctamins (Anoctamins 6, 9 and 10) containing a GFP (green fluorescent protein) tag in C-terminus were already cloned into pcDNA3.1 (+) vectors (Invitrogen, V790-20).

pcDNA™3.1(+) is a 5.4 kb vector derived from pcDNA™3 designed for high-level stable and non-replicative transient expression in mammalian hosts. The vector contains an ampicillin resistance gene, which was used for selection of transformed bacteria.

A triple hemagglutinin tag was inserted in the anoctamins' cDNAs (Anoctamins 6, 9 and 10) constructs containing a GFP tag in C-terminus. The 3-HA tag was inserted in an apparent extracellular loop in order to be used as a marker of the anoctamins located at the plasma membrane. Thus, when an immunofluorescence experiment is done with cells transfected with these constructs, the antibody that binds to the 3-HA tag should stain the membrane proteins without permeabilization of the plasma membrane.

The double-tagged anoctamin constructs were cloned into pLVX-TRE3G (Clontech, 631191) lentiviral vector using the In Fusion® HD Cloning Kit (Clontech, 631187), with the purpose of creating lentiviral particles to transduce cells and create stably transfected cell lines. pLVX-Tet3G (Clontech, 631358) lentiviral vector encoding the Tet-On 3G transactivator protein was used for inducible gene expression. pLVX-TRE3G contains a puromycin resistance gene and pLVX-Tet3G contains a G418 (geneticin) resistance gene.

Vectors' maps and pLVX-TRE3G cloning sites are displayed in Appendix 1.

2.1.2) Production of competent bacteria

The bacterial strain used for cloning, mutagenesis and DNA amplification was XL1-Blue (Stratagene), which is tetracycline resistant. XL1-Blue cells are endonuclease (endA) deficient, which greatly improves the quality of miniprep DNA, and are recombination (recA) deficient, improving insert stability. XL1-Blue Genotype: *recA1 endA1 gyrA96 thi-1 hsdR17 supE44 relA1 lac* [F´ *proAB lacI*^{q}*ZΔM15* Tn*10* (Tet^{r})].

For production of competent bacteria, 200 µL of XL1-Blue competent cells were grown in LB medium (NZYTech, MB028) supplemented with tetracycline (NZYTech, MB02201) overnight at 37°C with vigorous shaking (220 rpm). This solution was diluted 1/100 into a larger volume of LB medium, typically 200 mL, which was also grown at 37°C (220 rpm) to final concentration of bacteria corresponding to an absorbance between 0.45 and 0.55 at 590 nm. Bacteria were transferred to ice and pelleted by centrifugation (1000 g for 15 min at 4°C). The bacterial pellet was then ressuspended, incubated on ice for 15 min in 33 mL RF1 buffer (100 mM RbCl, 50 mM $MnCl_2$, 30 mM KCH_3COO, 10 mM $CaCl_2$, 15% (w/v) glycerol, pH 5.8; all from Sigma-Aldrich) and re-pelleted by centrifugation (1000 g for 15 min at 4°C). This second pellet was ressuspended and incubated on ice for 15 min in 8 mL of RF2 buffer (10 mM MOPS, 10 mM RbCl, 75 mM $CaCl_2$, 15% (w/v) glycerol, pH 6.8; all from Sigma-Aldrich). 200 µl aliquots were then rapidly frozen with liquid nitrogen and stored at -80°C for further use.

2.1.3) Transformation of competent bacteria

Bacteria were transformed by incubating a 200 µL aliquot of competent cells with DNA (10 µL of ligation products; 15 µL of the PCR product – mutagenesis; 10 ng of plasmid DNA) for 30 min on ice, followed by heat-shock (1 min and 30 s at 42°C), incubation for 2 min on ice, and then incubation in antibiotic-free LB medium for 1 h at 37°C at 300 rpm. Bacteria were then pelleted (6000 g for 2 min), the supernatant was discarded and the pellet was ressuspended in the remaining supernatant medium. This suspension was then plated into LB-agar (Sigma-Aldrich, L2897) supplemented with selection antibiotic (100 µg/mL ampicillin, Sigma-Aldrich, A9518) and left to grow overnight at 37ºC at 220 rpm.

Transformed bacterial colonies were grown in LB medium supplemented with 100 µg/mL ampicillin and used to extract plasmid DNA. Clones were stored in liquid LB medium supplemented with 50% (w/v) glycerol at -20°C.

2.1.4) Plasmid DNA extraction and quantification

Small scale plasmid DNA was purified with the NZYMiniprep kit (NZYTech, MB010). The protocol is based on an alkaline lysis of the bacterial cells in the presence of SDS, to denature bacterial proteins, followed by a centrifugation step to remove cellular debris, genomic DNA and denatured proteins, and adsorption of the plasmid DNA in the supernatant to an anionic exchange matrix in the presence of high saline concentrations. After adsorption, the DNA is washed and eluted in water. Sequence of plasmid DNA preparations was confirmed by DNA sequencing (2.1.6 – DNA sequencing) at least once for every plasmid.

Whenever a high quantity of DNA was necessary for further experiments (for example for lentivirus production), large-scale preparation of highly pure plasmid DNA was achieved using NZYMaxiprep kit (NZYTech, MB051).

DNA concentration was determined by measurement of absorbance at 260 nm using a Nanodrop ND-1000 spectrophotometer (Thermo Scientific), and its purity was evaluated by assessment of the ratio A260/A280 (Absorbance at 260 nm/Absorbance at 280 nm). Only DNA samples with ratios above 1.8 were considered pure enough for further use.

2.1.5) Genomic DNA extraction

Genomic DNA (gDNA) extraction was performed to confirm the correct insertion of the anoctamins' constructs in the genome of stably transfected cells.

To achieve this, cells were trypsinized and harvested in microcentrifuge tubes. Cells were then pelleted and washed with PBS. Next, the proteins were precipitated, the supernatant was collected and added to a tube containing isopropanol to precipitate the DNA. The DNA was then pelleted, washed with ethanol, and air-dried for 15 min. Finally, the DNA was rehydrated for 1 h at 65ºC.

2.1.6) DNA sequencing

Plasmid DNAs were purified as described in 2.1.4 – Plasmid DNA extraction and quantification. The sequencing reactions were performed by StabVida using Sanger sequencing.

The primers used for sequencing were specific for each anoctamin (ordered through StabVida), and are shown in Appendix 2.

The sequences obtained were analysed through comparison with the reference human sequence of each anoctamin (Anoctamin 6 – Reference Q4KMQ2, Anoctamin 9 - Reference A1A5B4, Anoctamin 10 – Reference Q9NW15, all from UniProt[126]) using the software Geneious[127].

2.1.7) Mutagenesis

The 3-HA (triple hemagglutinin) tag was inserted in Ano6, Ano9, and Ano10-GFP constructs by mutagenesis. The 3-HA tag was introduced in a predicted extracellular loop for each anoctamin, as already mentioned above.

In the first mutagenesis attempt for each anoctamin, the localizations of the 3-HA tag were selected using the predicted structure of these anoctamins available in Uniprot[126] (Ano6 – Reference Q4KMQ2, Ano9 - Reference A1A5B4, Ano10 – Reference Q9NW15). For Ano9, the first mutagenesis was performed by a co-worker, Sara Afonso. Since the localizations of these first tags were not adequate (because they were most likely not exposed to the exterior of the cell) – 2.1.8 – Protein modelling, Appendix 4 – a second mutagenesis was achieved for each anoctamin. In this second attempt, the localization of the tags were chosen using a predicted structure of the proteins created by protein modelling based on the crystal structure of nhTMEM16[74] (work performed by a co-worker, Hugo Botelho, see 2.1.8 – Protein modelling to determine the best localization for the HA tags, Appendix 4).

The mutagenesis reactions were performed using the KOD Hot Start Kit (Novagene, 71086) with complementary pairs of the custom designed HPLC-purified mutagenic primers described in Appendix 3 – Table 2 (ordered from StabVida).

The mutagenesis reaction is a regular PCR reaction, with primers that are not completely complementary to the template sequence; instead, they contain the 3-HA tag meant to be inserted. The PCR programs used are displayed in Appendix 3 – Table 3.

The result of these mutagenesis reactions is a mixture of the template plasmid and a new plasmid containing the desired insertion. After confirming the amplification by electrophoresis using a 0.8 % agarose gel, the PCR products were incubated 1 h at 37ºC with *DpnI* (Invitrogen, ER1702), a restriction enzyme that specifically hydrolyses methylated DNA. This results in complete degradation of the template DNA, heavily methylated because of its bacterial origin, leaving the mutated DNA, synthesized *in vitro*, intact.

After the hydrolysis step, bacteria were transformed with the PCR products and grown in LB agar plates with 100 µg/mL ampicillin. The correct insertion of the 3-HA tag was first confirmed using “colony PCR” with primers that bind at 5’ and 3’ of the inserted sequence (primers and PCR programs in Appendix 3 – Tables 4 and 5). The “colony PCR” reaction consists of a normal PCR, using the DNA directly from the bacterial colony (without DNA extraction and purification). The plasmid DNA of the bacterial colonies with the correct size of the insertion was then extracted (2.1.4 – Plasmid DNA extraction and quantification) and the insertion was finally confirmed by DNA sequencing (2.1.6 – DNA sequencing, and Appendix 2).

2.1.8) Protein modelling to determine the best localization for the HA tags

As already referred, for Ano6, Ano9 and Ano10, it was necessary to insert the 3-HA tag in two different positions. The first attempt was performed according to the predicted sequences available in UniProt[126].

After DNA sequencing of the mutagenesis products, cells were transfected with the double-tagged constructs in order to determine whether the 3-HA tag was indeed inserted in a loop located at the extracellular side of the plasma membrane.

For Ano6, after transient transfection (2.2.3 – Transient transfections) with the first construct, it was not possible to detect the 3-HA tag staining outside of the cell (i.e. when performed an immunofluorescence assay without membrane permeabilization – 2.4.1 – Immunofluorescence of anoctamins – no signal was detected, see Appendix 4 – Fig.40). Moreover, the number of transfected cells was always low. Regarding this issue, two approaches were followed. In the first one, an immunofluorescence assay with membrane permeabilization was made using a membrane antibody as control (E-cadherin), and an antibody for Ano6. The results obtained suggest that Ano6 was retained in the ER, not trafficking to the membrane, as no overlay between E-cadherin and Ano6 was observed (Appendix 4 – Fig.42). For the second approach, Ano6 structural models were generated using the I-TASSER server[128] (work performed by a co-worker, Hugo Botelho and included here with permission, see Appendix 4). With this method, the predicted structure of Ano6 was found to be completely unfolded, possibly explaining the ER retention of the protein (Appendix 4 – Fig.38).

I-TASSER (Iterative Threading ASSEmbly Refinement) is a hierarchical method for protein structure and function prediction. Structural templates are first identified from the PDB, followed by the construction of full-length atomic models. Finally, the 3D models are developed using a protein function database.

The amino acid sequences for the three anoctamins were submitted to the server and the structure of the TMEM16 protein from the fungus *Nectria haematococca* (nhTMEM16)[74] was used as a template for the modelling. Initially, models were obtained for Ano6, Ano9 and Ano10 structures without the tags (GFP and 3-HA). Using these models it was possible to select with more confidence a presumable extracellular loop in which the insertion of the 3-HA tag would: *i*) be exposed to the exterior of the cell; and *ii*) be less likely to affect the protein structure. After choosing the new localizations for the tags, the structural models of the first and second constructs of each anoctamin were also obtained using the I-TASSER server to determine those two aspects. All figures were prepared with PyMOL[129] (work performed by a co-worker, Hugo Botelho and included here with permission, see Appendix 4).

For Ano6, the correct localization of the 3-HA tag in the second construct (predicted by the structural model) was confirmed by an immunofluorescence assay on transiently transfected cells without plasma membrane permeabilization (Appendix 4 – Fig.43 and 44).

For Ano9, although the transfection rates as well as the GFP expression were high, the first construct did not show any membrane staining of the 3-HA tag (Appendix 4 – Fig.46). Nevertheless, the cellular localization of Ano9 is still unknown, with some studies suggesting that it is mainly cytoplasmic[84]. However, since the second construct of Ano6 based on the model showed the desired results, another mutagenesis was performed for Ano9, also choosing the

localization of the 3-HA tag in a probable extracellular loop (based on the structural model). After transient transfection with this construct, it was again not possible to detect the 3-HA tag without membrane permeabilization (Appendix 4 – Fig.48). Even though these results did not match what it was expected, this construct was used for further experiments, including the generation of stable cell lines overexpressing Ano9. This decision was made based on the still unknown localization of this protein, and because the two structural models of the construct seemed to have the correct localization of the tag. In this case, if Ano9 is not really in the membrane under normal cellular conditions, maybe the knockdown of other cellular components could alter this situation. This hypothesis will be further studied with the siRNA screens.

For Ano10, although the structural model of the first construct appeared to be similar to the native protein and with the 3-HA tag located in an extracellular loop, it was never possible to transfect cells with it (Appendix 4 – Fig.50). For this reason, another mutagenesis was performed. With this second construct the cells could be transfected but with a very low transfection rate. In this case it was not possible to detect clearly the 3-HA tag without plasma membrane permeabilization (Appendix 4 – Fig.51). However, similarly to Ano9, the cellular localization of this protein is still controversial, so the further experiments were also done using this construct.

2.1.9) Cloning

The double-tagged constructs of Ano6 and Ano9 were cloned into pLVX-TRE3G using the In Fusion® HD Cloning Kit, with the purpose of creating lentiviral particles to transduce human cells and thus create stably transfected cell lines with homogeneous transgene expression. As the Ano10 mutagenesis caused some difficulties, the cloning of this anoctamin into the pLVX-TRE3G vector is currently being done.

The cDNAs of the constructs were amplified through PCR reactions (primers and PCR programs in Appendix 3 – Tables 6 and 7) creating 16 bp extensions in both C- and N- terminals.

The pLVX-TRE3G was linearized using *BamHI* (Promega, R6021) and *MluI* (Fermentas, ER0561) (2h at 37ºC) restriction enzymes which create sticky ends complementary to the anoctamins' primer extensions.

The linearized vector as well as the anoctamins cDNAs with extensions were spin-column purified using the NZYGelpure kit (NZYTech, MB011). The In-Fusion cloning reaction was then performed (In Fusion HD Cloning Kit – Appendix 5 – Table 8) and afterwards competent cells were transformed with the cloning reaction product. The In-Fusion HD Cloning Kit was first tested using positive and negative controls provided in the kit (Appendix 5 – Table 9).

The correct insertion was confirmed through "colony PCR" (using primers that bind to the anoctamin, to confirm that it was inserted in the vector – Appendix 3 – Tables 4 and 5) and the plasmid DNA of the colonies in which the band size was correct was extracted. The cloning products were first digested with specific restriction enzymes (that digest differently according to the presence or absence of the insertion of the anoctamin) and then sequenced (StabVida).

2.1.10) Production of lentiviral particles

Lentiviral particles with pLVX-Tet-3G, pLVX-TRE3G-Ano6 3-HA GFP and pLVX-TRE3G-Ano9 3-HA GFP DNAs were produced in HEK (Human embryonic kidney) 293T cells (2.2.1 – Cell lines and culture conditions and Appendix 5 – Fig.52).

The cells were seeded at a density of 5 x 10^5 cells per well of a 6-well plate in DMEM (Dulbecco's Modified Eagle Medium with high glucose and L-glutamine, Lonza - BioWhittaker, BE12-604F) + 10% Foetal Bovine Serum (FBS, Gibco Life Technologies, 10270) and incubated for 24 h at 37ºC, 5% CO_2. Then, cells were transfected with 5 µg of DNA per well – 1.96 µg of pLVX (pLVX-Tet-3G, pLVX-TRE3G-Ano6 3-HA GFP or pLVX-TRE3G-Ano9 3-HA GFP), 1.96 µg of packaging plasmid pCMV-dR8.74psPAX2, 0.98 µg of pRev (plasmid containing Rev, a protein necessary for mRNA translation) and 98 ng of envelop plasmid VSV-G/pMD2.G. The protocol used for this transfection was the protocol of Jetpei (Polyplus – 2.2.3 – Transient transfections). The cells were incubated for 18 h at 37ºC, 5% CO_2.

The medium was then changed to DMEM + 10% FBS to remove the transfection reagent and the cells were incubated for 30 h at 37ºC, 5% CO_2.

The media containing the lentivirus (the three different lentivirus were produced by different cells) were harvested and the packaging cells were discarded. The viral particles harvested were immediately used to transduce cells or were stored at -80ºC for further use.

2.1.11) Lentiviral infection – Generation of stably transduced cells

Cells (CFBE 41o-, CFBE wt- and F508del-CFTR, CFBE mCherry wt- and F508del-CFTR and HeLa H_2B mCherry – 2.2.1 – Cell lines and culture conditions) were plated on p60 plates at a concentration of 8x10^5 cells per plate in 3 mL of EMEM (Eagle's Minimum Essential Media with L-Glutamine, Lonza - BioWhittaker, BE12-611F)/DMEM (according to the cell type) + 10% FBS and were incubated for 24 h at 37ºC, 5% CO_2.

The cells were co-infected with 1 mL of pLVX-Tet3G, 1 mL of pLVX-TRE3G-Ano6 3-HA GFP or pLVX-TRE3G-Ano9 3-HA GFP and 1 mL of EMEM + 10% FBS with Polybrene (Hexadimethrine bromide, Sigma-Aldrich, H9268-5G) infection enhancer (8 µg/mL final concentration). The plates were centrifuged at 10 g for 1 h at 25ºC and then incubated for 24 h at 37ºC, 5% CO_2.

The medium was changed to EMEM/DMEM + 10% FBS without antibiotics and the cells were incubated for 24 h at 37ºC, 5% CO_2.

The medium was then changed to EMEM/DMEM + 10% FBS containing half of the concentration needed of each antibiotic to kill all the non-infected cells (1 µg/mL of puromycin – selection of pLVX-TRE3G-Ano6/9 3-HA GFP – and 200 µg/mL of G418 – selection of pLVX-Tet3G). The antibiotic concentrations were determined through the results obtained from the antibiotic dose-dependent survival curves (Appendix 6, Fig. 55 and 56).

The cells were incubated for 48 h at 37ºC, 5% CO_2 and the medium was then changed to EMEM/DMEM + 10% FBS supplemented with 2 µg/mL of puromycin and 400 µg/mL of G418. Afterwards the medium was changed every 48 h and the cells were kept in culture at 37ºC, 5% CO_2.

To analyse the expression of the desired proteins in the stably transduced cells, 1 µg/mL of doxycycline (Sigma-Aldrich, D9891) was added. The protein expression was detected through its GFP fluorescence.

The correct insertion of the anoctamins' constructs on the different cell types was confirmed through sequencing of the extracted gDNA (2.1.5 – Genomic DNA extraction; 2.1.6 – DNA sequencing) from the cells.

2.1.12) Cell sorting

CFBE 41o- and CFBE mCherry wt and F508del-CFTR stably overexpressing Ano6 or Ano9 3-HA GFP were sorted using BD FACSAria™ II cell sorter in IMM (Instituto de Medicina Molecular, Lisboa).

The cells were induced with 1 µg/mL of doxycycline in order to be selected according to their GFP fluorescence intensity.

Using the FSC-A (forward scatter) and SSC (side scatter) parameters it was possible to look at the mixture of cells and distinguish them based off of size and internal complexity. With these two parameters only living cells were selected. The next step was to use FSC-A and FSC-H parameters to select single cells (singlets, i.e. cells that are not attached to other cells) among the living cells. After these two steps of gating, the GFP negative and the GFP positive cells with higher fluorescence intensity were selected and sorted.

The results of the sorting as well as the immunofluorescence results with sorted cells are displayed in Appendix 7 – Fig. 58-87.

2.2) Cell culture

2.2.1) Cell lines and culture conditions

Cystic Fibrosis Bronchial Epithelial cells (CFBE 41o- cells)[130], further referred to as CFBE, were cultured in EMEM supplemented with 10% FBS. These immortalized cells were developed from bronchial epithelial cells from an F508del-CFTR homozygous CF patient and allowed the development of other types of cells used on this work.

CFBE cells stably overexpressing wt-CFTR or F508del-CFTR (CFBE wt-CFTR or CFBE F508del-CFTR)[131] were grown in EMEM supplemented with 10% FBS and 2 µg/mL of puromycin (Sigma-Aldrich, P8833).

CFBE cells stably overexpressing wt-CFTR or F508del-CFTR with a mCherry tag in N-terminus and with a FLAG tag (octapeptide: DYKDDDDK) inserted in the fourth extracellular loop under Tet-On promoter induction (CFBE mCherry wt-CFTR or CFBE mCherry F508del-CFTR) were created in our laboratory[132]. These cells were cultured in DMEM supplemented with 10% FBS, 2 µg/mL of puromycin and 100 µg/mL of blasticidin (InvivoGEN, ant-bl-1). A schematic representation of this construct is shown in Appendix 8 – Fig.88.

Human Embryonic Kidney 293T cells (HEK 293T)[133, 134] were cultured in DMEM supplemented with 10% FBS.

Human cervical carcinoma cells (HeLa Kyoto)[135, 136] stably expressing H_2B histone attached to mCherry (HeLa H_2B mCherry) were a kind gift from Dr. Gerlich's Group (IMBA – Institute of Molecular Biotechnology, Vienna, Austria). The cells were grown in DMEM supplemented with 10% FBS, and 0.5 µg/mL of puromycin.

CFBE, CFBE wt/F508del CFTR, CFBE mCherry wt/F508del CFTR or HeLa H_2B mCherry cells stably overexpressing Ano6 or Ano9 3-HA GFP under Tet-On promoter induction were produced as described in 2.1.11 – Lentiviral infection – Generation of stably transduced cells. The selection of infected cells was made using 400 µg/mL of G418 (Geneticin, Sigma-Aldrich, A1720) and 2 µg/mL of puromycin. Among these cells, only CFBE did not have resistance for puromycin, so the other cells were only selected by G418. Whenever the presence of a more homogeneous cell population was required, the cells were sorted as previously described in 2.1.12 - Cell sorting.

All cell lines were maintained at 37ºC in a humidified atmosphere of 5% (v/v) CO_2. All cells were tested for mycoplasma infection, being mycoplasma free.

2.2.2) Polarized cells

For polarization-dependent assays, specifically immunofluorescence assays in polarized cells and micro-Ussing chamber, cells were seeded onto collagen IV (Sigma-Aldrich, C7521) coated Costar 12mm Snapwell filter inserts with 0.4 µm Pore Polyester Membrane and 1.12 cm^2 surface area (Corning, 3801). Cells were seeded on the apical side of the filter at a density of 3 x 10^5 cells per filter, using normal cell media without antibiotics. The filters were maintained in liquid-liquid interface. After 2 days of incubation, the amount of FBS in the media was changed from 10% to 5%, and cells took 2-7 days to polarize.

The transepithelial electrical resistance (TEER) was routinely measured using a volt-ohmmeter (Millicell-ERS, Millipore, MERS00001). Experiments were performed when a confluent monolayer was formed, as judged by a TEER above 600 Ω/cm^2. When this was achieved, cells were induced with 1 µg/mL doxycycline in both basal and apical side.

2.2.3) Transient transfections

CFBE cells or HEK 293T cells were transfected using cationic liposomes or polymers.

Lipofection is based on the ability of cationic lipids to form unilamelar liposomes that adsorb nucleic acid molecules to their surface and are internalized by the cells. The transfection result is protein expression (plasmids) or down-regulation of the target genes (siRNAs). In this work, three liposomal formulations were used, Lipofectamine 2000 (Invitrogen, 11668019), Fugene HD (Promega, E2311) and JetPei® (Polyplus, 101-40N).

A polymer was also used for transfections (Xfect Transfection Reagent, Clontech, 631317), which is a biodegradable transfection polymer with low cytotoxicity and high transfection efficiency. It can be used to transfect a broad range of cell types in a serum-compatible protocol.

For transfection with plasmids which encode for GFP fusion proteins, transfection efficiency could be estimated by direct counting of fluorescent vs. non fluorescent cells under a

fluorescence microscope – Leica DMI 6000B. For transfection with siRNAs, the efficiency was estimated by the decrease of fluorescence of the target gene (namely Ano6).

Transfection with Lipofectamine 2000

Lipofectamine and DNA/siRNA were incubated separately for 5 min in Opti-MEM Reduced Serum Medium (Gibco, 31985) and then the diluted DNA/siRNA was added to diluted Lipofectamine (1:2 ratio). DNA/siRNA-lipid complex was incubated for 20-30 min at room temperature and then added to 70-80% confluent cells (seeded the day before). Medium was changed after 6 h and 24 h. When using plasmid DNA, the experiments were performed 48 h post-transfection, and when using siRNA transfections, doxycycline was added 24 h post-transfection, and the experiments were performed after 48 h of induction.

Also with Lipofectamine, a solid phase reverse transfection protocol was used for siRNA screens. Plates were coated by Hugo Botelho with customized siRNAs (SilencerH Select, Ambion)[137] in a sucrose and Lipofectamine solution.

The cells were seeded on top of the coating, allowing them to take up the different siRNAs from the solid phase. Doxycycline was added after 24 h of siRNA transfection, and the experiments were performed 48 h post-induction.

Transfection with Fugene HD

Fugene and DNA were separately incubated for 5 min in Opti-MEM, in a Fugene:DNA ratio of 3:1. The solutions were mixed together and allowed to incubate for 15 min at room temperature. The mix was then added dropwise to either 70-80% confluent cells (seeded the day before) or to freshly trypsinized cells. Medium was changed after 24 h and the experiments were performed 48 h post-transfection.

Transfection with JetPei

JetPei and DNA were separately diluted in NaCl 150 mM. The Jetpei-NaCl solution was added to the DNA-NaCl mix, and this final mixture was incubated for 15 to 30 min at room temperature. The mix was then added dropwise to attached cells (seeded the day before) with Opti-MEM medium only. Medium was changed after 6 h and 24 h, and the experiments were performed 48 h post-transfection.

Transfection with Xfect Transfection Reagent

This transfection protocol was used for transient transfection of HEK 293T cells with the lentiviral vectors, in order to test if the Tet-On inducible system was functional.

DNA (pLVX-TRE3G-Ano6/9 3-HA GFP and pLVX-Tet3G) was diluted in Xfect Reaction Buffer and the solution was mixed by vortexing for 5 s. Xfect Polymer was added to the diluted plasmid DNA (ratio DNA:Xfect Polymer 3:1) and the solutions were mixed by vortexing. The DNA-Polymer solution was incubated for 10 min at room temperature to allow nanoparticle

complexes to form. This nanoparticle complex solution was added dropwise to the attached cells, and the cells were incubated for 4 h at 37ºC. The nanoparticle complexes were removed, replacing the medium for fresh complete medium containing doxycycline to induce the expression of the desired anoctamins, and the cells were incubated again at 37ºC until time of analysis (24 h).

2.3) Generation of Knockout cells – CRISPR/Cas9 system

Bacteria and archaeal clustered regularly interspaced short palindromic repeats (CRISPR) systems rely on CRISPR RNAs (crRNAs) in complex with CRISPR-associated (Cas) proteins to direct degradation of complementary sequences present in invading viral and plasmid DNA. An *in vitro* reconstitution of the *Streptococcus pyogenes* type II CRISPR system demonstrated that crRNA fused to a normally trans-encoded tracrRNA is sufficient to direct Cas9 protein to cleave specific target DNA sequences matching the crRNA. This system is now explored in eukaryotic organisms, making genome engineering an easier approach[138].

In eukaryotic cells, Cas9 can be directed to cleave a sequence of interest using crRNA-tracrRNA fusion transcripts, or “guide RNAs” (gRNAs). These gRNAs induce precise cleavage at endogenous genomic loci in human cells, in a process requiring for the PAM (protospacer-adjacent motif) sequence (a DNA sequence immediately following the DNA sequence targeted by Cas9)[139] (see Fig.6).

Cas9 generates double breaks in the DNA, which are repaired through cellular mechanisms: Nonhomologous end joining (NHEJ) and High fidelity homology-directed repair (HDR). NHEJ is a fast repair mechanism that ligates the two broken DNA ends possibly resulting in point mutations and deletions, frequently disrupting open reading frames and leading to gene knockouts (see Fig.6). HDR is used for the introduction of specific nucleotide changes in the target gene, using a homologous template[140].

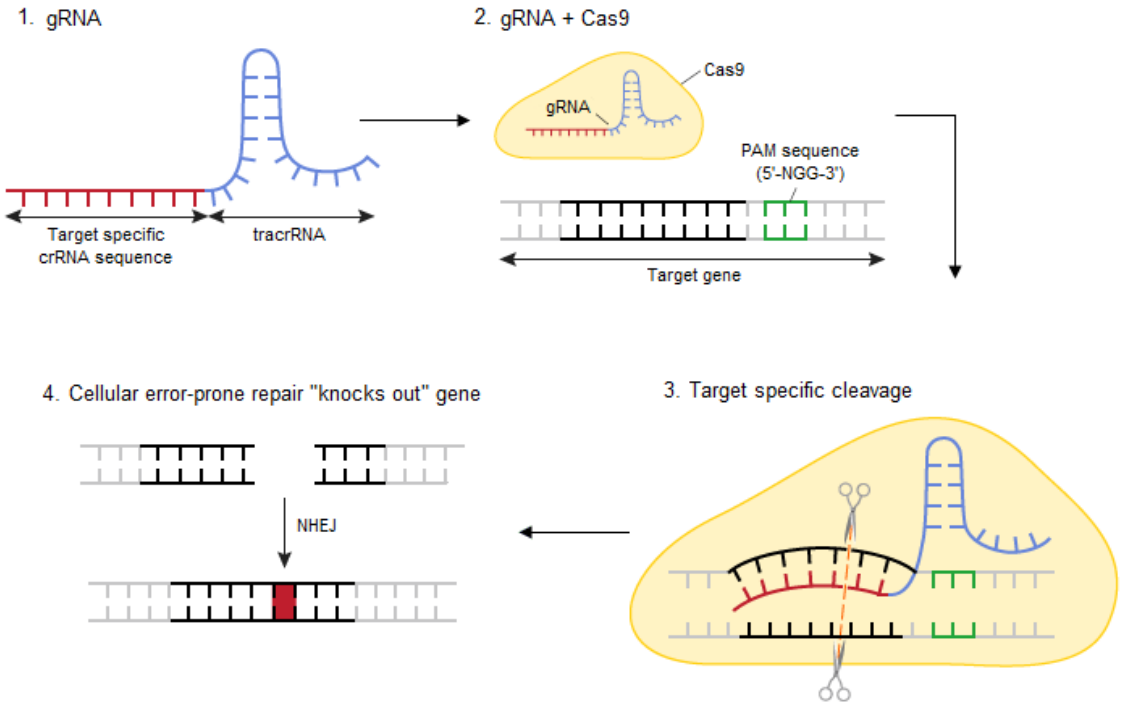

Figure 6 - **CRISPR/Cas9 system for targeted genome editing. Representation of gRNA guiding Cas9 to the target gene, followed by target specific cleavage by Cas9. DNA is then repaired by NHEJ (Nonhomologous end joining), which is a fast repair mechanism that ligates the two broken DNA ends possibly resulting in point mutations and deletions, frequently disrupting open reading frames and leading to gene knockouts. Adapted from [141].**

This system was used in CFBE, CFBE wt- and F508del-CFTR cells to achieve the knockout of Ano6. To accomplish this, cells were seeded in a T_{25} flask (Thermo Scientific, 130189) at a concentration of 8 x 10^5 cells per flask and were incubated for 24 h at 37ºC, 5% CO_2. The cells were then transfected with 5 µg of DNA – 1.5 µg of each gRNA (two different gRNAs were simultaneously used to improve knockout efficiency), 1.5 µg of Cas9 plasmid with a GFP tag and 500 ng of a plasmid containing the gene that confers resistance to hygromycin – using the Jetpei protocol (2.2.3 – Transient transfections, and Appendix 9). After 24 h the medium was changed to EMEM + 10% FBS without antibiotics, and the cells were incubated for 48 h at 37ºC, 5% CO_2. The cells were then trypsinized to a p100 plate (Thermo Scientific, 130182) using EMEM + 10% FBS with 100 µg/mL hygromycin (Sigma-Aldrich, H772). The cells were again incubated for 48 h at 37ºC, 5% CO_2 and then the medium was changed to EMEM + 10% FBS with 200 µg/mL hygromycin. The most suitable concentration of hygromycin was determined through the results obtained from the antibiotic dose-dependent survival curves (Appendix 6 – Fig.57). Afterwards the medium was changed every 48 h and the cells were kept in culture at 37ºC, 5% CO_2. After approximately 10 days, clones were picked to a 24-well plate (Thermo Scientific, 930186) using cloning discs with trypsin (Sigma-Aldrich, Z374431).

Due to the slow growth of the clones, the knockout of Ano6 has not yet been confirmed. However, the transfection could be followed by the green fluorescence of the transfected cells conferred by Cas9-GFP plasmid (Fig. 7, 8 and 9), and through the survival of the cells when incubated with hygromycin. Whenever possible, the knockout will be ascertained using Western Blot and through sequencing (Stabvida).

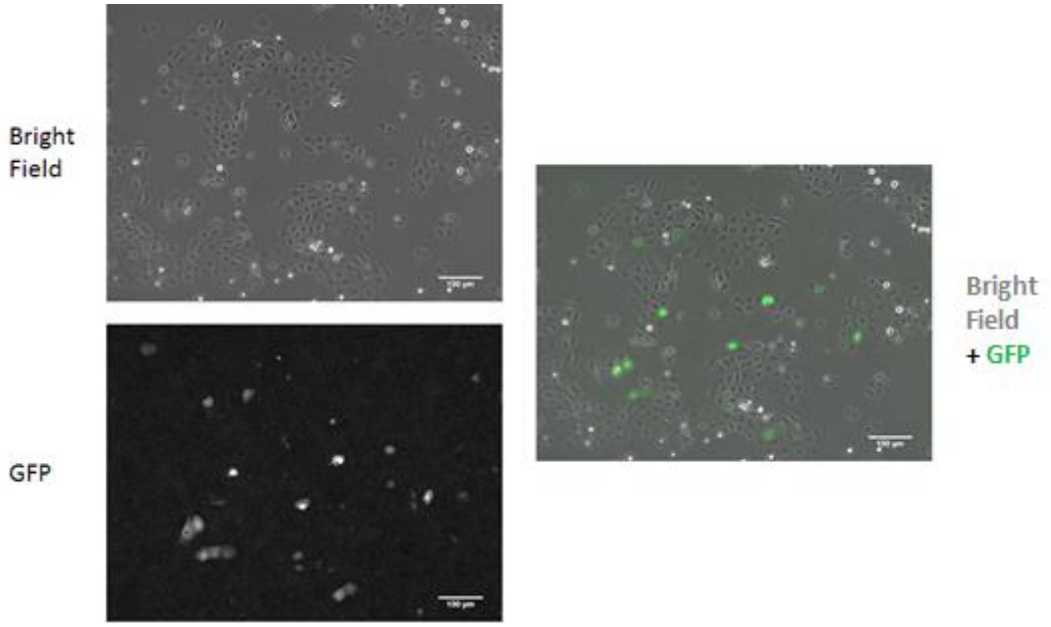

Figure 7 – **CFBE parental cells transfected with the plasmids necessary for Ano6 knockout. With the GFP fluorescence (bottom left image) it is possible to detect the cells transfected with the Cas9-GFP plasmid, which means that the Ano6 knockout is possible in these cells. Images were acquired with the 10x objective. Scale bar represents 100 µm.**

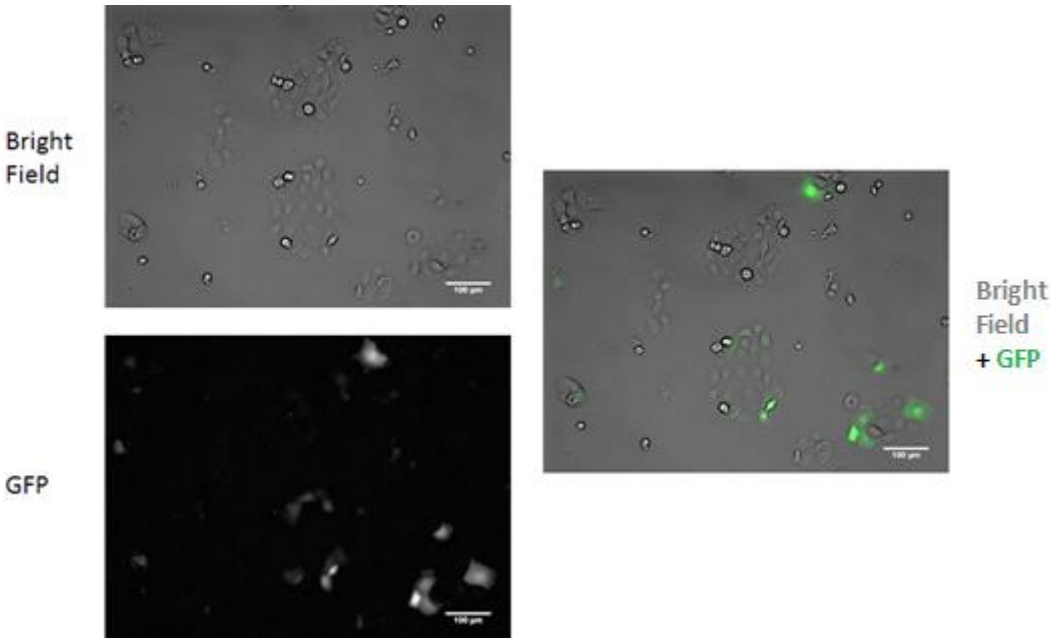

Figure 8 - **CFBE wt-CFTR cells transfected with the plasmids necessary for Ano6 knockout. With the GFP fluorescence (bottom left image) it is possible to detect the cells transfected with the Cas9-GFP plasmid, which means that the Ano6 knockout is possible in these cells. Images were acquired with the 10x objective. Scale bar represents 100 µm.**

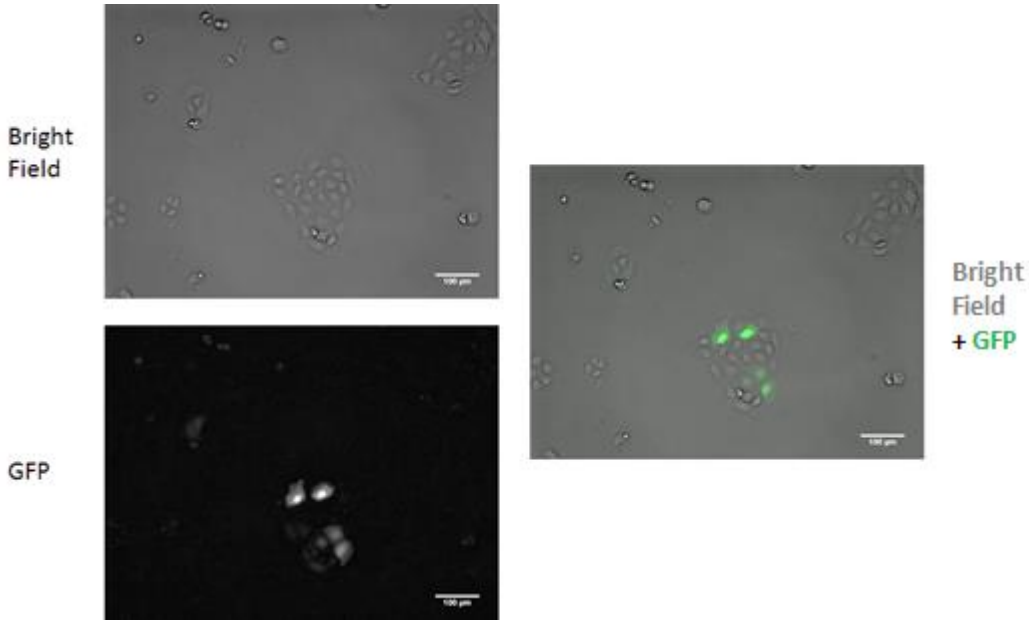

Figure 9 - **CFBE F508del-CFTR cells transfected with the plasmids necessary for Ano6 knockout. With the GFP fluorescence (bottom left image) it is possible to detect the cells transfected with the Cas9-GFP plasmid, which means that the Ano6 knockout is possible in these cells. Images were acquired with the 10x objective. Scale bar represents 100 µm.**

2.3.1) gRNA design and synthesis

As already stated, the purpose of using the CRISPR/Cas9 system was to create cells that do not express Ano6 (Ano6 knockout). To achieve this goal, it was necessary to design proper gRNAs and to select the genomic sequence of this gene that is specifically recognized by them.

The selected target sequence for Ano6 is a 23 bp genomic site with the form 5'-N_{20}NGG-3'. Target specificity of Cas9 protein relies on the presence of specific nucleotides 3' to the protospacer sequence (the previously referred protospacer adjacent motif (PAM)). However this PAM motif is only present in the genomic region and it is not included in the gRNAs.

Ano6 DNA sequence from the NCBI database[142] was analysed, selecting two different 23 bp genomic sequences matching the criteria[143]. This selection was made with the help of a co-worker, Ines Pankonien. The final sequences were blasted using NCBI's nucleotide BLAST tool, in order to select only sequences that were specific for the *ANO6* gene.

The gRNA sequences are displayed in Appendix 9.

2.4) Protein Analysis

2.4.1) Immunofluorescence of anoctamins

Non-polarized cells

Cells were grown in cover slips in 24-well plates or in 8-wells labteks (Sigma-Aldrich, C7182). Two types of protocols were used: one in which the plasma membranes were

permeabilized (using 0.5% Triton X-100 (v/v) (Amersham Biosciences, 17-1315-01) diluted in phosphate buffered saline (PBS)) and the other without membrane permeabilization.

In the first protocol, cells were washed 3 times with PBS (137 mM NaCl (Calbiochem, 7760); 2.7 mM KCl (Sigma-Aldrich, P9541); 10 mM Na_2HPO_4 (Sigma-Aldrich, S9763); 1.8 mM KH_2PO_4 (Fluka, 60229); pH 7.4) supplemented with 0.7 mM of $CaCl_2$ (Sigma-Aldrich, 223506) and 1.1 mM of $MgCl_2$ (Merck Millipore, 105833) (termed PBS++ from now on) and fixed for 10 min with 4% (v/v) paraformaldehyde (PFA) (Merck Millipore, 14003). Next, the cells were washed 3 times with PBS, permeabilized for 5 min with 0.5% Triton X-100 (v/v) and washed again 3 times with PBS. The cells were then incubated at room temperature with a specific primary antibody diluted in PBS with bovine serum albumin (BSA) (Sigma-Aldrich, A9647) 1% (w/v) for 1 h (the negative controls were incubated with PBS with BSA 1% (w/v) instead of the primary antibody). The cells were washed 3 times with PBS and incubated at room temperature in the dark with the secondary antibody diluted in PBS with BSA 1% (w/v) for 1 h. The cells were then washed 3 times with PBS and incubated 10 min in the dark with Hoechst 33342 Fluorescent Stain (Life Technologies, H3570). The cover slips were mounted in glass slides with Vectashield mounting medium (Vector Laboratories, H-1000) and sealed.

In the protocol without membrane permeabilization, the cells were first washed 3 times with PBS++ and kept on ice in an ice cold chamber for 15 min. Then they were incubated with the primary antibody for 2 h in the cold chamber. Next, the cells were washed 3 times with PBS++ and fixed with 4% (v/v) paraformaldehyde for 10 min, outside the cold chamber. The remaining protocol is equal to the final steps of the permeabilization protocol (from the washings before the incubation with the secondary antibody to the mounting in glass slides).

Immunofluorescence staining was observed in the Leica DMI 6000B fluorescence microscope, which was also used to acquire the images.

The antibodies used for immunofluorescence are displayed in Appendix 10 – Table 11.

Polarized cells

CFBE cells were polarized as described in section 2.2.2 – Polarized cells.

Filters were washed 3 times for 5 min with PBS++ at room temperature on both apical and basolateral sides. All treatments were applied to both sides of the filters. The cells were fixed with PFA 4% (v/v) for 30 min, and then washed again 3 times for 5 min with PBS++. Next, the cells were permeabilized using triton X-100 0.5% (v/v) for 15 min. After a blocking step of 20 min with BSA 1% (w/v), the filters were removed from their supports using a scalpel. Each filter was placed in one well of a 12 or 24-well plate (Thermo Scientific, 130185 – 12-well plate) and were incubated overnight at 4ºC with the primary antibodies in 1% (w/v) BSA. Afterwards the filters were subjected to a more stringent washing step using PBS with 0.05% of triton X-100. After, the filters were incubated with a mix of the secondary antibody and nuclear dye ToPro3 Iodide (Life Technologies, T3605) (1:750) for 1 h at room temperature. Finally, the filters were mounted on slides with Vectashield anti-fading mounting medium and sealed.

The antibodies used are displayed in Appendix 10 – Table 11.

Live-cell imaging

HeLa H_2B mCherry cells were seeded in a p60 plate in a concentration of 1.5 x 10^5 cells/mL, using DMEM without phenol red (Lonza, BE12-917F) supplemented with 25 mM HEPES (Gibco, 15630) and 2 mM L-glutamine (Gibco, A2916801). Images were acquired every 20 min in Leica DMI 6000B fluorescence microscope during 20 h in bright field and with the mCherry filter. The cell division was observed through the mCherry staining of the nuclei (H_2B histone) and the acquired images were used to make a film (gif/avi) – Fig.10.

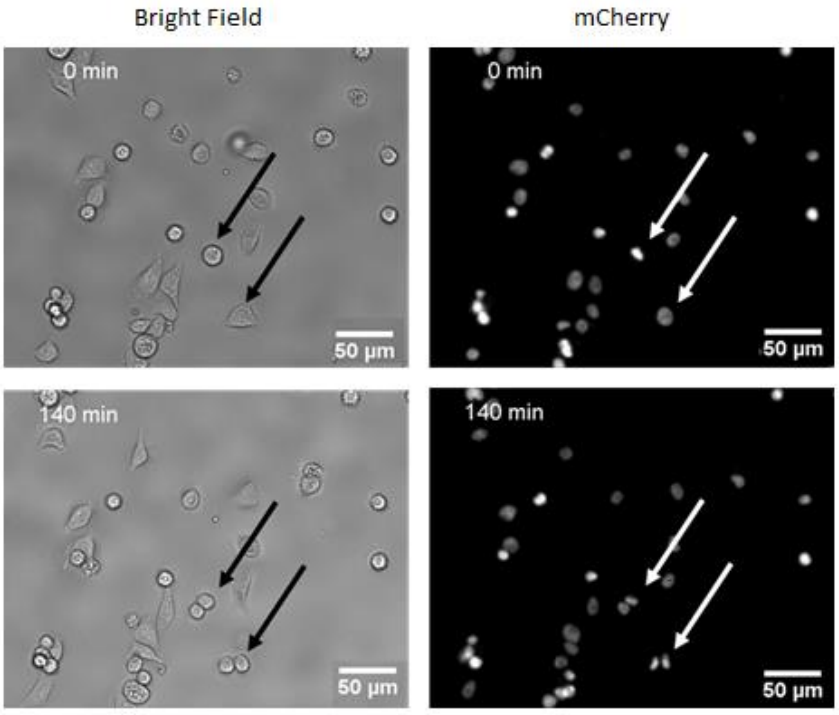

Figure 10 – **Live-cell imaging of HeLa H_2B mCherry cells. Images were acquired at the beginning of the experiment (0 min) and at 140 min, with the 10x objective. Cell division can be detected through bright field and mCherry nuclear staining, as indicated by arrows. Scale bar represents 50 µm.**

HeLa H_2B mCherry cells were also stably transfected with Ano6 3-HA GFP or Ano9 3-HA GFP, but it was not yet possible to sort the cells (selecting only the GFP positive cells). However, when the cells are sorted, live-cell imaging will also be performed with these cells, in order to study the cellular localization of overexpressed Ano6 and Ano9. The cell division will be observed through the mCherry staining of the nuclei, and the localization of these anoctamins will be assessed using the GFP channel.

2.4.2) Image acquisition, processing and analysis

For non-polarized cells, images were acquired using the Leica DMI6000B microscope. According to the experiments, all channels available in the microscope were used: DAPI/Hoechst, GFP, Alexa Fluor 568/mCherry and Alexa Fluor 647/Cy5.

With non-polarized cells used in siRNA screens (anoctamins traffic assay), automatic imaging was possible using the Leica DMI6000B microscope.

Automatic image analysis was performed with open source software tools (CellProfiler and R) using specific pipelines appropriate for traffic assays.

For polarized cells, images were acquired using a Leica TCS SPE confocal microscope with a 63x oil objective. In this case, fluorescence was accessed in three different channels – GFP, Alexa Fluor 568 and ToPro3. Image edition was performed using Visage Imaging Amira 5.3.3 for section's 3D reconstruction, made available by Professor Sólveig Thorsteindóttir at DevEM/CE3C.

2.4.3) Western Blot

Cell lysis and protein collection

Cells were grown on 6-well plates or p35 plates. To extract the protein, cells were washed twice with cold PBS and lysed with sample buffer (1.5% (w/v) SDS; 5% (v/v) glycerol; 0.01% (w/v) bromophenol blue; 0.05 mM dithiotreitol; 0.095 M Tris, pH 6.8). DNA was sheared using benzonase 25U/mL (Sigma-Aldrich) in the presence of $MgCl_2$ 2.5 mM. The cells with sample buffer were centrifuged at 13000 rpm for 5 min at 4ºC and the supernatant was collect.

Protein quantification

Total protein concentration in different samples was assessed by a Bradford assay[144]. A regression line was made using increasing concentrations of BSA.

The protein solutions were incubated 5 min with BioRad Protein Assay Reagent (Bio-Rad, 500-0006EDU) and the absorbance was measured at 595 nm using the spectrophotometer (Jasco V-560 UV/Vis Spectrophotometer).

SDS-PAGE

Protein extracts were separated by SDS-Polyacrylamide gel electrophoresis (PAGE) on 7 or 10% (w/v) separating and 4% stacking gels at 100-150V followed by transfer onto PVDF (Polyvinylidene Fluoride) membranes (Millipore) at 400 mA for 1 h 30 min.

After blocking with 5% (w/v) non-fat milk in phosphate buffered saline (PBS, NaCl 137 mM; KCl 2.7 mM; KH_2PO_4 1.5 mM; Na_2HPO_4 6,5 mM, pH 7.4) containing 0.1% (v/v) Tween (PBS-T) for 1 h, the membranes were probed overnight at 4ºC with primary antibodies diluted in 5% (w/v) milk in PBS-T.

The cells were then washed three times during 10 min with PBS-T, followed by incubation for 1 h at RT with horseradish peroxidase-conjugated secondary antibodies in 5% (w/v) milk-PBS-T. Chemiluminescent detection was performed using Chemidoc XRS+ analyser (BioRad) and the signal was developed with the Clarity Western ECL Substrate (Bio-Rad, 170-5061). Finally, the quantification was performed with the ImageLab software (Bio-Rad).

The antibodies used for Western Blot are displayed in Appendix 10 – Table 12.

2.4.4) Biotinylation

Cells were grown in p60 plates until confluence was reached and incubated at 4ºC with NHS LC Biotin buffer (1 mg biotin (EZ-Link Hydrazide-LC-Biotin, Thermo Scientific, 21339)/1 mL PBS with 1 mM $MgCl_2$, 0.1 mM $CaCl_2$, pH 8.2) for 1 h protected from the light. Cells were lysed

with 1 mL of BL buffer (25 mM HEPES, 1% (v/v) Triton X-100, 10% (v/v) glycerol, pH 8.2), supplemented with a 1x Complete protease inhibitor cocktail (PIC, Roche, 11697498001) and collected with a cell scraper. Cell membranes and debris were pelleted by centrifugation at 14,000 rcf for 10 min at 4ºC. 100 µL of the supernatants were collected (whole cell lysate). The remaining samples were incubated overnight at 4ºC with streptavidin beads (Thermo Scientific, 20353). The beads were pelleted, washed 2x with PBS and 1x with BL buffer and the samples were then analysed by Western Blot.

2.5) Functional Analysis

2.5.1) Iodide efflux

Iodide efflux assays were performed to determine the viability of the double-tagged anoctamins. Two different protocols were use: one for cells transiently transfected with the double-tagged anoctamins, and the other for the stably transfected cells.

Protocol for transiently transfected cells

First, HEK 293T cells were seeded in 6-well plates and transfected according to the Fugene protocol (2.2.3 – Transient transfections). Cells transfected with empty pLVX-TRE3G vector were used as control, and all transfections were perform in duplicate: one to stimulate with 100 µM ATP and the other to readout as unstimulated sample.

Loading buffer (136 mM NaI, 3 mM KNO_3, 2 mM $Ca(NO_3)_2$, 0.5 mM $MgSO_4$, 10 mM glucose, 20 mM HEPES, pH 7.5) and efflux buffer (136 mM $NaNO_3$, 3 mM KNO_3, 2 mM $Ca(NO_3)_2$, 0.5 mM $MgSO_4$, 10 mM glucose, 20 mM HEPES, pH 7.5) were pre warmed to 37ºC.

The cells were first washed twice with 2 mL of loading buffer and then incubated with 2 mL of loading buffer for 30 min at 37ºC. Following this incubation period, the cells were washed four times with 2 mL of efflux buffer. The cells were then equilibrated in 2 mL of efflux buffer for 10 min at 37ºC. After the equilibration period, 2 mL of efflux buffer was added to the unstimulated set of cells and 2 mL of efflux buffer with 100 µM ATP was added to the stimulated set. Both sets were incubated for 5 min at 37ºC. The cells were washed with 3 mL of efflux buffer and then were lysed with 1 mL of efflux buffer with 0.5% Triton X-100 for 5 min. The lysate was collected to a 1.5 mL tube and centrifuged at 13,000 rpm for 5 min.

All the samples were read with the iodide electrode to calculate the amount of iodide remaining in the cells. In order to compare the remaining iodide in the stimulated and unstimulated cells, 15 µL of the lysate was used for protein quantification (2.4.3 – Western Blot – Protein quantification).

Protocol for stably transfected cells

Cells were incubated for 1 h in loading buffer (13 mM NaI, 3 mM KNO_3, 2 mM $Ca(NO_3)_2$, 20 mM HEPES, and 11 mM D-glucose, pH 7.4) and then washed 10 times with efflux buffer (136 mM $NaNO_3$ replacing NaI in the loading buffer). Anoctamin-mediated iodide efflux was

measured at room temperature using an iodide selective electrode (Thermo Electron Corp, MP225). The measurements were made at 1 min intervals, being the cells stimulated with 100 µM ATP only from min 1 to 4.

2.5.2) Micro-Ussing chamber

For micro-Ussing chamber experiments, inducible CFBE cells overexpressing Ano6 or Ano9 3-HA GFP were seeded at approximately 3 x 10^5 cells/mL onto collagen IV-coated Costar 12 mm Snapwell Insert with 0.4 µm Pore Polyester Membrane and 1.12 cm^2 area, as referred in 2.2.2 – Polarized cells. Transepithelial electrical resistance (TEER) was routinely measured using a volt-ohmmeter.

Monolayers were mounted in modified perfused micro-Ussing chambers and analysed under open-circuit conditions. Anoctamins' activity was measured when a confluent monolayer was formed, as judged by a TEER above 600 Ω/cm^2. Anoctamins were activated with ATP (100 µM) and anoctamin inhibition was achieved with $CaCC_{inh}$-A01 (30 µM).

Briefly, the apical and basolateral surfaces of CFBE cells were continuously perfused with Ringer solution (145 mM NaCl, 0.4 mM KH_2PO_4, 1.6 mM K_2HPO_4, 5 mM D-glucose, 1 mM $MgCl_2$, and 1.3 mM Ca-gluconate), at a rate of 3-5 mL/min. pH was adjusted to 7.4 and the experiments were carried out at 37ºC under open circuit conditions.

Following a 15-20 min stabilization period, two additions of ATP 100 µM (anoctamins' activator) and one of the CaCC inhibitor $CaCC_{inh}$-A01 were performed sequentially (apical side). Next, $CaCC_{inh}$-A01 and ATP were simultaneously added. After a 30 min washout period, ATP was again added to the apical side, followed by an addition of ATP to the basolateral side of the filter.

Transepithelial resistance (R_{te}) was determined by applying short (1 s) current pulses (I = 0.5 µA) and the corresponding changes in transepithelial voltage (V_{te}) were recorded continuously. The equivalent short-circuit currents ($I_{eq\text{-}SC}$) were calculated by Ohm's law from V_{te} and R_{te} ($I_{eq\text{-}SC} = V_{te}/R_{te}$), with appropriate correction for fluid resistance.

2.6) Microscopy assay for siRNA screens

2.6.1) siRNAs

The siRNAs used in this experiment were part of a library of siRNAs shown to have an effect (positive or negative) on CFTR traffic to the plasma membrane ("hits" from the CFTR screen) in a primary screen performed in A549 cells (human alveolar epithelial cells) performed by Shehrazade Daihimène – [145] and unpublished data. "Scrambled" non-targeting siRNA was used as a negative control.

2.6.2) siRNA pilot screen

To first try the reverse transfection in the stably transfected cells and to assess the suitability of the screening platform to the identification of genes that affect Ano6 traffic, a pilot screen was performed using a labtek coated with 384 spots of different siRNAs pre-mixed with

lipofectamine. CFBE Ano6 3-HA GFP cells were grown to confluence and then split to 50% confluence. After 24 h, cells were trypsinized to an antibiotic-free medium and seeded on the siRNA-spotted labtek (10^5 cells in 2 mL).

Ano6 expression was induced 24 h after seeding with antibiotic-free medium supplemented with 1 µg/mL doxycycline. Immunofluorescence experiments were performed 48 h after induction (72 h post-siRNA transfection). Automatic imaging was made using the Leica DMI6000B microscope.

Automatic image analysis was performed with open source software tools (CellProfiler and R) using specific pipelines appropriate for traffic assays. The first algorithm used calculated the illumination correction functions for background subtraction (for each channel). The second pipeline comprises background subtraction, cell segmentation, fluorescence integration and basic quality control. These quality control steps exclude cells which do not significantly express Ano6 3-HA GFP, have atypical morphology or contain saturated pixels. Next, an algorithm for quantification of GFP (Ano6) or Cy5 (3-HA) signal was used. In this pipeline the nuclei were identified as primary objects. Cells containing too large or too small nuclei, cells with nuclei with wrong eccentricity and localized too close to the image border were removed from the data analysis. Secondary objects were identified expanding from the nuclei on the images acquired in the GFP or Cy5 channels.

The fluorescence quantification data allowed the determination of the anoctamins traffic in each cell according to the following formula:

$$Anoctamin\ Traffic\ Efficiency = \frac{PM\ ANO}{Total\ ANO} = \frac{Cy5\ Integrated\ Fluorescence}{GFP\ Integrated\ Fluorescence}$$

For each image, the anoctamin traffic efficiency was considered the median for all the cells in the image. After, a custom R script[146] was used to exclude out of focus images and images with high background fluorescence.

After averaging the anoctamin traffic efficiency for all images from the same siRNA treatment, the effect of different siRNAs on the anoctamins traffic was compared with the results obtained with the "scrambled" siRNA treatments, using the following formula:

$$Deviation\ score = \frac{Traffic\ effienciency - Traffic\ efficiency_{Scrambled}}{2 \times SEM_{Scrambled}}$$

$SEM_{Scrambled}$ is the standard error of the mean for the "Traffic Efficiency" with the treatment with scrambled siRNA. Significant effects on the traffic efficiency were considered when the magnitude was larger than twice the scrambled siRNA SEM. Therefore, genes in which the deviation score was above +1, were considered traffic enhancers. Accordingly, genes having a deviation score below -1 were considered traffic inhibitors.

2.7) Statistical Analysis

Student's t-test for paired or unpaired samples was used as appropriate. $P<0.05$ was accepted as significant.

3. Results and discussion

3.1) Generation of stable cell lines overexpressing the double-tagged anoctamin constructs

3.1.1) Characterization of the cell lines

To achieve the main goal of this project, i.e., to identify regulators of anoctamins' traffic and study their interaction with CFTR and other anoctamin family members, it was necessary to develop a cellular model capable of detecting and discriminating between the total cellular protein and the membrane fraction of the protein.

Regarding this objective, double-tagged constructs of anoctamin 6, 9 and 10 (Ano6, Ano9 and Ano10) were generated. These constructs contain a GFP tagged to the C-terminus, as well as a 3-HA (triple hemagglutinin) tag in a putative transmembrane loop of each anoctamin so as to be outside the cell whenever the protein is at the plasma membrane (mutagenesis was performed as described in Materials and methods – 2.1.7 – Mutagenesis). For Ano6 and Ano9 it was possible to clone the respective constructs into a lentiviral vector (pLVX-TRE3G), allowing the transduction of CFBE cells and thereby generating stably transfected cell lines under an inducible (Tet-On) promoter induction.

Since CFBE cells derive from the bronchial epithelium of a CF patient, these cells represent a good model of the processes occurring in CF. Moreover, the initial experiments were performed with CFBE 41o- (parental) cells, which do not overexpress other proteins (like CFBE wt- or F508del-CFTR), having a higher resemblance to *in vivo* cellular conditions. Additionally, the microscope used for automated inverted fluorescence (Leica DMI 6000B) shows a leakage between the GFP and the mCherry channel (GFP – Emission >515 nm; mCherry – Emission >590 nm), as the excitation wavelength of GFP is not narrow enough to prevent simultaneous mCherry excitation. Consequently, mCherry emission is detected in the GFP channel. Given this observation, the quantifications of total and membrane proteins are more accurate using these cells which do not have another fluorescent protein present.

Representative fluorescence images of stably transfected CFBE cells overexpressing Ano6 or Ano9 3-HA GFP (before and after sorting) are represented in Fig. 11 and 13, respectively. Signal-to-noise ratios of GFP fluorescence of both cells types, and Cy5 (3-HA tag) signal of Ano6 (also before and after sorting) are represented in Fig. 12 and 14. This measurement compares the level of a desired signal (in this case, GFP or Cy5 fluorescence intensity) to the level of background fluorescence. Thus, when it is higher, the desired signal is more easily distinguishable from the background noise. The signal-to-noise ratio is calculated using the following formula:

$$\text{Signal-to-noise ratio} = \frac{Cell\ fluorescence\ Intensity - Background\ fluorescence\ Intensity}{Background\ fluorescence\ Intensity}$$

CFBE Ano6 3-HA GFP cells show a considerable membrane expression of Ano6, as observed with the anti-HA antibody (Cy5 secondary antibody – Fig.11). However, a large amount of the protein also appears to be intracellular, more precisely around the nucleus, suggesting a localization in the endoplasmic reticulum (ER) – Fig.11, GFP panel. Ano6 has been identified as a major component of the ORCC[49] and as a scramblase[92], being consequently localized at the plasma membrane, which is in agreement with these obtained results. On the contrary, some

studies described Ano6 only as an intracellular and possibly ER protein[147] which is also partially observed in the present results. Yet, Ano6 used in the reported experiments was cloned from mouse tissues and tagged with GFP, while the one used in the present work is human. Moreover, the first mutagenesis we performed for the insertion of the 3-HA tag in the Ano6 construct (Material and methods – 2.1.7 – Mutagenesis and Appendix 4 – Fig.42) revealed the same results, with a total cytoplasmic localization of Ano6. These discrepancies can thus be due to a structural modification of the protein caused by the insertion of tags, which disrupt the normal protein traffic to the plasma membrane.

Due to the heterologous Ano6 expression detected in the initial and unsorted population (Fig.11 – Left panel (before sorting)), these cells were sorted by flow cytometry in order to select only the cells with the highest GFP signal intensity (Fig.11 – Right panel (after sorting)). After sorting, both GFP and Cy5 signal-to-noise ratios significantly increased (Fig.12). Therefore, this sorted cell line appears to be a *bona fide* model to perform siRNA screens, since the membrane fraction and the total protein can be correctly distinguished.

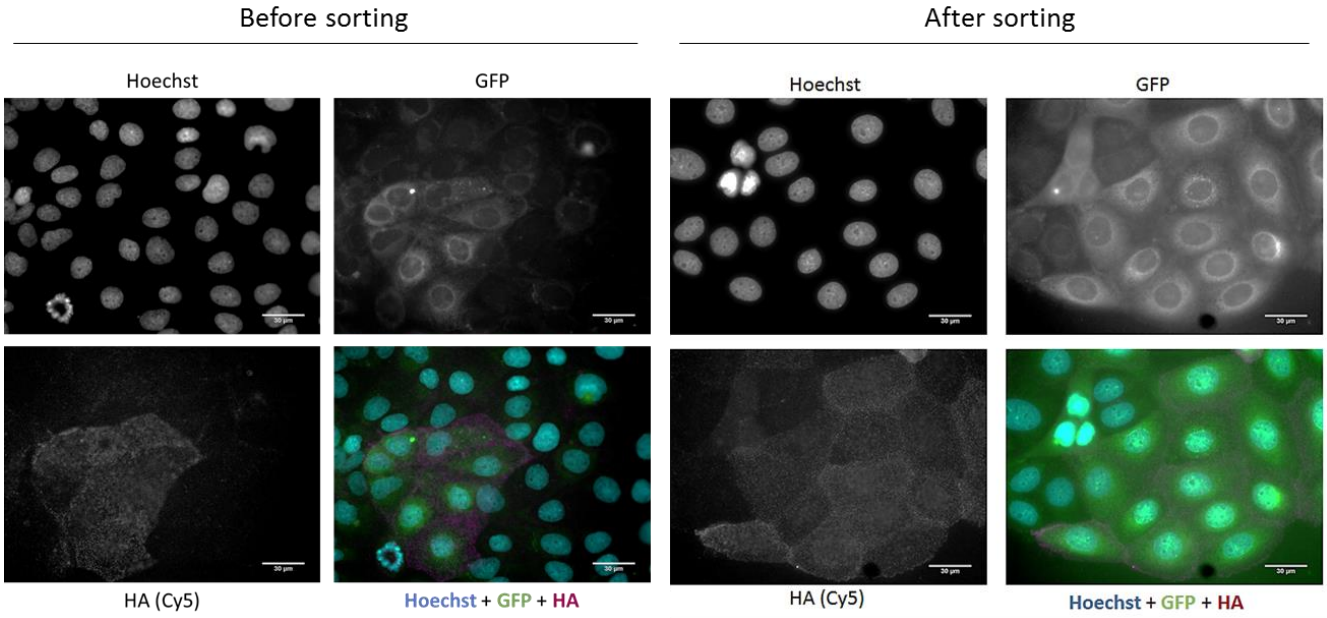

Figure 11 - **Immunofluorescence images of CFBE cells stably overexpressing Ano6 3-HA GFP. The expression of Ano6 was induced by the addition of 1 µg/mL of doxycycline for 48 h. Left panel – Unsorted cells; Right panel – Cells sorted for their GFP fluorescence. Hoechst – Nuclei; GFP – Total Ano6; Cy5 – PM Ano6 (detected with an anti-HA antibody). After sorting (right panel) it is possible to observe a more homogeneous population in both the GFP and Cy5 channels, being these cells a more adequate model to perform siRNA screens. Images were acquired with the 40x objective in a Leica DMI 6000B microscope. Scale bar represents 30 µm.**

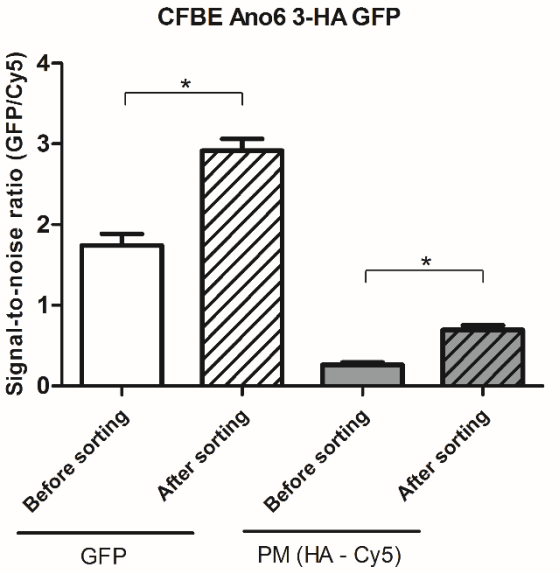

Figure 12 - **Signal-to-noise ratios of GFP and Cy5 fluorescence in CFBE Ano6 3-HA GFP cells (n = 100 cells). With these results, it is possible to detect a significant increase in the signal-to-noise ratio in both channels when the cells are sorted, meaning that the difference between signal and background is higher. Accordingly, these sorted cells are a better model for siRNA screens. * P<0.05 was accepted as significant.**

For CFBE cells stably expressing the Ano9 construct it was possible to detect a higher GFP fluorescence (higher signal-to-noise ratio) when compared with CFBE cells overexpressing Ano6 (Fig.14). Moreover, as observed with CFBE Ano6 3-HA GFP cells, the cell sorting for CFBE Ano9 3-HA GFP significantly increased the GFP signal-to-noise ratio (Fig. 13 and 14).

For this cell line, however, as previously noticed with transient transfections (Materials and methods – 2.1.8 – Protein modelling to determine the best localization for the HA tags and Appendix 4 – Fig.48), membrane expression of Ano9 was not detected. This was observed for the two mutagenesis strategies for this construct (insertion of the 3-HA tag), even though the second structural model appeared to have the correct localization of the tag, i.e., in an extracellular loop (Appendix 4 – Fig.45). Nevertheless, the cellular localization of Ano9 is still controversial, being mostly reported as an intracellular protein[80]. Therefore, cell lines overexpressing this Ano9 construct were generated in order to also study the subcellular localization of this protein. If Ano9 is not in the plasma membrane under physiological cellular conditions, possibly the knockdown of other cellular components could alter this situation. This hypothesis will be further studied with the siRNA screens.

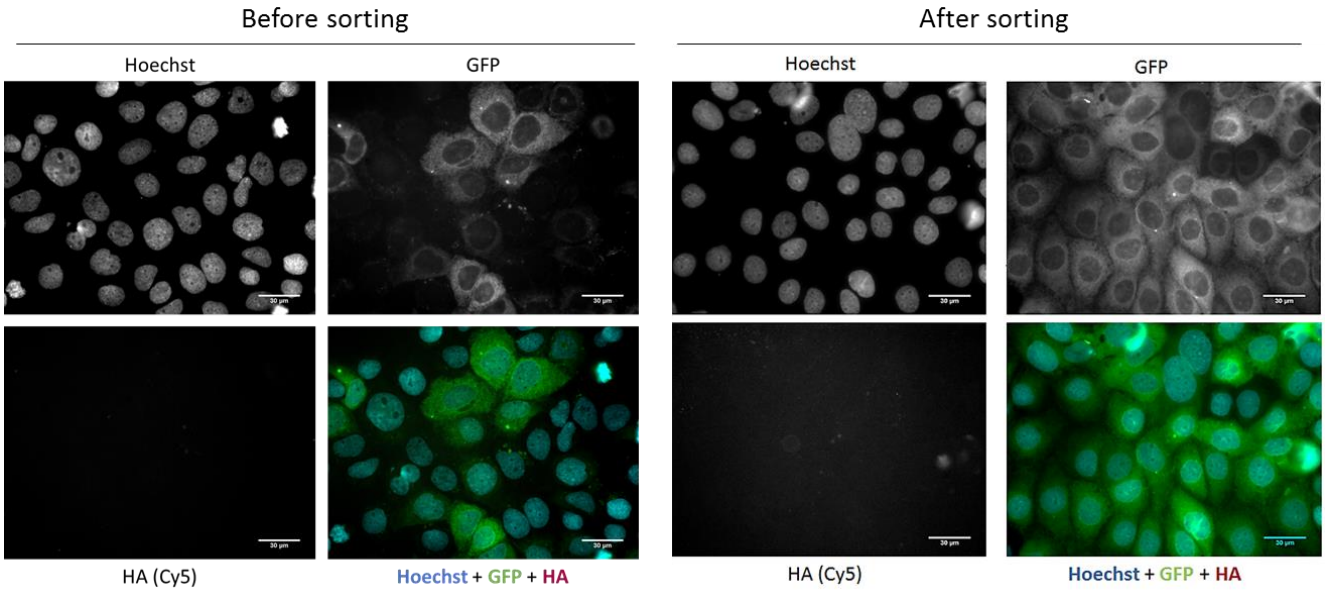

Figure 13 – **Immunofluorescence images of CFBE cells stably overexpressing Ano9 3-HA GFP. The expression of Ano9 was induced by the addition of 1 µg/mL of doxycycline for 48 h. Left panel – Unsorted cells; Right panel – Cells sorted for their GFP fluorescence. Hoechst – Nuclei; GFP – Total Ano9; Cy5 – PM Ano9. After sorting (right panel) it is possible to observe a more homogeneous GFP expression, being these cells a more adequate model to perform siRNA screens. However, no membrane signal was detected either before or after sorting. Images were acquired with the 40x objective in a Leica DMI 6000B microscope. Scale bar represents 30 µm.**

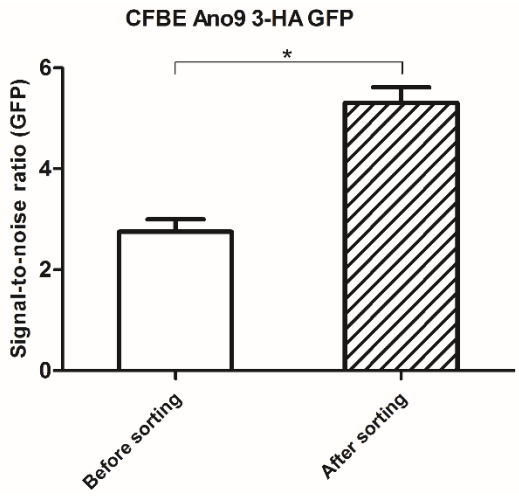

Figure 14 - **Signal-to-noise ratios of GFP in CFBE Ano9 3-HA GFP cells (n = 100 cells). With these results, it is possible to detect a significant increase in the signal-to-noise ratio of GFP fluorescence when the cells are sorted, meaning that the difference between signal and background is higher. Accordingly, these sorted cells are a better model for siRNA screens. * P<0.05 was accepted as significant.**

CFBE Ano6 and Ano9 3-HA GFP were also characterized by Western Blot (Fig.15), where the results obtained were consistent with what was shown by Immunofluorescence assays. The protein was extracted from cells induced with 1 µg/mL of doxycycline for 48 h, and the anti-GFP antibody (Appendix 10 – Table 12) was used to detect both Ano6 and Ano9. This protein analysis was performed before and after cell sorting. The GFP-Ano quantification was normalized to α-tubulin (loading control).

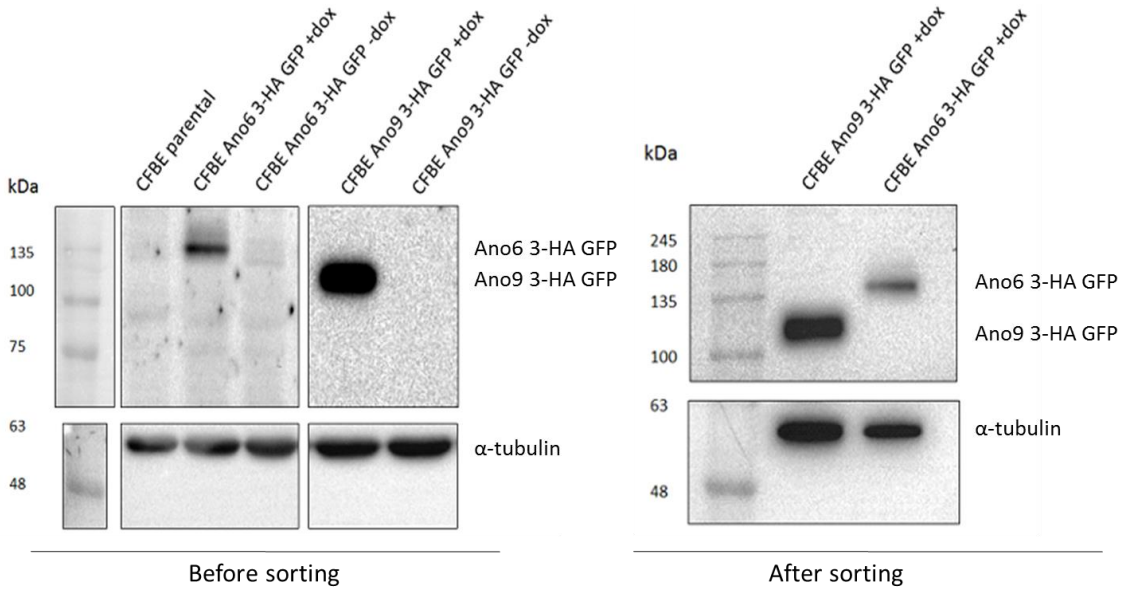

Figure 15 – **Western Blot of CFBE Ano6/9 3-HA GFP cells before (left) and after (right) cell sorting, using an anti-GFP antibody. CFBE parental cells or non-induced cells were used as negative control and α-tubulin was used as loading control. The expression of Ano6 and Ano9 is only detected with doxycycline induction (+dox), and it was significantly increased after cell sorting – see Fig.16.**

As it can be observed in Fig.15 and 16, Ano9 expression (measured through GFP fluorescence) seems to be higher than that of Ano6 in the respective stable cell lines. Moreover, as observed with the immunofluorescence assays, GFP signal highly increased after cell sorting, providing more robust cellular models to use in further experiments.

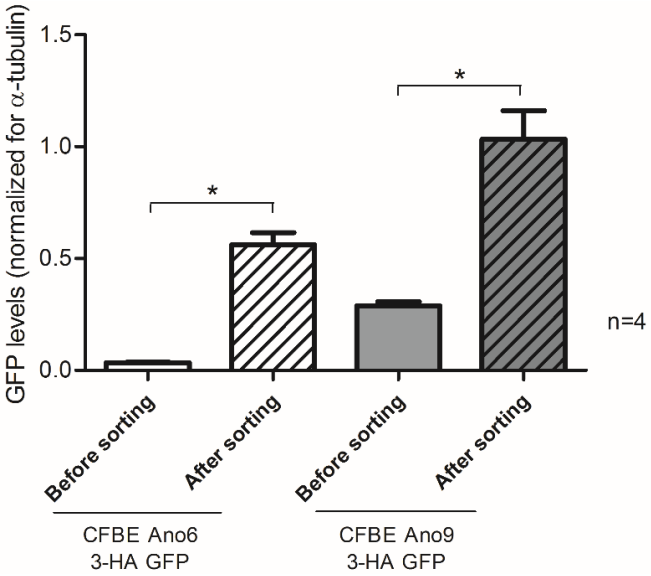

Figure 16 - **Quantification of GFP levels of the Western Blot represented in Fig.15. After sorting it is possible to detect a significant increase in both Ano6 and Ano9 (GFP) expression. * P<0.05 was accepted as significant.**

CFBE mCherry wt- and F508del-CFTR cells stably expressing Ano6 or Ano9 3-HA GFP were also generated and sorted according to their GFP fluorescence intensity. However, due to the time limitations, the characterization of these cell lines was not yet possible to complete.

CFBE wt- and F508del-CFTR cells as well as HeLa H_2B mCherry cells were also stably transfected with Ano6 and Ano9 constructs, and sorting of these cells is pending.

3.1.2) Functional analysis

3.1.2.1) Iodide Efflux

Before generating the stable cell lines overexpressing Ano6 and Ano9, it was necessary to test the ion channel function of these proteins to determine whether the insertion of the tags was not altering their function.

Although Ano9 was previously reported as an intracellular protein with no ion channel function[80], Ano6 was identified as a component of the ORCC[49]. Hence, the detection of increased ion currents with cells overexpressing the Ano6 construct is expected. The absence of increased currents would imply that the tags were probably disrupting the channel function and possibly its structure, which would preclude the next steps of the project.

Thus, to test the functions of Ano6 and Ano9 3-HA GFP, the Iodide (I^-) efflux technique was firstly used. In this assay, the efflux of I^- was measured in HEK 293T cells transiently transfected with these constructs. HEK 293T cells were used in detriment of CFBE cells since their transfection rate is considerably higher. HEK 293T cells transfected with the "empty" pLVX-TRE3G vector were used as control.

This assay was performed as explained in Materials and Methods – 2.5.1 – Iodide efflux. The amount of I^- that remained inside the cell with or without stimulation with ATP was measured. In order to do relative comparison of the results obtained with different anoctamins, the intracellular I^- concentrations obtained for each were normalized by dividing I^- concentration by the concentration of protein. The efflux of I^- was then calculated by subtracting the value of ATP-stimulated cells from non-stimulated cells. Since this technique is based on the calculation of the amount of I^- that remains inside the cells, it was expected that, when channels are functional the stimulation with ATP leads to a decrease of intracellular I^-.

As shown in Fig.17, HEK 293T cells transfected with Ano6 3-HA GFP show a significant 5-fold increase in the efflux of I^- in comparison to the "empty vector" transfected cells, while cells transfected with Ano9 3-HA GFP show a 3-fold increase in the ATP response.

Since other possible endogenous ion channels are taken into account with the "empty vector" transfected cells, these results suggest that the overexpression of the double-tagged constructs leads to an increase of I^- transport. If this increase is due to I^- transport directly conducted by the transfected proteins or if it is caused by a regulation of other channels is still unknown. However, as already referred, although Ano6 was described as a membrane localized protein and as an ion channel[49], which is in agreement with the present results, Ano9 was mostly considered an intracellular protein[80]. Consequently, the increased I^- efflux detected with the overexpression of the Ano9 construct suggests a possible interaction with other ion channels.

Nevertheless, these results support the notion that the insertion of the tags did not disrupt the function of the proteins, which was essential to proceed with this work.

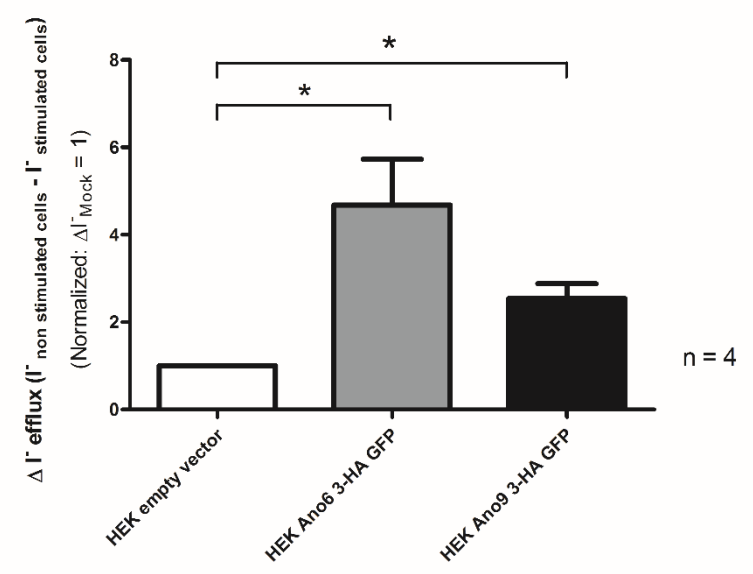

Figure 17 – **Iodide efflux assay for transiently transfected HEK 293T cells. The transfection with the Ano6 construct led to a 5-fold increase of I^- export, while the transfection with the Ano9 construct showed a 3-fold increase, when compared with HEK 293T cells transfected with empty vector. * P<0.05 was accepted as significant.**

After the generation of stably transfected CFBE cell lines, the activity of the overexpressed anoctamins was also assessed using the iodide efflux technique. However, for these cells, the assay used consisted in measuring the I^- that goes out ("efflux") of the cells (measured in the media) in 1-min intervals, before and after ATP stimulation. This assay is preferable to the previous one in assessing the proteins' functions since it measures close time-points, which enables a more comprehensive view of the response to ATP stimulation. However, this assay was not used in the previously shown HEK 293T transiently transfected cells because they detach too easily. Nevertheless, the previous assay also gives valid results.

This assay was performed with CFBE Ano6/Ano9 3-HA GFP cells, and the non-induced cells (cells without addition of doxycycline) were used as control.

As depicted in Fig.18, only Ano6 overexpression led to an increase of I^- transport. However, the ATP stimulation is not specific for anoctamins, being also highly variable among different experiments.

Furthermore, the overexpression of Ano9 appears to decrease the I^- currents when compared with the controls. Also, there was almost no variation in this response. Previous reports have shown that overexpression of Ano9 inhibits Ano1 currents[82]. This inhibiting role of Ano9 could help to explain the findings in this work. However, inhibition of other channels may also be involved. Studies to validate Ano9 communication with other proteins need to be performed.

Although these results differ from the observed in HEK 293T cells transiently transfected with Ano6/9 3-HA GFP, these differences can be explained by the specific type of cells used (HEK 293T cells in the first experiment, and CFBE cells in the second). Differences in Ano9 expression are not a plausible reason for these discrepancies because HEK 293T cells showed a high transfection rate (above 50%, data not shown), and CFBE Ano9 cells were sorted, so that overexpressing of this protein is observed in almost every cell. An explanation could be the Ano9

insertion into the genome of the cells, which can affect other proteins and pathways, differently from what is observed with the transient transfections.

Interestingly, according to different studies, HEK 293T cells do not express endogenous Ano1 (or if they do, the expression of Ano1 is extremely low)[78]. Nevertheless, a relationship between Ano1 and Ano9 has been reported[82] which could explain the differences observed in these two cell types, as CFBE cells express certainly endogenous Ano1.

Another important consideration is the previously mentioned lack of specificity of ATP, being extremely difficult to identify the channels that are activated with its addition. The use of inhibitors of anoctamins would be a possible alternative. However, this also presents a challenge, since there are no specific inhibitors available for each anoctamin[148].

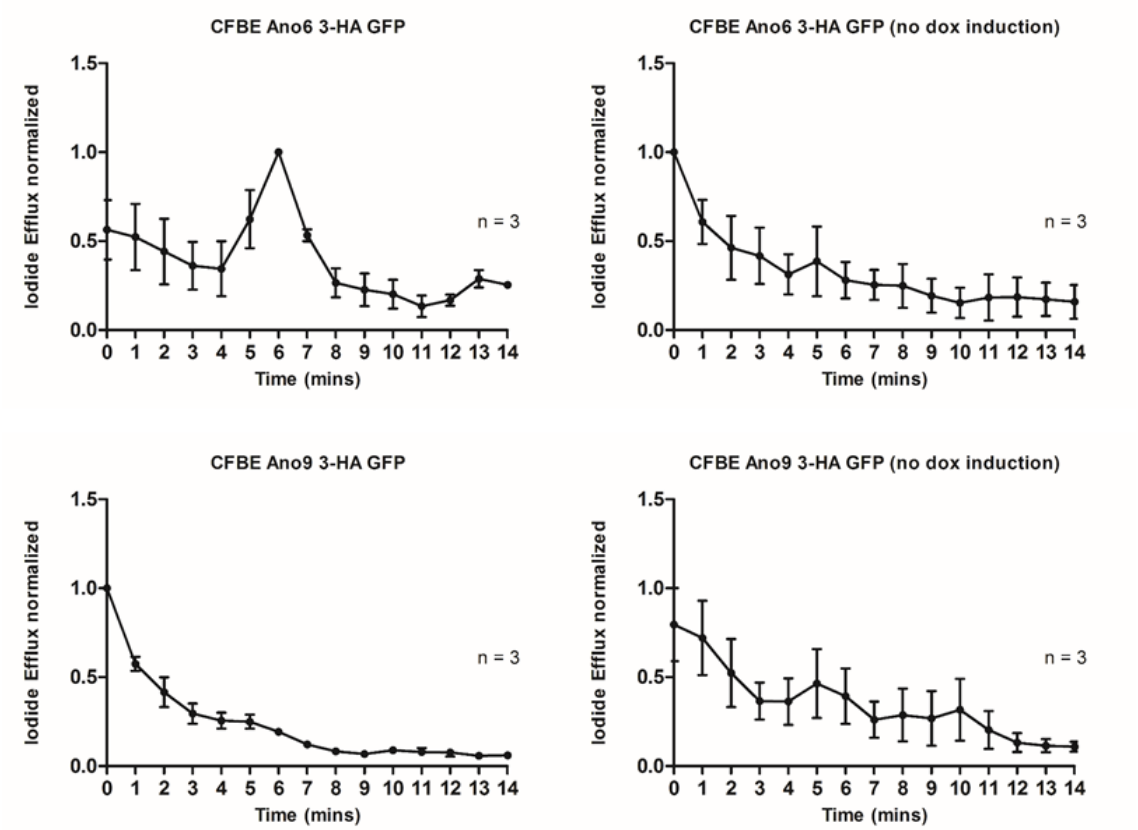

Figure 18 – **Iodide efflux measurements at 15 time-points using CFBE cells stably overexpressing Ano6 or Ano9. 100 µM ATP was added at 5 min time point. CFBE overexpressing Ano6 show an increased I^- efflux when stimulated with ATP compared to the non-induced CFBE Ano6 cells (control), while CFBE overexpressing Ano9 show an apparent decrease in I^- efflux in comparison to the control cells (CFBE Ano9 without doxycycline induction).**

3.1.2.2) Micro-Ussing chamber

Micro-Ussing chamber experiments were performed in CFBE Ano6 and Ano9 3-HA cells to confirm the results obtained with the iodide efflux and to test their function in polarized cells, which represents a more physiological condition. In these experiments, CFBE cells overexpressing Ano6 or Ano9 were seeded onto collagen IV-coated permeable supports to form monolayers of polarized cells, as described in Materials and methods – 2.5.2 – Micro-Ussing chamber. Monolayers were mounted in perfused micro-Ussing chambers and analysed under

open-circuit conditions. Transepithelial voltages (V_{te}) were measured and equivalent short-circuit currents (I_{eq-SC}) were calculated according to Ohm's law (Fig. 19 and 20). Anoctamins were activated by 100 µM ATP, and 30 µM of $CaCC_{inh}$-A01 (CaCC inhibitor) was used to block the channels. The same CFBE Ano6 and Ano9 cells but without doxycycline induction were used as controls.

The activation of anoctamins is thought to be achieved through the ATP stimulation of apical purinergic $P2Y_2$ receptors[150]. Activation of the $P2Y_2$ receptors leads to the stimulation of phospholipase C (PLC) and inositol triphosphate (IP_3) release, which ultimately causes the release of calcium (Ca^{2+}) from the ER to the cytoplasm[151]. The increase of intracellular Ca^{2+} then leads to the activation of anoctamins. Additionally, activation of basolateral potassium (K^+) channels, results in hyperpolarization of the cell membrane and increases the driving force for apical anion efflux[152] (see Fig.31).

In this study, using dox-induced CFBE Ano6 3-HA GFP cells, application of ATP from the apical side originated a negative voltage deflection (Fig.19). Accordingly, the calculated I_{eq-SC} increased in comparison to non-induced controls (Fig.19 – D), which is consistent with the iodide efflux results showing an ion channel function of Ano6. After ATP washout, a second ATP stimulation was performed. The calculated I_{eq-SC} significantly decreased compared to the first addition (Fig.19 – B and D). This result reflects the desensitization of the purinergic receptors[153], causing a smaller release of intracellular Ca^{2+} and, consequently, a smaller activation of the channels (Fig.19 – A, B and D).

The addition of ATP to the basolateral side showed only a modest response (small negative voltage deflection – Fig.19 – C), with no statistical difference compared to the response of control cells. This result suggests an asymmetric distribution of Ano6 between the apical and basolateral membranes, being mostly localized at the apical side. However, the occurrence of a negative voltage deflection can be explained by the activation of basolateral K^+ channels, since basolateral application of ATP to human airway epithelial cells has shown to activate Cl^- secretion indirectly, by activating K^+ channels[154].

Moreover, the distribution of purinergic receptors in the apical and basolateral sides of epithelial cells has also been reported as being asymmetric[46, 155]. Studies performed in 16HBE14o- (Human bronchial epithelial cells) and Caco-2 cells (Human colon epithelial cancer cells) showed that the $P2Y_2$ receptor was expressed at the apical membrane. However, in 16HBE14o- cells, the receptor was also expressed at lower levels in the lateral membrane below the tight junctions[155], which is in agreement with the small response obtained with the basolateral addition of ATP in the present work (using CFBE cells – also human bronchial epithelial cells). Furthermore, ER Ca^{2+} stores have been reported as preferentially distributed towards the apical membrane in airway epithelial cells. Accordingly, it has been described that basolateral activation of $P2Y_2$ receptors with ATP, although causes an increase in intracellular Ca^{2+} concentration, failed to activate apical Ca^{2+} sensitive channels. Apical administration of ATP has also been shown to be unable to activate basolateral Ca^{2+}-activated K^+ cannels, suggesting a compartmentalization of Ca^{2+} signalling in airway epithelia[149].

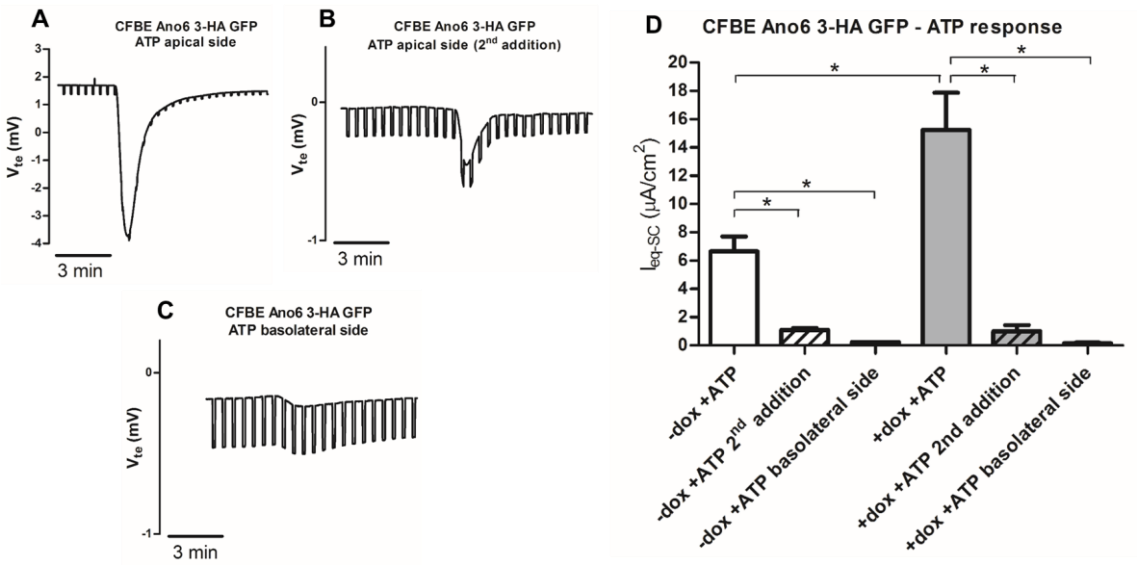

Figure 19 - **Original micro-Ussing chamber (open circuit) recordings for CFBE Ano6 3-HA GFP induced cells (+dox). Non-induced CFBE Ano6 cells were used as control (-dox). A negative voltage deflection can be observed after addition of ATP. A – First addition of 100 µM ATP to the apical side of the filter. B – Second addition of 100 µM ATP to the apical side of the filter. C – Addition of 100 µM ATP to the basolateral side of the filter. D – Bar graph that summarizes calculated $I_{eq\text{-}sc}$ ($\mu A/cm^2$) for the first and second addition of ATP to the apical side of the filter, as well as to the basolateral side, for both doxycycline induced and non-induced CFBE Ano6 cells. * P<0.05 was accepted as significant.**

Regarding Dox-induced CFBE Ano9 3-HA GFP cells, ATP addition to the apical side of the filter (Fig.20) also originated a negative voltage deflection. However, the $I_{eq\text{-}SC}$ calculated in these cells did not show significant differences from the non-induced control cells (Fig.20 – D), although it appears slightly reduced. These results reproduce the previous observations shown with the iodide efflux assays in the same cells.

Similarly to what was detected in CFBE Ano6 3-HA GFP cells after the second ATP application, the calculated $I_{eq\text{-}SC}$ significantly decreased in comparison to first ATP stimulation (Fig.20 – B and C). This result reflects once more the desensitization of the purinergic receptors[153]. Moreover, activation of ion currents and thus negative voltage deflection by basolateral addition of ATP was also reduced in these cells (Fig.20 – C and D), with no statistical difference when compared to the response of non-induced control cells. This can again be explained by the asymmetric distribution of purinergic receptors[155] and the Ca^{2+} signalling compartmentalization[149]. Furthermore, Ano9 may also not be expressed in the plasma membrane[82] as already described.

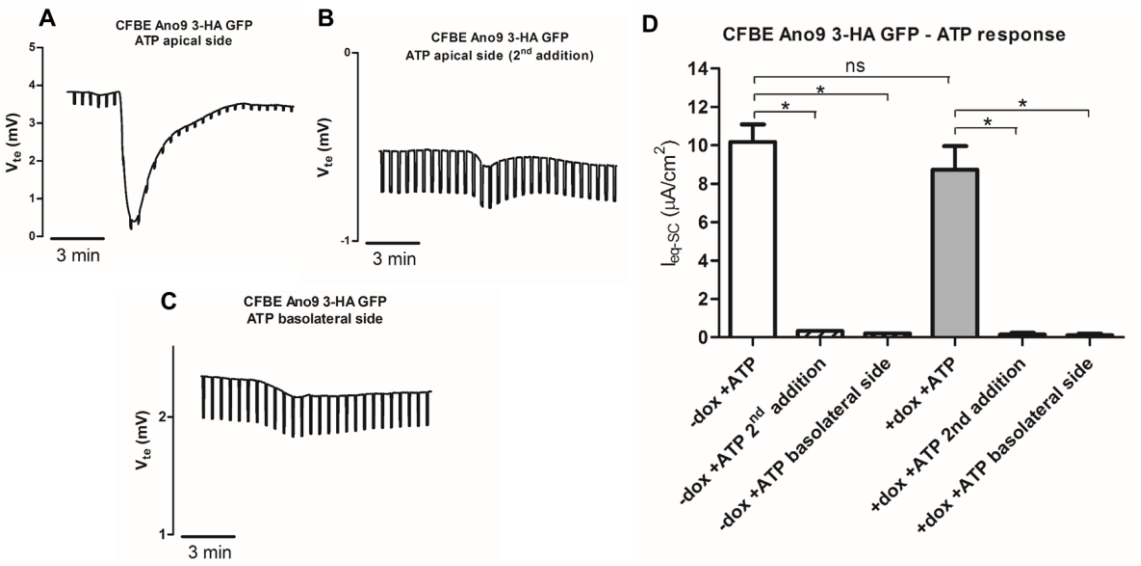

Figure 20 - **Original micro-Ussing chamber (open circuit) recordings for CFBE Ano9 3-HA GFP induced cells (+dox). Non-induced CFBE Ano9 cells were used as control (-dox). A negative voltage deflection can be observed after addition of ATP. A – First addition of 100 µM ATP to the apical side of the filter. B – Second addition of 100 µM ATP to the apical side of the filter. C – Addition of 100 µM ATP to the basolateral side of the filter. D – Bar graph that summarizes calculated I_{eq-sc} (µA/cm^2) for the first and second addition of ATP to the apical side of the filter, as well as to the basolateral side, for both doxycycline induced and non-induced CFBE Ano9 cells. * P<0.05 was accepted as significant.**

For both cell types, the stimulation by ATP in the presence of inhibitor $CaCC_{inh}$-A01 resulted in an extremely reduced I_{eq-SC} (Fig.21 – A). Hence, this inhibitor can be used to eliminate almost all currents produced by anoctamins (98.8% and 98.9% of inhibition of CFBE Ano6 and Ano9, respectively). Furthermore, the effects of $CaCC_{inh}$-A01 on epithelial ion transport in both cell types (and controls) were reversible, since after washout of the inhibitor, ATP addition originated negative voltage deflections (Fig.21 – B). However, these inhibitors are not specific for anoctamins[148], which does not allow discrimination of the currents caused by each anoctamin or other ion channels.

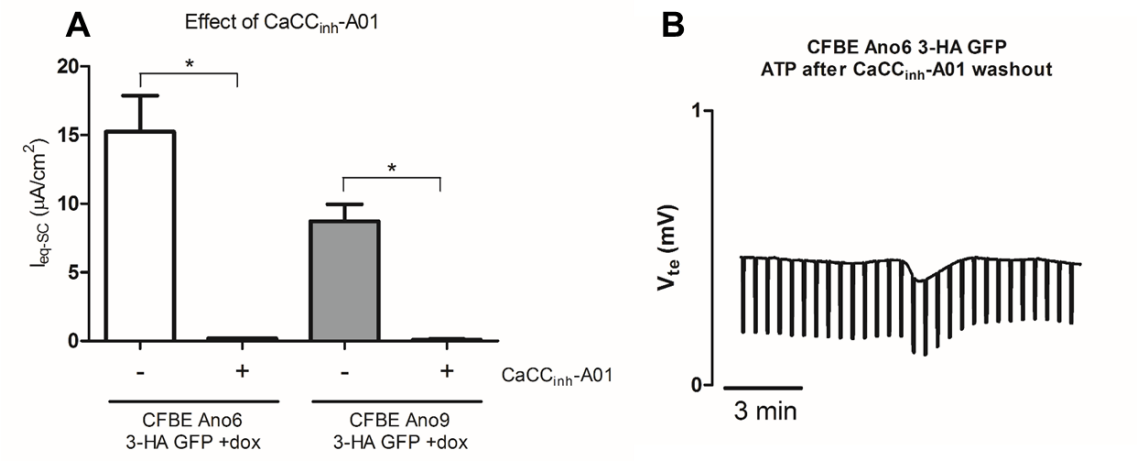

Figure 21 - **Effect of $CaCC_{inh}$-A01 on I_{eq-SC} values. A – The simultaneous addition of 30 µM $CaCC_{inh}$-A01 and 100 µM ATP led to a significant decrease in I_{eq-SC} in both cell types, meaning that this inhibitor is strongly (although not specifically) inhibiting the activation of anoctamins by ATP. * P<0.05 was accepted as significant. B – Original micro-Ussing chamber recordings of an example of ATP addition (on CFBE Ano6 3-HA GFP cells) after $CaCC_{inh}$-A01 washout, showing that its inhibitory effect is reversible.**

An additional interesting aspect of this experiment is that cells overexpressing Ano6 had lower transepithelial resistance (TEER) than CFBE Ano9 3-HA cells. These results could suggest that Ano6 is somehow involved in cellular dedifferentiation, possibly through the "loosening" of tight junctions, which would be in accordance with the role of Ano6 in cancer progression that has been seen in several studies[100].

3.1.3) Intracellular localization of anoctamins

3.1.3.1) Immunostaining in polarized cells

After performing micro-Ussing chamber experiments, the same CFBE Ano6/9 3-HA GFP cell monolayers were then stained as described in Materials and methods – 2.4.1 – Immunofluorescence of anoctamins. Images of cells on filters were acquired using confocal microscopy.

The staining of these polarized cells for Ano6 and Ano9 3-HA GFP were determined by GFP fluorescence which confirmed their overexpression in the cells and helped to validate the micro-Ussing chamber results. However, the main goal of this experiment was to detect differences in the intracellular localization of these anoctamins in polarized cells.

For an optimal identification of the cellular localization of Ano6 and Ano9, it would be necessary to compare its expression to (at least) plasma membrane and ER markers. However, due to the fact that the confocal microscope used only has three lasers (488 nm, 532 nm and 635 nm), and that the TOPRO3 staining was visible in the mCherry channel, it was only possible to use the lasers of 488 nm (GFP) and 635 nm (TOPRO3).

Nevertheless, the images acquired allow the detection of differences between Ano6 and Ano9 localization.

In CFBE Ano6 3-HA GFP cells (Fig. 22 and 23), Ano6 seems to be localized at the plasma membrane, although it can also be detected in the cytoplasm at significant levels. Interestingly, Ano6 expression was detected not only in the apical membrane, but also, in some cells, in the basolateral membrane.

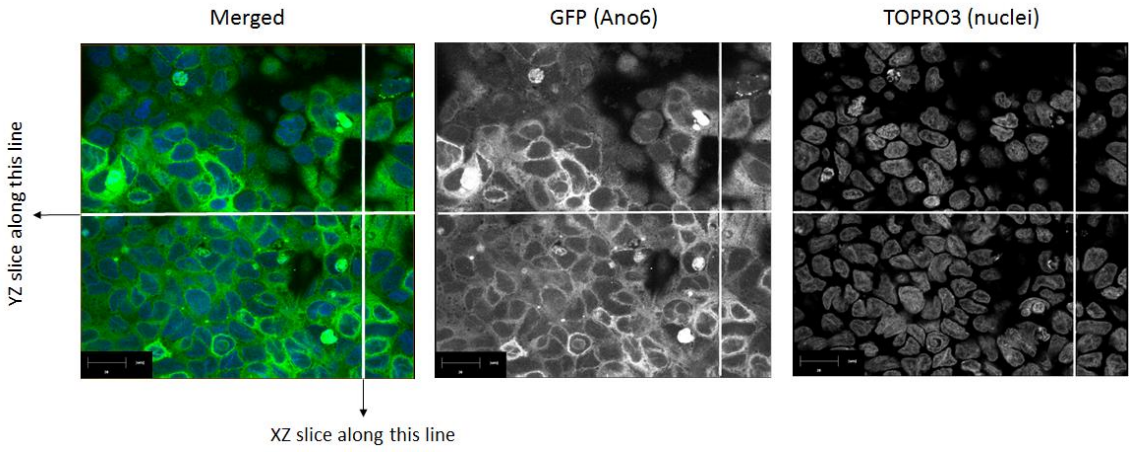

Figure 22 – **Intracellular localization of Ano6 in CFBE Ano6 3-HA GFP cells as determined by GFP fluorescence. Images were acquired using a Leica TCS SPE confocal microscope with a 63x oil objective. Ano6 (GFP) and nuclei (TOPRO3) are represented in centre and right images, respectively. In the left image Ano6 and nuclei images are merged, corresponding to green and blue colours, respectively. 3D reconstructions were performed along the YZ**

and XZ lines represented in the image. Scale bar represents 20 µm (Images acquired by the core-microscopy technician of the laboratory Luis Marques).

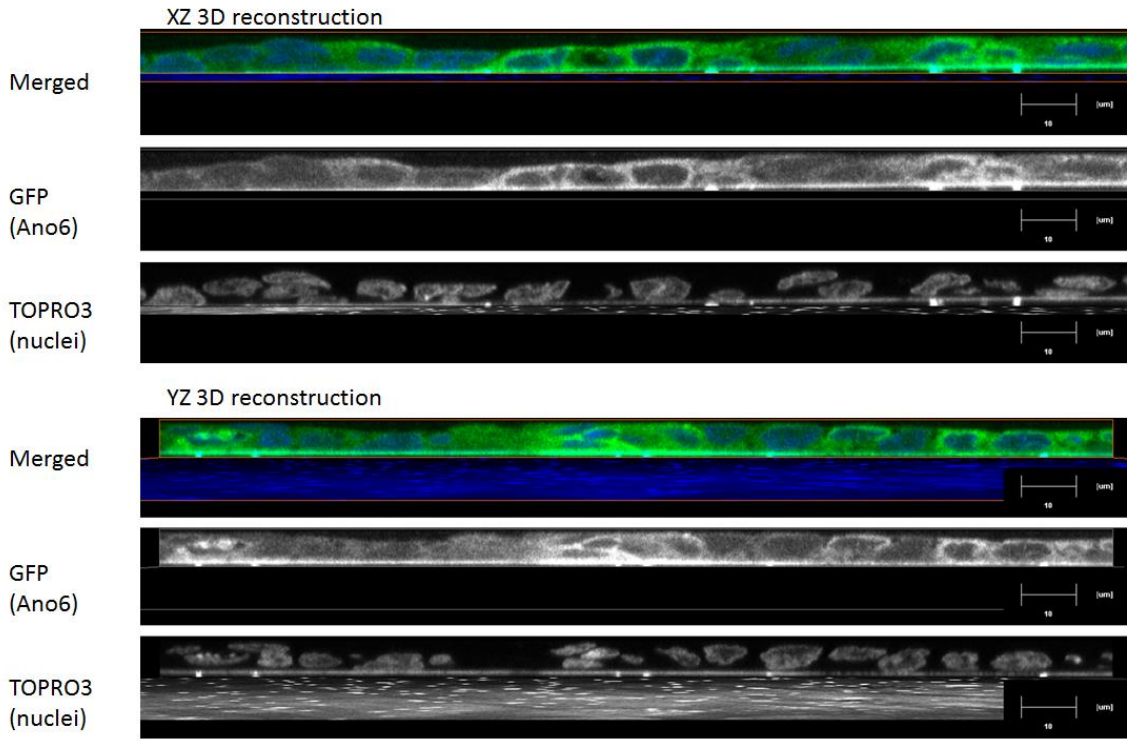

Figure 23 – **3D reconstruction of the images represented in Fig.22. Scale bar represents 10 µm. (Images reconstructed by the core-microscopy technician of the laboratory Luis Marques).**

In contrast to CFBE Ano6 3-HA GFP cells, for CFBE Ano9 3-HA GFP cells, Ano9 seems to be mostly localized in the cytoplasm, rather than at the plasma membrane. These observations result from comparison of images for Ano6 and Ano9 (Fig. 23 and 25, respectively). For Ano6, it is visible from the GFP fluorescence (Fig.23, GFP panel), that there is almost no separation (or "space") between the cells, which means that Ano6 is likely in the plasma membrane. However, for Ano9, the GFP fluorescence (Fig.25, GFP panel) is mostly located around the nuclei. These results are in agreement with previous studies reporting that Ano9 is mostly localized in the cytoplasm[82] and are also consistent with our results from the micro-Ussing experiments, where currents in Dox-induced cells overexpressing Ano9 had no significant difference from the non-induced control cells.

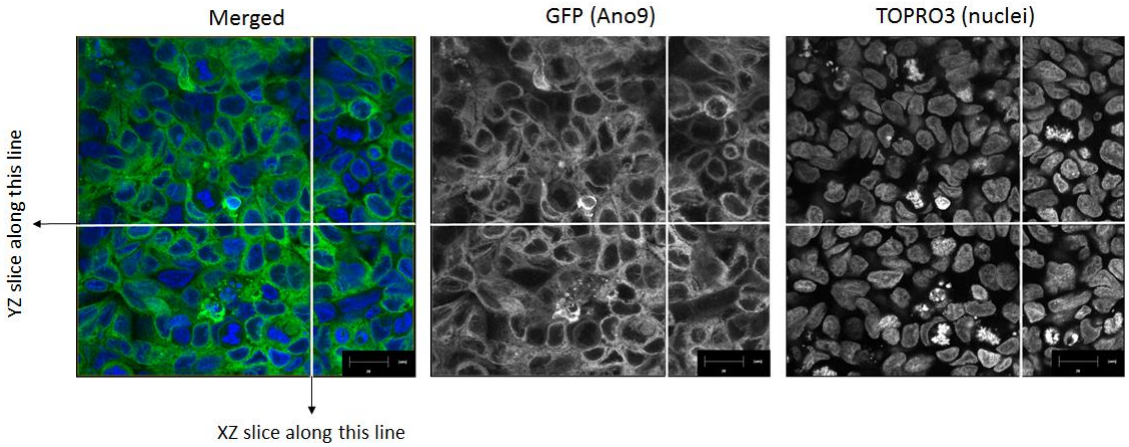

Figure 24 - **Intracellular localization of Ano9 in CFBE Ano9 3-HA GFP cells as determined by GFP fluorescence. Images were acquired using a Leica TCS SPE confocal microscope with a 63x oil objective. Ano9 (GFP) and nuclei (TOPRO3) are represented in centre and right images, respectively. In the left image Ano9 and nuclei images are merged, corresponding to green and blue colours, respectively. 3D reconstructions were performed along the YZ and XZ lines represented in the image. Scale bar represents 20 µm (Images acquired by the core-microscopy technician of the laboratory Luis Marques).**

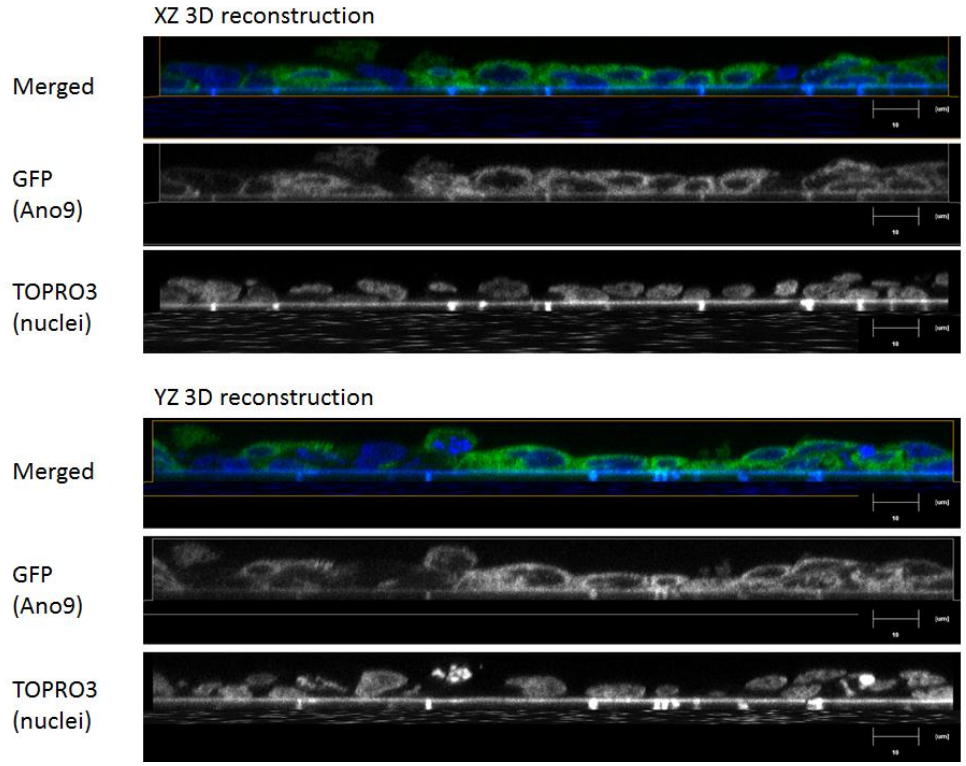

Figure 25 - **3D reconstruction of the images represented in Fig.24. Scale bar represents 10 µm. (Images reconstructed by the core-microscopy technician of the laboratory Luis Marques).**

Nonetheless, as already stated, these preliminary results need further confirmation, namely by using markers for the apical and basolateral membranes, as well as for cell junctions. Furthermore, the localization of Ano6 to the basolateral membrane is inconsistent with the almost inexistent currents created by the basolateral addition of ATP in micro-Ussing chamber

experiments. However, as already referred, the lower levels of $P2Y_2$ receptors at the basolateral membrane[155] can explain those differences.

3.1.3.2) Biotinylation

In order to confirm whether overexpressed Ano9 in CFBE cells is trafficking to the plasma membrane, a cell-surface biotinylation assay was performed. In this assay CFBE cells overexpressing Ano6 were used as control, since previous experiments with these cells allowed the detection of Ano6 in the plasma membrane.

In this experiment, a Western Blot was performed using the whole-cell lysate and the plasma membrane fraction (cell-surface biotinylated) – Fig.26. The anti-GFP antibody was used to detect both Ano6 and Ano9.

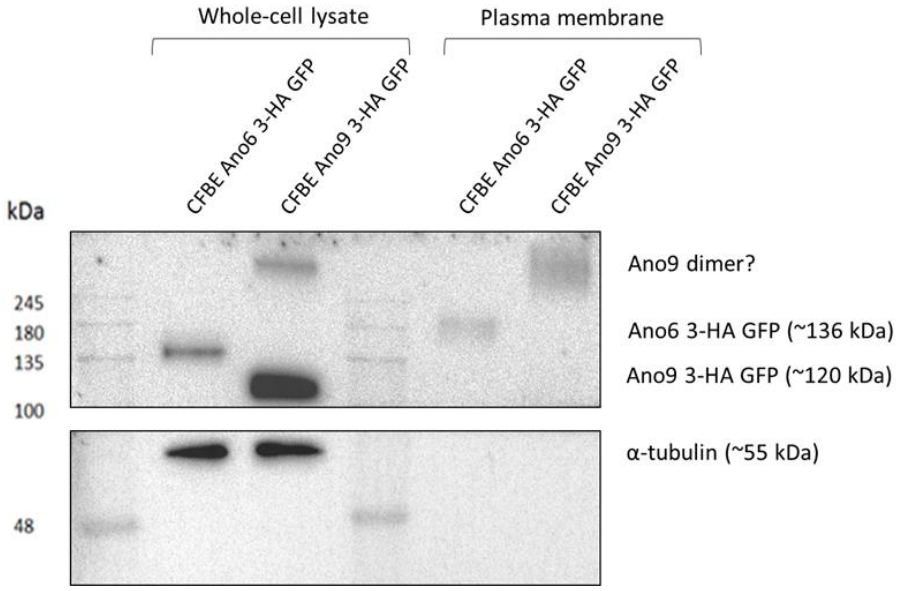

Figure 26 - **Western Blot of a biotinylation assay performed with CFBE Ano6 and Ano9 3-HA GFP. A band corresponding to Ano6 3-HA GFP is detected in both the whole-cell lysate sample and membrane fraction (~136 kDa in the first and slightly higher in the second). For Ano9, two bands are detected in the whole-cell lysate, possibly corresponding to a monomer and a dimer of Ano9 (~120 kDa and >245 kDa, respectively), while only the highest is detected in the membrane fraction. α-tubulin, as expected, is only detected in the whole-cell lysate (~55 kDa), meaning that the plasma membrane proteins were correctly isolated.**

α-tubulin was used as loading control for the whole-cell lysate and as a control for the specificity of the cell-surface biotinylation technique to detect only plasma membrane proteins. Tubulin is not expected to be identified in the plasma membrane fractions since it is a structural component of microtubules, which are cytoplasmic cytoskeletal elements, and indeed it was not detected by the cell-surface biotinylation.

As it can be observed in Fig.26, Ano6 was detected in both whole-cell lysate and in the membrane fraction by cell-surface biotinylation (~136 kDa: Ano6 – 106 kDa, GFP – 27 kDa, 3-HA – 3 kDa). However, in the membrane fraction, Ano6 appears with a higher molecular weight, possibly because of the glycosylation it undergoes until reaching the plasma membrane. To confirm that this corresponds indeed to a glycosylated form, a glycosidase assay needs to be performed.

In the whole-cell lysate blot for Ano9 (Fig.26) two bands (of ~120 kDa: Ano9 – 90 kDa, GFP – 27 kDa, 3-HA – 3 kDa; and >245 kDa, respectively) were detected. The lower molecular weight band matches the expected size for Ano9 3-HA GFP with 120 kDa. In the plasma membrane fraction, however, it is not possible to detect this lower molecular weight band, while the one of >245 kDa remains present. Although this band could be due to an unspecific antibody interaction, it is not detected in CFBE cells overexpressing Ano6 (using the same antibody). This strongly suggests that this band may represent a homodimer of Ano9 (or a heterodimer of Ano9 and other anoctamin – possibly Ano1), which resists to chemical reduction with DTT (present in the sample buffer).

Several studies show that anoctamins form homodimers and the occurrence of heterodimers has not been yet excluded. Moreover, dimerization of Ano1 and Ano2 has already been reported[68], as well as the inhibition of Ano1 currents by Ano9 expression[82], as referred above, which may also suggest a possible interaction between these two family members. Regarding all these observations, it is possible that the band of higher molecular weight that we observed (Fig.26) corresponds to an anoctamin homo/heterodimer. We plan to send this band to be assessed by mass spectrometry to solve this issue.

3.2) Establishment of microscopy-based assays to be used in siRNA screens

In order to determine whether the stable cell lines created are adequate for microscopy-based siRNA screens, CFBE Ano6 3-HA GFP cells (sorted by flow cytometry and above characterized) were used to perform a pilot screen. To this end, image acquisition and analysis were performed as described in Materials and methods – 2.4.2 – Image acquisition, processing and analysis and 2.6.2 – siRNA pilot screen.

For this pilot screen, we used a labtek spotted with 384 siRNAs which target 231 genes previously found to affect wt-CFTR traffic in a primary screen using human alveolar epithelial A549 cells (Amaral lab, unpublished data). “Scrambled” non-targeting siRNA was used as a negative control.

Results from this pilot screen (Fig.27) identified 71 siRNA hits affecting Ano6 traffic: 34 inhibitor genes, i.e., targeted by Ano6-activating siRNAs, and 37 enhancer genes, i.e., targeted by siRNAs inhibiting Ano6 traffic. Among the 34 inhibitors of Ano6 traffic, 4 were targeted by 2 siRNAs, and among the 37 enhancers, 5 were targeted by 2 siRNAs.

The summary of these results and the deviation scores of hits targeted by 2 siRNAs are shown in Fig. 27 and 28, while the images acquired for these hits (with background corrections) are presented in Fig. 29 and 30. The scores of remaining hits (those resulting from only one siRNA), are displayed in Tables 13 and 14 in Appendix 11, where the names of the genes affecting Ano6 traffic as well as their effects on wt- and F508del-CFTR traffic are also specified.

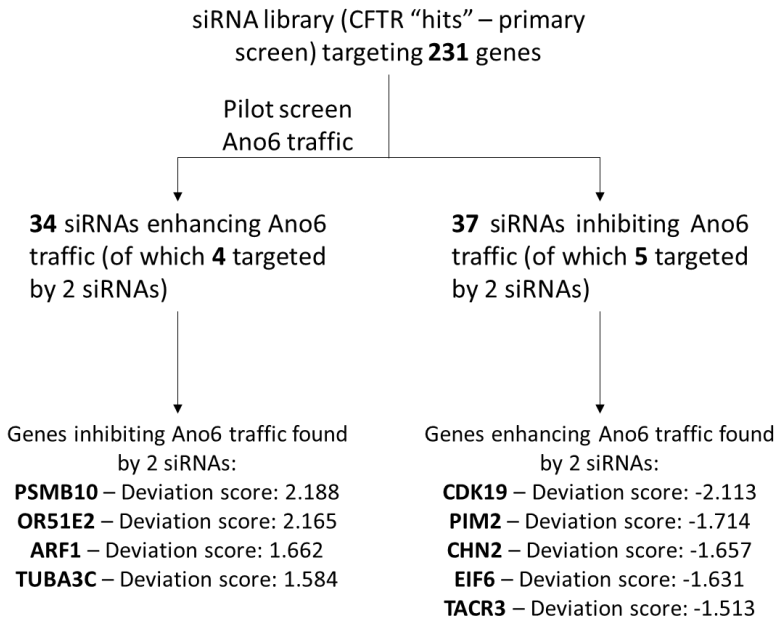

Figure 27 – **Workflow of the pilot screen aimed at identifying Ano6 traffic regulators and summary of hits that were found by 2 different siRNAs and respective scores.**

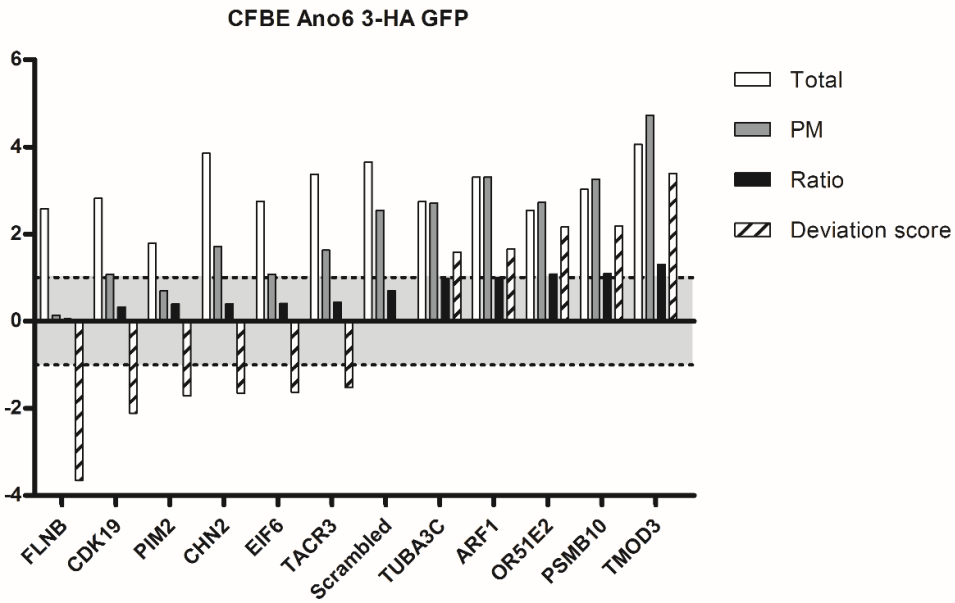

Figure 28 – **Graph representing screen data for total Ano6, plasma membrane Ano6, ratio total Ano6/PM Ano6 and deviation score of the ratio for the top enhancer and inhibitor hits. Genes with negative deviation scores are enhancers of Ano6 traffic (their siRNAs inhibit Ano6 traffic) and genes with positive deviation scores are inhibitors of Ano6 traffic (their siRNAs enhance Ano6 traffic).**

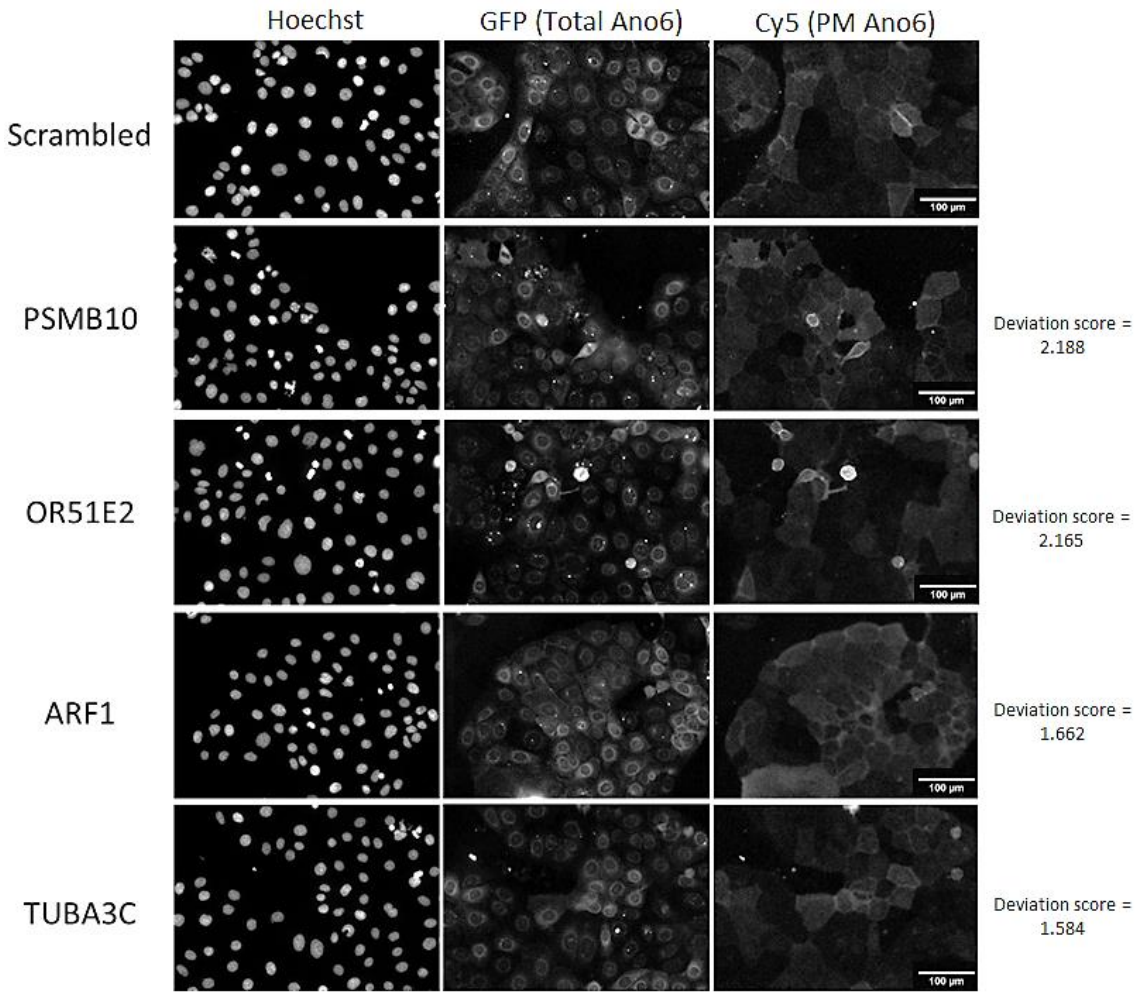

Figure 29 – **Representative images of cells under the effect of the top siRNA hits enhancing Ano6 traffic to the plasma membrane. Images were acquired with the 10x objective. Scale bar represents 100 µm.**

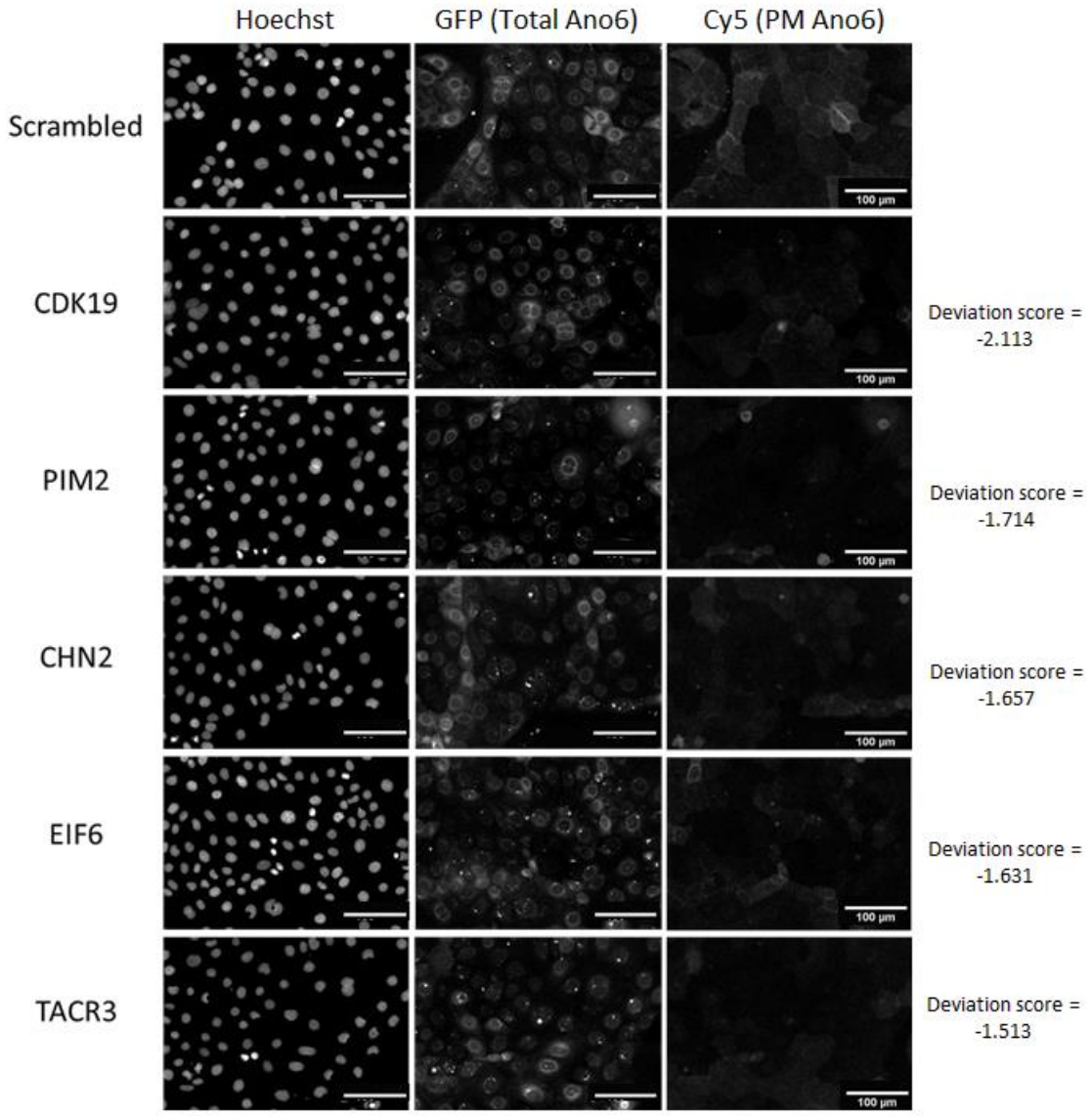

Figure 30 – **Representative images of cells under the effect of the top siRNA hits inhibiting Ano6 traffic to the plasma membrane. Images were acquired with the 10x objective. Scale bar represents 100 µm.**

The genes detected as inhibitors and enhancers of Ano6 traffic were separately clustered using the DAVID (Database for Annotation, Visualization and Integrated Discovery) Bioinformatics Resource, using a high classification stringency.

The results obtained for the most important biological processes regulated by the genes inhibiting Ano6 traffic include (from the most to the less significantly enriched): G-protein coupled receptor protein signalling (8 genes), ion transport (5 genes), establishment of protein localization (4 genes), neurological system process (4 genes), second-messenger-mediated signalling (3 genes), response to hormone stimulus (3 genes), intracellular transport (3 genes), proteolysis (3 genes), protein phosphorylation (3 genes), and cell adhesion (3 genes).

For genes that enhance Ano6 traffic the results obtained include (from the most to the less significantly enriched): G-protein coupled receptor protein signalling pathway (12 genes),

sensory perception of chemical stimulus (4 genes), regulation of apoptosis (3 genes), and protein phosphorylation (3 genes).

This pilot screen allowed not only the detection of some genes that influence Ano6 traffic, but also the calculation of this assay's dynamic range. Dynamic range measures the ratio between the strongest signal on a fluorescence channel and the minimum discernible signal. This measurement is particularly important for the detection of PM and total Ano6, in order to determine if the differences of Ano6 expression in these channels are sufficient to be correctly quantified in further screens. In this pilot screen the dynamic range was 40 for PM Ano6 and 18 for total Ano6, meaning that the maximum signal of each channel was 40 and 18 times higher, respectively, compared to the minimum signal. These results then suggest that, with this model, the differences in PM and total Ano6 signals can be correctly distinguished.

A validation screen for CFTR traffic enhancers and inhibitors, performed on CFBE mCherry wt- and F508del-CFTR cells in our laboratory by Hugo Botelho[145] (and unpublished), showed some similar hits, suggesting a relationship between CFTR and Ano6 traffic pathways. The most important biological processes regulated by genes affecting CFTR include: G-protein coupled receptor protein signalling pathway (e.g.: ITPR2 - Inositol 1,4,5-trisphosphate receptor, type 2), cell surface receptor linked signal transduction, ion homeostasis (e.g.: ATP2C1 – ATPase, Ca^{2+} transporting, type 2C, member 1), neurological system process (e.g.: OR2AG1 – Olfactory receptor, family 2, subfamily AG, member 1), response to hormone stimulus (e.g.: LDLR – Low density lipoprotein receptor), protein phosphorylation (e.g.: ROR1 – Receptor tyrosine kinase-like orphan receptor 1), and intracellular protein transport (e.g.: COPBI – Coatomer protein complex, subunit beta 1).

The results in this pilot screen for Ano6 traffic showed that G-protein coupled receptor protein signalling is the most significantly enriched pathway, represented by a total of 20 genes among the 71 hits. This is consistent with the fact that activation of anoctamins is related with this signalling pathway, which suggest that Ano6 traffic to the plasma membrane and activation are correlated. Indeed, ATP binding to G_q-coupled purinergic receptors, particularly $P2Y_2$ receptors (the most predominant receptor in bronchial epithelia[156]) activates G protein (G_q) which stimulates phospholipase C (PLC). PLC stimulation catalyses the hydrolysis of phosphatidylinositol 4,5-bisphosphate (PIP_2) into inositol 1,4,5-trisphosphate (IP_3) and diacylglycerol (DAG). IP_3 then binds to IP_3 receptors, particularly to Ca^{2+} channels in the ER, which leads to the increase of cytosolic Ca^{2+} [151]. This increase then causes the activation of Ca^{2+} activated chloride channels, namely anoctamins. Interestingly, the IP_3 receptor type 2 was also a hit in both the Ano6 pilot screen and CFTR validation screen.

Although targeted by only one siRNA, other channels like ENaC and Ano1 also showed to have an effect on the traffic of Ano6. The knockdown of these two genes was shown to increase Ano6 traffic, i.e., these proteins seem to be inhibitors of Ano6 traffic.

Taking together the results obtained in the present work and reported data on anoctamins, CFTR and ENaC, we propose a working model of these ion channels in airway epithelial cells (Fig.31).

Extracellular ATP stimulates Cl^- secretion through $P2Y_2$ purinergic receptors via both Ca^{2+}-independent signalling and intracellular Ca^{2+}-dependent pathways by opening CFTR, CaCCs (Ano1)[157] and according to the current study also Ano6. However, Ano6 is only activated by

apical ATP although it locates on both apical and basolateral sides (shown by immunostainings). Additionally, Cl^- secretion in polarized epithelia requires parallel activation of apical Cl^- channels and basolateral K^+ channels also by $P2Y_2$ receptors (basolateral) to generate the driving force for Cl^- exit through the apical membrane[46]. Moreover, apical $P2Y_2$ activation has shown to inhibit ENaC, possibly by a PIP_2-dependent mechanism[158]. This inhibition consequently diminishes the Na^+ influx and creates an electrochemical driving force leading also to Cl^- secretion via Ca^{2+} activated Cl^- channels[151, 159].

As already referred, G_q-protein receptor signalling is associated with the activation of anoctamins and CFTR. Apart from changes of intracellular Ca^{2+}, another consequence of PIP_2 hydrolysis is the formation of DAG and its activation of PKC, which regulates Cl^- secretion via CFTR[149].

Crosstalk between cAMP- and Ca^{2+}-dependent Cl^- secretion may occur at different levels, strengthening the concept of interaction between anoctamins and CFTR. For example, purinergic receptors ($P2Y_2$/$P2Y_6$) increase both intracellular cAMP and Ca^{2+}; intracellular Ca^{2+} affects the activity of enzymes that control intracellular cAMP; and CFTR translocates G_q-coupled receptors to the plasma membrane that leads to intracellular Ca^{2+} increase and consequently to the activation of anoctamins (Ano1 and Ano6)[120, 160, 161]. Additionally, it has been shown that Ano6 interacts with CFTR either directly or indirectly via scaffold proteins[120]. As it has been found within this thesis Ano6 expression is also affected by Ano1 as well as ENaC by unknown mechanisms. Furthermore, CFTR is known to regulate ENaC[162]. Together, all these facts suggest a relationship between these membrane channels in the airway epithelium. Further research is required to unravel the mechanisms of this crosstalk.

Another interesting observation resulting from this pilot screen was that regulators of apoptosis increase Ano6 traffic to the membrane. This supports the notion of Ano6 being involved in cell death[49].

Altogether, these results indicate that the cells expressing double-tagged Ano6 that we used in this pilot screen constitute a robust model for future high-content siRNA microscopy screens. Moreover, the results obtained are very encouraging to pursue more in-depth studies to identify regulators of anoctamins, as well as to further study the interaction between anoctamins, ENaC and CFTR. Nonetheless, the use of larger siRNA libraries, the increase of replicates for every siRNA and a secondary validation of primary hits (confirmation with additional siRNAs for the same gene) are crucial steps to achieve this goal.

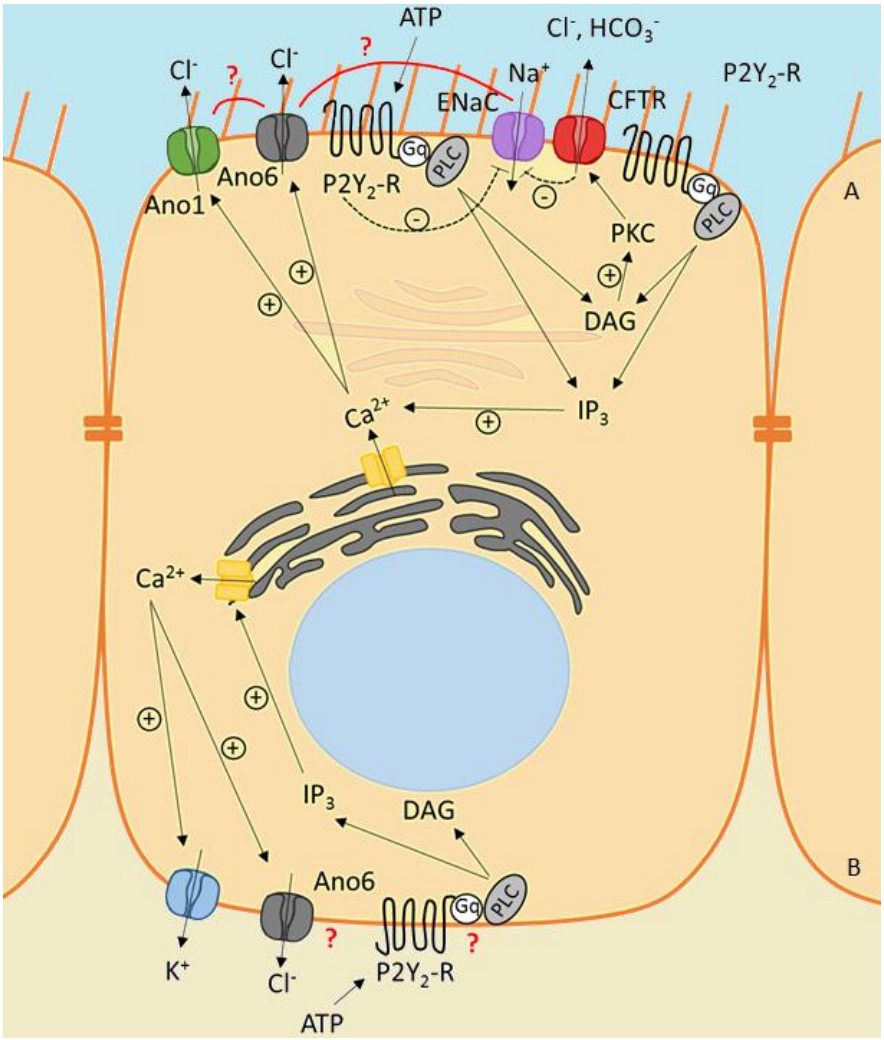

Figure 31 - **Model of ion transport across airway epithelial cells. A – Apical membrane; B – Basolateral membrane. $P2Y_2$ purinergic receptors ($P2Y_2$-R) are represented in both apical and basolateral membranes, although they have been reported as mostly localized at the apical membrane[155]. Ano1, Ano6, CFTR and ENaC are represented in the apical membrane. Ano6 is also possibly localized at the basolateral membrane. K^+ channel is represented in the basolateral membrane, being responsible for the driving force that increases anion efflux across the apical membrane. Ca^{2+} channel is located at the ER, where IP_3 binds, originating the release of Ca^{2+} ions to the cytoplasm, which then leads to the activation of Ca^{2+}-activated channels. ATP stimulation of $P2Y_2$-R was also shown to inhibit ENaC-mediated Na^+ influx, possibly due to PIP_2 hydrolysis. CFTR inhibits ENaC. ENaC and Ano1 possibly interact with Ano6, although through unknown mechanisms.**

4. Concluding remarks

We have herein generated novel cellular models stably expressing 3-HA – GFP double-tagged Ano6 and Ano9 under an inducible (Tet-On) promoter. The purpose of the new cell models is to study the traffic of anoctamins in automated fluorescence microscopy screens and to identify factor that affect their traffic by siRNA-knockdown.

The new cell lines were characterized regarding the anoctamins' cellular expression, localization and function. Ano6 was found to be localized at the plasma membrane, and showed increased ion currents upon stimulation with ATP, confirming its known function as a channel. In contrast, overexpressed Ano9 showed a predominantly intracellular localization and no ATP-activated ion currents, which is also suggested by other studies. Thus, these cell lines appear to be good models for further studies on anoctamins' traffic, regulation, localization and interaction with other ion channels/proteins in the airway epithelium. Moreover, these models are valuable tools to explore the roles of anoctamins in disease, particularly in CF.

In addition, the novel CFBE cell line overexpressing Ano6 was used in a pilot siRNA screen which identified 71 genes affecting the traffic of Ano6: 34 genes inhibiting and 37 enhancing Ano6 traffic. The results thus obtained demonstrate that the traffic of Ano6 to the plasma membrane is affected by several genes that affect CFTR traffic, increasing the interest and motivation for further studies on these proteins' interactions. Moreover, these preliminary results also showed that Ano1 and ENaC affect Ano6 traffic, which further indicates a relation among these ion channels and reflects the relevance of the study of this protein family of anoctamins to find alternative therapeutic targets for CF.

Altogether, these results suggest that the new CFBE cell line expressing double-tagged Ano6, which we generated and validated with this pilot screen, constitutes a *bona fide* model for future high-content siRNA microscopy screens.

Future work using the Ano9 overexpressing cell line will demonstrate the feasibility of this cell line for similar studies. Furthermore, a novel generated Ano10 construct will also be used to develop a similar stable (inducible) cell line (see next section).

In conclusion, the work developed during this MSc thesis not only supports the importance of anoctamins' study to a better comprehension of epithelial ion transport, but also reinforces the relevance of these proteins for the development of "bypass therapies" to overcome the ion transport defects caused by the loss of functional CFTR in CF.

5. Future perspectives

The results obtained here with the robust cellular models generated are very encouraging to further pursue the study of anoctamins' regulators, as well as the study of the crosstalk between anoctamins and CFTR.

The main proposed objective for this project (i.e. to perform siRNA screens to detect traffic regulators of anoctamins) was only initiated in the time frame available for this thesis. However, since the mutagenesis, cloning, and production of stable cell lines were the limiting steps of the present work, interesting experiments can now be planned and designed for future work, as next described.

Firstly, Ano10 is being cloned into the same lentiviral vector as Ano6 and Ano9 (pLVX-TRE3G), so that similar stable cell lines with inducible expression of double-tagged Ano10 (GFP and 3-HA) can be generated. This will allow the study of one more "epithelial anoctamin", and possibly help unveiling its intriguing functions. As the lentiviral infection is a heterologous process, resulting in different transgene expression among the stably transfected cells, it will be necessary (as for the Ano6/Ano9 cells) to perform cell sorting (according to the cells' GFP fluorescence) in order to obtain cell populations with more homogeneous anoctamin expression. When sorted, these cells will provide more reliable results in future experiments.

Secondly, the crosstalk between anoctamins and CFTR and among anoctamins is a highly interesting topic to study. Thus, to determine whether CFTR and anoctamins physically interact, co-immunoprecipitation assays of CFTR and Ano6, Ano9 and Ano10 should be performed. To this end, we could use CFBE wt- and F508del-CFTR stably expressing Ano6, Ano9 and Ano10 to perform co-immunoprecipitations using anti-CFTR and anti-GFP antibodies.

The interaction among the various anoctamins is also an exciting subject. The results (blots) presented here from the cell-surface biotinylation assays showed that, besides the expected band corresponding to Ano9, an additional band of higher molecular weight was also observed. This band may represent an Ano9 homodimer or a heterodimer. To identify the unknown protein(s) present in this band, the sample will be sent for analysis by NanoLC-MS/MS (nanoscale liquid chromatography coupled to tandem mass spectrometry). To further search for interactions among anoctamin family members, co-immunoprecipitation assays will also be performed.

Thirdly, to further define the functional interaction between CFTR and anoctamins, it would be very important to determine how anoctamins affect CFTR currents, and vice-versa. To this end, it is possible to use cells that overexpress wt- or mutant CFTR, and simultaneously Ano6, 9 or 10. Functional assays like micro-Ussing chamber and iodide efflux are valuable tools in this matter, since these techniques allow to detect whether CFTR function is compromised or enhanced by the overexpression of these anoctamins. Similarly, it would also be pertinent to study CFTR in cells with absence of each one of the anoctamins under study. To this end, the Ano6 knockout cell line has already been initiated in CFBE 41o-, CFBE wt- and CFBE F508del-CFTR cells, although the absence of Ano6 has not yet been confirmed. For the remaining anoctamins studied in this project, the gRNAs are currently being designed. Since the antibiotic selection and the growth of the knockout clones are two major limiting steps, the cells transfected with the plasmids needed for anoctamin knockout (gRNAs and the Cas9 GFP tagged

plasmid) will also be sorted according to their GFP fluorescence. Once the anoctamin knockout in these cells is confirmed, they could be used to study CFTR function, also by functional assays like iodide efflux and micro-Ussing chamber. These experiments would allow the detection of differences in CFTR function caused by the absence of each of these anoctamins. Furthermore, functional assays using these knockout cells can permit to distinguish the contribution of each anoctamin to the currents caused by ATP stimulation, overcoming the problem of lack of specific anoctamin inhibitors. Since there is evidence suggesting that Ano9 overexpression inhibits Ano1 currents, the Ano9 knockout in cells overexpressing Ano1 (created by Joana Lérias, from our research group) could confirm if the absence of Ano9 enhances the currents created by Ano1. If Co-IP assays lead to the detection of interactions between anoctamins, those results can also be confirmed using this knockout strategy.

Fourthly, as anoctamins were shown to affect cell movement and proliferation, wound healing assays can also be made using anoctamin knockout cells or cells overexpressing anoctamins. The results obtained with these studies could provide insight into the role of these proteins in disease. Moreover, HeLa H_2B mCherry cells stably expressing double-tagged Ano6, 9 and 10, will be used to perform live-cell imaging assays with the objective of studying the subcellular localization of overexpressed anoctamins during different phases of the cell cycle.

Fifthly, the first double-tagged constructs of Ano6, Ano9 and Ano10 that were not used for further experiments (as their HA-tags were not facing the exterior of the cell) might be useful to study anoctamins' traffic. Particularly the first Ano6 construct, which probably originates a misfolded protein, can be used to test compounds that promote the correct protein folding and trafficking to the membrane. Since some compounds have already been shown to partially rescue traffic of F508del-CFTR, allowing some amount of protein to reach the plasma membrane, it would be interesting to study the effect of these compounds in misfolded Ano6. This would possibly improve the understanding of the mechanism of action of these compounds.

Finally, although there are many experiments that can be performed with these new cellular models of anoctamins, the main goal is use them to perform high-content siRNA screens so as to identify novel genes regulating the traffic of Ano6, Ano9 and Ano10. The pilot screen performed here with CFBE Ano6 cells revealed that this is a robust system to identify novel genes affecting the traffic of this anoctamin. Accordingly, additional screens will be performed with the stably transfected cell lines expressing the other anoctamins. The main objective is to use a high-content siRNA library, so that we gain deep insight into the pathways that regulate anoctamins traffic.

The continuation of the work developed during this project is thus crucial to deepen the knowledge on this protein family of increasing biological relevance. The understanding of the crosstalk between CFTR and anoctamins, as well as their regulation pathways is essential to possibly find alternative pharmacological targets for CF disease. If the functional interactions between CFTR and this protein family are indeed revealed, new drugs can be designed to enhance Cl^- secretion (possibly by overstimulating anoctamins, since their expression/activity in the airways is much lower than that of CFTR) and restore the basic defect in all CF patients, independently of the CFTR mutation types they bear.

6. References

[1] Collins, F. S. Cystic Fibrosis: Molecular Biology and Therapeutic Implications. *Science.* **256,** 774–779 (1992);

[2] Amaral, M. D. Novel personalized therapies for cystic fibrosis: treating the basic defect in all patients. *J. Intern. Med.* **277,** 155–166 (2015);

[3] Bobadilla, J. L., Macek, M., Fine, J. P. & Farrell, P. M. Cystic fibrosis: A worldwide analysis of CFTR mutations - Correlation with incidence data and application to screening. *Hum. Mutat.* **19,** 575–606 (2002);

[4] O'Sullivan, B. P. & Freedman, S. D. Cystic fibrosis. *Lancet* **373,** 1891–1904 (2009);

[5] Andersen, H. Cystic Fibrosis of the pancreas and its relation to celiac disease. *Am J Dis Child* **56,** 344–399 (1938);

[6] Riordan, J. R. *et al.* Identification the Cystic Fibrosis Gene : Cloning and Characterization of Complementary DNA. *Science.* **245,** 1066–73 (1989);

[7] Hug, M. J., Tamada, T. & Bridges, R. J. CFTR and bicarbonate secretion to epithelial cells. *News Physiol. Sci.* **18,** 38–42 (2003);

[8] Sheppard, D. N. & Welsh, M. J. Structure and function of the CFTR chloride channel. *Physiol. Rev.* **79,** S23–S45 (1999);

[9] Reddy, M. M., Light, M. J. & Quinton, P. M. Activation of the epithelial Na+ channel (ENaC) requires CFTR Cl- channel function. *Nature* **402,** 301–304 (1999);

[10] Kunzelmann, K., Kathöfer, S. & Greger, R. Na+ and Cl- conductances in airway epithelial cells: increased Na+ conductance in cystic fibrosis. *Pflügers Arch. Eur. J. Physiol.* **431,** 1–9 (1995);

[11] Cohen, T. S. & Prince, A. Cystic fibrosis: a mucosal immunodeficiency syndrome. *Nat. Med.* **18,** 509–519 (2012);

[12] Gaspar, M. C., Couet, W., Olivier, J.-C., Pais, A. A. C. C. & Sousa, J. J. S. Pseudomonas aeruginosa infection in cystic fibrosis lung disease and new perspectives of treatment: a review. *Eur. J. Clin. Microbiol. Infect. Dis.* **32,** 1231–52 (2013);

[13] Rowe, S., Miller, S. & Sorscher, E. Cystic fibrosis. *N Engl J Med* **352,** 1992–2001 (2005);

[14] Saiman, L. Microbiology of early CF lung disease. *Paediatr. Respir. Rev.* **5,** 367–369 (2004);

[15] Cutting, G. R. Cystic fibrosis genetics: from molecular understanding to clinical application. *Nat. Rev. Genet.* **16,** 45–56 (2014);

[16] Zielenski, J. Genotype and phenotype in cystic fibrosis. *Respiration* **67,** 117–133 (2000);

[17] Kerem, B. *et al.* Identification of the Cystic Fibrosis gene: Genetic Analysis. *Science.* **245,** 1073–1080 (1989);

[18] Ratjen, F. & Döring, G. Cystic fibrosis. *Lancet* **361,** 681–689 (2003);

[19] Quinton, P. Physiological Basis of Cystic Fibrosis: A Historical Perspective. *Physiol Rev* **79,** S3–S22 (1999);

[20] Stern, M. *et al.* European Cystic Fibrosis Society Standards of Care: Quality Management in cystic fibrosis. *J. Cyst. Fibros.* **13,** S43–S59 (2014);

[21] CF Foundation Patient Registry Data: https://www.cff.org/2013_CFF_Patient_Registry_Annual_Data_Report.pdf;

[22] Amaral, M. D. & Farinha, C. M. Rescuing mutant CFTR: a multi-task approach to a better outcome in treating cystic fibrosis. *Curr. Pharm. Des.* **19,** 3497–508 (2013);

[23] Crystal, R. G. *et al.* Administration of an adenovirus containing the human CFTR cDNA to the respiratory tract of individuals with cystic fibrosis. *Nat. Genet.* **8,** 42–51 (1994);

[24] Crystal, R. G. The Challenge of Using Gene- or Cell-Based Therapies to Treat Lung Disease. *Mol. Ther.* **20,** 1077–1078 (2012);

[25] Alton, E. W. F. W. et al. Repeated nebulisation of non-viral CFTR gene therapy in patients with cystic fibrosis: a randomised, double-blind, placebo-controlled, phase 2b trial. *Lancet Respir Med* **2600**, 1–9 (2015);

[26] Riordan, J. R. CFTR function and prospects for therapy. *Annu. Rev. Biochem.* **77,** 701–726 (2008);

[27] Solomon, G. M., Marshall, S. G., Ramsey, B. W. & Rowe, S. M. Breakthrough therapies: Cystic fibrosis (CF) potentiators and correctors. *Pediatr. Pulmonol.* (2015);

[28] McCarthy, V. a. & Harris, A. The CFTR gene and regulation of its expression. *Pediatr. Pulmonol*., 1–8 (2005);

[29] Bell, S. C., De Boeck, K. & Amaral, M. D. New pharmacological approaches for cystic fibrosis: Promises, progress, pitfalls. *Pharmacol. Ther.* **145,** 19–34 (2014);

[30] De Boeck, K. & Amaral, M. D. *Lancet Resp Med*, submitted (2015);

[31] The Cystic Fibrosis mutation database. http://www.genet.sickkids.on.ca/app;

[32] Amaral, M. D. & Kunzelmann, K. Molecular targeting of CFTR as a therapeutic approach to cystic fibrosis. *Trends Pharmacol. Sci.* **28,** 334–341 (2007);

[33] Li, C. & Naren, A. P. Macromolecular complexes of cystic fibrosis transmembrane conductance regulator and its interacting partners. *Pharmacol. Ther.* **108,** 208–223 (2005);

[34] Gadsby, D. C., Vergani, P. & Csanády, L. The ABC protein turned chloride channel whose failure causes cystic fibrosis. *Nature* **440,** 477–483 (2006);

[35] Riordan, J. R. Assembly of functional CFTR chloride channels. *Annu. Rev. Physiol.* **67,** 701–718 (2005);

[36] Amaral, M. D. Processing of CFTR: Traversing the cellular maze - How much CFTR needs to go through to avoid cystic fibrosis? *Pediatr. Pulmonol.* **39,** 479–491 (2005);

[37] Linsdell, P. & Hanrahan, J. W. Glutathione permeability of CFTR. *Am. J. Physiol.* **275,** C323–C326 (1998);

[38] Wei, L. *et al.* Interaction between calcium-activated chloride channels and the cystic fibrosis transmembrane conductance regulator. *Pflügers Arch. Eur. J. Physiol.* **438,** 635–641 (1999);

[39] Perez-Cornejo, P. & Arreola, J. Regulation of Ca2+-activated chloride channels by cAMP and CFTR in parotid acinar cells. *Biochem. Biophys. Res. Commun.* **316,** 612–617 (2004);

[40] Ousingsawat, J., Kongsuphol, P., Schreiber, R. & Kunzelmann, K. CFTR and TMEM16A are separate but functionally related Cl - channels. *Cell. Physiol. Biochem.* **28,** 715–724 (2011);

[41] Kunzelmann, K. & Schreiber, R. CFTR, a regulator of channels. *J. Membr. Biol.* **168,** 1–8 (1999);

[42] Schwiebert, E. M. *et al.* CFTR regulates outwardly rectifying chloride channels through an autocrine mechanism involving ATP. *Cell* **81,** 1063–1073 (1995);

[43] Kunzelmann, K. *et al.* The cystic fibrosis transmembrane conductance regulator attenuates the endogenous Ca2+ activated Cl- conductance of Xenopus oocytes. *Pflugers Arch. Eur. J. Physiol.* **435,** 178–181 (1997);

[44] Perez-Cornejo, P. & Arreola, J. Regulation of Ca2+-activated chloride channels by cAMP and CFTR in parotid acinar cells. *Biochem. Biophys. Res. Commun.* **316,** 612–617 (2004);

[45] Clarke, LL., Boucher RC. Chloride secretory response to extracellular ATP in human normal and cystic fibrosis nasal epithelia. *Am J Physiol.* **263,** 348-356 (1992);

[46] Mall, M. *et al.* Modulation of Ca2+-activated Cl- secretion by basolateral K+ channels in human normal and cystic fibrosis airway epithelia. *Pediatr. Res.* **53,** 608–618 (2003);

[47] Yang, Y. D. *et al.* TMEM16A confers receptor-activated calcium-dependent chloride conductance. *Nature* **455,** 1210–1215 (2008);

[48] Caputo, A. *et al.* TMEM16A, a membrane protein associated with calcium-dependent chloride channel activity. *Science* **322,** 590–594 (2008);

[49] Martins, J. R. *et al.* Anoctamin 6 is an essential component of the outwardly rectifying chloride channel. *Proc. Natl. Acad. Sci.* **108,** 18168–18172 (2011);

[50] Kunzelmann, K. TMEM16, LRRC8A, bestrophin: chloride channels controlled by Ca2+ and cell volume. *Trends Biochem. Sci.* 1–9 (2015);

[51] Miledi, R. A calcium-dependent transient outward current in Xenopus laevis oocytes. *Proc. R. Soc. Lond. B. Biol. Sci.* **215,** 491–497 (1982);

[52] Bader, B., Bertrand, D. & Schwartzt, E. A. Voltage-Activated and Calcium-Activated Currents studied in solitary rod inner segments from the salamander retina. *J Physiol* **331,** 253–284 (1982);

[53] Kunzelmann, K., Milenkovic, V. M., Spitzner, M., Soria, R. B. & Schreiber, R. Calcium-dependent chloride conductance in epithelia: Is there a contribution by Bestrophin? *Pflugers Arch. Eur. J. Physiol.* **454,** 879–889 (2007);

[54] André, S. *et al.* Axotomy-induced expression of calcium-activated chloride current in subpopulations of mouse dorsal root ganglion neurons. *J. Neurophysiol.* **90,** 3764–3773 (2003);

[55] Matthews, H. R. & Reisert, J. Calcium, the two-faced messenger of olfactory transduction and adaptation. *Curr. Opin. Neurobiol.* **13,** 469–475 (2003);

[56] Angermann, J. E., Sanguinetti, A. R., Kenyon, J. L., Leblanc, N. & Greenwood, I. a. Mechanism of the inhibition of Ca2+-activated Cl- currents by phosphorylation in pulmonary arterial smooth muscle cells. *J. Gen. Physiol.* **128,** 73–87 (2006);

[57] Lalonde, M., Kelly, M. & Barnes, S. Calcium-activated chloride channels in the retina. *Channels* **2,** 252–260 (2008);

[58] Verkman, A. S. & Galietta, L. J. V. Chloride channels as drug targets. *Nat. Rev. Drug Discov.* **8,** 153–171 (2009);

[59] Ferrera, L., Zegarra-Moran, O. & Galietta, L. J. V. Ca^{2+} -Activated Cl^{-} Channels. *Compr. Physiol.* **1,** 2155–2174 (2011);

[60] Galietta, L. J. V. The TMEM16 protein family: a new class of chloride channels? *Biophys. J.* **97,** 3047–3053 (2009);

[61] Hartzell, C., Putzier, I. & Arreola, J. Calcium-activated chloride channels. *Annu. Rev. Physiol.* **67,** 719–758 (2005);

[62] Gruber, a D., Schreur, K. D., Ji, H. L., Fuller, C. M. & Pauli, B. U. Molecular cloning and transmembrane structure of hCLCA2 from human lung, trachea, and mammary gland. *Am. J. Physiol.* **276,** C1261–C1270 (1999);

[63] Huang, P. *et al.* Regulation of human CLC-3 channels by multifunctional Ca2+/calmodulin-dependent protein kinase. *J. Biol. Chem.* **276,** 20093–20100 (2001);

[64] Qu, Z., Wei, R. W., Mann, W. & Hartzell, H. C. Two bestrophins cloned from Xenopus laevis oocytes express Ca(2+)-activated Cl(-) currents. *J. Biol. Chem.* **278,** 49563–49572 (2003);

[65] Gibson, A. *et al.* HCLCA1 and mCLCA3 are secreted non-integral membrane proteins and therefore are not ion channels. *J. Biol. Chem.* **280,** 27205–27212 (2005);

[66] Eggermont, J. Calcium-activated chloride channels: (un)known, (un)loved? *Proc. Am. Thorac. Soc.* **1,** 22–27 (2004);

[67] Schroeder, B. C., Cheng, T., Jan, Y. N. & Jan, L. Y. Expression Cloning of TMEM16A as a Calcium-Activated Chloride Channel Subunit. *Cell* **134,** 1019–1029 (2008);

[68] Kunzelmann, K. *et al.* Anoctamins. *Pflugers Arch. Eur. J. Physiol.* **462,** 195–208 (2011);

[69] Hartzell, H. C., Yu, K., Xiao, Q., Chien, L.-T. & Qu, Z. Anoctamin/TMEM16 family members are Ca2+-activated Cl- channels. *J. Physiol.* **587,** 2127–2139 (2009);

[70] Milenkovic, V. M., Brockmann, M., Stöhr, H., Weber, B. H. & Strauss, O. Evolution and functional divergence of the anoctamin family of membrane proteins. *BMC Evol. Biol.* **10,** 319 (2010);

[71] Pedemonte, N. & Galietta, L. J. V. Structure and function of TMEM16 proteins (anoctamins). *Physiol. Rev.* **94,** 419–59 (2014);

[72] Ferrera, L. *et al.* Regulation of TMEM16A chloride channel properties by alternative splicing. *J. Biol. Chem.* **284,** 33360–33368 (2009);

[73] Duran, C. & Hartzell, H. C. Physiological roles and diseases of Tmem16/Anoctamin proteins: are they all chloride channels? *Acta Pharmacol. Sin.* **32,** 685–692 (2011);

[74] Brunner, J. D., Lim, N. K., Schenck, S., Duerst, A. & Dutzler, R. X-ray structure of a calcium-activated TMEM16 lipid scramblase. *Nature* **516,** 207–212 (2014);

[75] HGNC (HUGO Gene Nomenclature Committee): http://www.genenames.org/;

[76] Yang, H. *et al.* TMEM16F Forms a Ca2+-Activated Cation Channel Required for Lipid Scrambling in Platelets during Blood Coagulation. *Cell* **151,** 111–122 (2012);

[77] Fallah, G. *et al.* TMEM16A(a)/anoctamin-1 shares a homodimeric architecture with CLC chloride channels. *Mol. Cell. Proteomics* **10,** M110.004697 (2011);

[78] Sheridan, J. T. *et al.* Characterization of the oligomeric structure of the Ca(2+)-activated Cl- channel Ano1/TMEM16A. *J. Biol. Chem.* **286,** 1381–1388 (2011);

[79] Tien, J., Lee, H. Y., Minor, D. L., Jan, Y. N. & Jan, L. Y. Identification of a dimerization domain in the TMEM16A calcium-activated chloride channel (CaCC). *Proc. Natl. Acad. Sci. U. S. A.* **110,** 6352–7 (2013);

[80] Schreiber, R. *et al.* Expression and function of epithelial anoctamins. *J. Biol. Chem.* **285,** 7838–7845 (2010);

[81] Kunzelmann, K. *et al.* Expression and function of epithelial anoctamins. *Exp. Physiol.* **97,** 184–192 (2012);

[82] Tian, Y., Schreiber, R. & Kunzelmann, K. Anoctamins are a family of Ca2+ activated Cl- channels. *J. Cell Sci.* (2012);

[83] Pifferi, S., Dibattista, M. & Menini, A. TMEM16B induces chloride currents activated by calcium in mammalian cells. *Pflugers Arch. Eur. J. Physiol.* **458,** 1023–1038 (2009);

[84] Ousingsawat, J. *et al.* Loss of TMEM16A causes a defect in epithelial Ca2+ -dependent chloride transport. *J. Biol. Chem.* **284,** 28698–28703 (2009);

[85] Romanenko, V. G. *et al.* Tmem16A encodes the Ca2+-activated Cl- channel in mouse submandibular salivary gland acinar cells. *J. Biol. Chem.* **285,** 12990–13001 (2010);

[86] Tian, Y. *et al.* Calmodulin-dependent activation of the epithelial calcium-dependent chloride channel TMEM16A. *FASEB J.* **25,** 1058–1068 (2011);

[87] Stöhr, H. *et al.* TMEM16B, a novel protein with calcium-dependent chloride channel activity, associates with a presynaptic protein complex in photoreceptor terminals. *J. Neurosci.* **29,** 6809–6818 (2009);

[88] Pifferi, S., Cenedese, V. & Menini, A. Anoctamin 2/TMEM16B: a calcium-activated chloride channel in olfactory transduction. *Exp. Physiol.* **97,** 193–9 (2012);

[89] Huang, F. *et al.* TMEM16C facilitates Na(+)-activated K(+) currents in rat sensory neurons and regulates pain processing. *Nat. Neurosci.* **16,** 1284–1290 (2013);

[90] Shimizu, T. *et al.* TMEM16F is a component of a Ca2+-activated Cl- channel but not a volume-sensitive outwardly rectifying Cl- channel. *Am. J. Physiol. Cell Physiol.* **304,** C748–59 (2013);

[91] Kunzelmann, K. *et al.* Molecular functions of anoctamin 6 (TMEM16F): A chloride channel, cation channel, or phospholipid scramblase? *Pflugers Arch. Eur. J. Physiol.* **466,** 407–414 (2014);

[92] Suzuki, J. & Nagata, S. Calcium-dependent phospholipid scrambling by TMEM16F. *Nature* **468,** 834–840 (2010);

[93] Sanyal, S. & Menon, A. K. Flipping lipids: Why an' what's the reason for? *ACS Chem. Biol.* **4,** 895–909 (2009);

[94] Lentz, BR. Exposure of platelet membrane phosphatidylserine regulates blood coagulation. *Prog Lipid Res*. **42,** 423-438 (2003);

[95] Suzuki, J. *et al.* Calcium-dependent phospholipid scramblase activity of TMEM16 protein family members. *J. Biol. Chem.* **288,** 13305–16 (2013);

[96] Almaça, J. *et al.* TMEM16 proteins produce volume-regulated chloride currents that are reduced in mice lacking TMEM16A. *J. Biol. Chem.* **284,** 28571–28578 (2009);

[97] Juul, C. a. *et al.* Anoctamin 6 differs from VRAC and VSOAC but is involved in apoptosis and supports volume regulation in the presence of Ca2+. *Pflugers Arch. Eur. J. Physiol.* 1–12 (2014);

[98] Malvezzi, M. *et al.* Ca2+-dependent phospholipid scrambling by a reconstituted TMEM16 ion channel. *Nat Commun* **4:** 2367 (2013);

[99] Scudieri, P. *et al.* Ion channel and lipid scramblase activity associated with expression of TMEM16F/ANO6 isoforms. *J. Physiol.* **593,** 3829–3848 (2015);

[100] Jacobsen, K. S. *et al.* The role of TMEM16A (ANO1) and TMEM16F (ANO6) in cell migration. *Pflugers Arch. Eur. J. Physiol.* **465,** 1753–1762 (2013);

[101] Szteyn, K. *et al.* Expression and Functional Significance of the Ca2+-Activated Cl- Channel ANO6 in Dendritic Cells. *Cell. Physiol. Biochem.* **30,** 1319–1332 (2012);

[102] Wanitchakool, P. *et al.* Role of anoctamins in cancer and apoptosis. *Phil Trans R Soc B* **369,** 1–8 (2014);

[103] Galindo, B. E. & Vacquier, V. D. Phylogeny of the TMEM16 protein family: some members are overexpressed in cancer. *Int. J. Mol. Med.* **16,** 919–924 (2005);

[104] Miwa, S., Nakajima, T., Murai, Y., Takano, Y. & Sugiyama, T. Mutation assay of the novel gene DOG1 in gastrointestinal stromal tumors (GISTs). *J. Gastroenterol.* **43,** 531–537 (2008);

[105] Kunzelmann, K. Ion channels and cancer. *J. Membr. Biol.* **205,** 159–173 (2005);

[106] Dutertre, M. *et al.* Exon-based clustering of murine breast tumor transcriptomes reveals alternative exons whose expression is associated with metastasis. *Cancer Res.* **70,** 896–905 (2010);

[107] West, R. B. *et al.* The novel marker, DOG1, is expressed ubiquitously in gastrointestinal stromal tumors irrespective of KIT or PDGFRA mutation status. *Am. J. Pathol.* **165,** 107–113 (2004);

[108] Britschgi, A. *et al.* Calcium-activated chloride channel ANO1 promotes breast cancer progression by activating EGFR and CAMK signaling. *Proc. Natl. Acad. Sci. U. S. A.* **110,** E1026–34 (2013);

[109] Carles, A. *et al.* Head and neck squamous cell carcinoma transcriptome analysis by comprehensive validated differential display. *Oncogene* **25,** 1821–1831 (2006);

[110] Huang, X., Godfrey, T. E., Gooding, W. E. & M.Gollin, S. Comprehensive Genome and Transcriptome Analysis of the 11q13 Amplicon in Human Oral Cancer and Synteny to the 7F5 Amplicon in Murine Oral Carcinoma. *Genes. Chromosomes Cancer* **45,** 1058–1069 (2006);

[111] Das, S. *et al.* NGEP, a prostate-specific plasma membrane protein that promotes the association of LNCaP cells. *Cancer Res.* **67,** 1594–1601 (2007);

[112] Tsutsumi, S. *et al.* The novel gene encoding a putative transmembrane protein is mutated in gnathodiaphyseal dysplasia (GDD). *Am. J. Hum. Genet.* **74,** 1255–1261 (2004);

[113] Marconi, C. *et al.* A novel missense mutation in ANO5/TMEM16E is causative for gnathodiaphyseal dyplasia in a large Italian pedigree. *Eur. J. Hum. Genet.* **21,** 613–619 (2013);

[114] Charlesworth, G. *et al.* Mutations in ANO3 cause dominant craniocervical dystonia: Ion channel implicated in pathogenesis. *Am. J. Hum. Genet.* **91,** 1041–1050 (2012);

[115] Balreira, A. *et al.* ANO10 mutations cause ataxia and coenzyme Q10 deficiency. *J. Neurol.* **261,** 2192–2198 (2014);

[116] Rock, J. R., Futtner, C. R. & Harfe, B. D. The transmembrane protein TMEM16A is required for normal development of the murine trachea. *Dev. Biol.* **321,** 141–149 (2008);

[117] Kojima, H. *et al.* Production and characterization of transformed B-lymphocytes expressing the membrane defect of Scott syndrome. *J. Clin. Invest.* **94,** 2237–2244 (1994);

[118] Faria, D., Schreiber, R., Kunzelmann, K. CFTR is activated through stimulation of purinergic P2Y2 receptors. *Pflugers Arch. Eur. J. Physiol.* **457,** 1373-1380 (2009);

[119] Namkung, W., Finkbeiner, W. E. & Verkman, A. S. CFTR-Adenylyl Cyclase I Association Responsible for UTP Activation of CFTR in Well-Differentiated Primary Human Bronchial Cell Cultures. *Mol. Biol. Cell* **21,** 2639–2648 (2010);

[120] Kunzelmann, K. & Mehta, A. CFTR: A hub for kinases and crosstalk of cAMP and Ca2+. *FEBS J.* **280,** 4417–4429 (2013);

[121] Rock, J. R. *et al.* Transmembrane protein 16A (TMEM16A) is a Ca2+ -regulated Cl- secretory channel in mouse airways. *J. Biol. Chem.* **284,** 14875–14880 (2009);

[122] Egan, M. *et al.* Defective regulation of outwardly rectifying Cl− channels by protein kinase A corrected by insertion of CFTR. *Nature* **358,** 581-584 (1992);

[123] Kongsuphol, P., Schreiber, R., Kraidith, K. & Kunzelmann, K. CFTR induces extracellular acid sensing in Xenopus oocytes which activates endogenous Ca 2+-activated Cl - conductance. *Pflugers Arch. Eur. J. Physiol.* **462,** 479–487 (2011);

[124] Anderson, M. P. & Welsh, M. J. Calcium and cAMP activate different chloride channels in the apical membrane of normal and cystic fibrosis epithelia. *Proc. Natl. Acad. Sci. U. S. A.* **88,** 6003–6007 (1991);

[125] Mall, M. a. & Galietta, L. J. V. Targeting ion channels in cystic fibrosis. *J. Cyst. Fibros.* **14,** 561-570 (2015);

[126] The Universal Protein Resource (UniProt): http://www.uniprot.org/;

[127] Geneious Software: http://www.geneious.com/download;

[128] Y Zhang. I-TASSER server for protein 3D structure prediction. *BMC Bioinformatics*, **9,** 40 (2008). http://zhanglab.ccmb.med.umich.edu/I-TASSER/;

[129] The PyMOL Molecular Graphics System, Version 1.7.5.0 Schrödinger, LLC**;**

[130] Ehrhardt, C. *et al.* Towards an in vitro model of cystic fibrosis small airway epithelium: characterisation of the human bronchial epithelial cell line CFBE41o-. *Cell Tissue Res.* **323,** 405–415 (2006);

[131] Bebok, Z. *et al.* Failure of cAMP agonists to activate rescued deltaF508 CFTR in CFBE41o- airway epithelial monolayers. *J. Physiol.* **569,** 601–615 (2005);

[132] Almaça, J. *et al.* Functional Genomics Assays to Study CFTR Traffic and ENaC Function. *Methods Mol. Biol.* **742,** 249–264 (2011);

[133] Graham, F. L., Smiley, J., Russell, W. C. & Nairn, R. Characteristics of a human cell line transformed by DNA from human adenovirus type 5. *J. Gen. Virol.* **36,** 59–74 (1977);

[134] Shaw, G., Morse, S., Ararat, M. & Graham, F. L. Preferential transformation of human neuronal cells by human adenoviruses and the origin of HEK 293 cells. *FASEB J.* **16,** 869–871 (2002);

[135] Hsu, S. *et al.* Genetic characteristics of the HeLa cell. *Science.* **191,** 392–394 (1976);

[136] Landry, J. J. M. *et al.* The genomic and transcriptomic landscape of a HeLa cell line. *G3 (Bethesda).* **3,** 1213–24 (2013);

[137] Erfle, H. *et al.* Reverse transfection on cell arrays for high content screening microscopy. *Nat. Protoc.* **2,** 392–399 (2007);

[138] Mali, P. *et al.* RNA-Guided Human Genome Engineering via Cas9. *Science.* **339,** 823–6 (2013);

[139] Cong, L., Ran, F., Cox, D., Lin, S. & Barretto, R. Multiplex Genome Engineering Using CRISPR / Cas Systems. *Science.* **819,** (2013);

[140] Singh, P., Schimenti, J. C. & Bolcun-Filas, E. A Mouse Geneticist's Practical Guide to CRISPR Applications. *Genetics.* **199,** 1–15 (2014);

[141] Clontech CRISPR/Cas9 system for targeted genome editing: http://www.clontech.com/US/Products/Genome_Editing/CRISPR_Cas9/Resources/About_CRISPR_Cas9;

[142] National Center for Biotechnology Information (NCBI) database: http://www.ncbi.nlm.nih.gov/gene/;

[143] Tool for gRNA design: http://www.e-crisp.org/E-CRISP/designcrispr.html;

[144] Bradford Protein Assay. *Bio-protocol* Bio101: e45 (2011). http://www.bio-protocol.org/e45;

[145] Botelho, H. M. *et al.* Protein Traffic Disorders: an Effective High-Throughput Fluorescence Microscopy Pipeline for Drug Discovery. *Sci. Rep.* **5,** 9038 (2015);

[146] R: The R Project for Statistical Computing: http://www.r-project.org/;

[147] Duran, C., Qu, Z., Osunkoya, a. O., Cui, Y. & Hartzell, H. C. ANOs 3-7 in the anoctamin/Tmem16 Cl- channel family are intracellular proteins. *AJP Cell Physiol*. **302**, C482–C493 (2012);

[148] Boedtkjer, D. M. B., Kim, S., Jensen, a B., Matchkov, V. M. & Andersson, K. E. New selective inhibitors of calcium-activated chloride channels-T16A inh -A01, CaCC inh -A01, and MONNA-what do they inhibit? *Br. J. Pharmacol*. (2015);

[149] Paradiso, a M., Ribeiro, C. M. & Boucher, R. C. Polarized signaling via purinoceptors in normal and cystic fibrosis airway epithelia. *J. Gen. Physiol*. **117**, 53–67 (2001);

[150] Zeng, W., Lee, M. G. & Muallem, S. Membrane-specific regulation of Cl- channels by purinergic receptors in rat submandibular gland acinar and duct cells. *J. Biol. Chem*. **272**, 32956–32965 (1997);

[151] Kellerman, D., Evans, R., Mathews, D. & Shaffer, C. Inhaled P2Y2 receptor agonists as a treatment for patients with Cystic Fibrosis lung disease. *Adv. Drug Deliv*. Rev. **54**, 1463–1474 (2002);

[152] Billet, A. & Hanrahan, J. W. The secret life of CFTR as a calcium-activated chloride channel. *J. Physiol*. **591**, 5273–5278 (2013);

[153] Chambers, L. a., Rollins, B. M. & Tarran, R. Liquid movement across the surface epithelium of large airways. *Respir. Physiol. Neurobiol*. **159**, 256–270 (2007);

[154] Schreiber, R. & Kunzelmann, K. Purinergic P2Y6 receptors induce Ca2+ and CFTR dependent Cl- secretion in mouse trachea. *Cell. Physiol. Biochem*. **16**, 99–108 (2005);

[155] Wolff, S. C., Qi, A.-D., Harden, T. K. & Nicholas, R. a. Polarized expression of human P2Y receptors in epithelial cells from kidney, lung, and colon. *Am. J. Physiol. Cell Physiol.* **288**, C624–32 (2005);

[156] Toczyłowska-Mamińska, R. & Dołowy, K. Ion transporting proteins of human bronchial epithelium. *J. Cell. Biochem*. **113**, 426–432 (2012);

[157] Hwang, T. H., Schwiebert, E. M. & Guggino, W. B. Apical and basolateral ATP stimulates tracheal epithelial chloride secretion via multiple purinergic receptors. *AJP Cell Physiol*. **270**, C1611–C1623 (1996);

[158] Kunzelmann, K. et al. Purinergic inhibition of the epithelial Na+ transport via hydrolysis of PIP2. *FASEB J.* **19**, 142–143 (2005);

[159] Idzko, M., Ferrari, D. & Eltzschig, H. K. Nucleotide signalling during inflammation. *Nature* **509**, 310–317 (2014);

[160] Martins, J. R. et al. F508del-CFTR increases intracellular Ca(2+) signaling that causes enhanced calcium-dependent Cl(-) conductance in cystic fibrosis. *Biochim. Biophys. Acta* **1812**, 1385–92 (2011);

[161] Kunzelmann, K. et al. Airway epithelial cells - Functional links between CFTR and anoctamin dependent Cl- secretion. *Int. J. Biochem. Cell Biol.* **44**, 1897–1900 (2012);

[162] Lazarowski, E. R. & Boucher, R. C. Purinergic receptors in airway epithelia. *Curr. Opin. Pharmacol*. **9**, 262–267 (2009);

[163] Santa Cruz Biotechnology CRISPR-Cas9 system: http://www.scbt.com/pt/crispr-cas9_system.html.

7. Appendices

7.1) Appendix 1 – Vectors

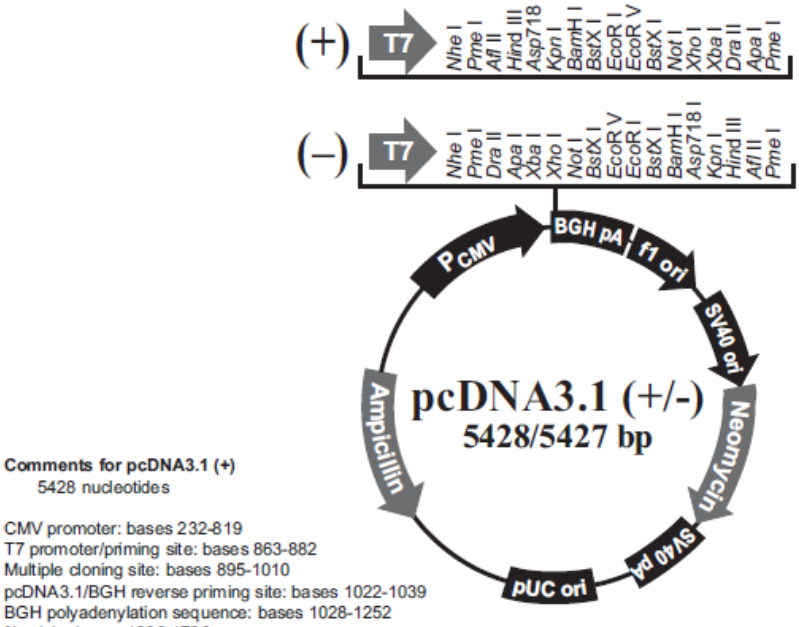

Comments for pcDNA3.1 (+)
5428 nucleotides

CMV promoter: bases 232-819
T7 promoter/priming site: bases 863-882
Multiple cloning site: bases 895-1010
pcDNA3.1/BGH reverse priming site: bases 1022-1039
BGH polyadenylation sequence: bases 1028-1252
f1 origin: bases 1298-1726
SV40 early promoter and origin: bases 1731-2074
Neomycin resistance gene (ORF): bases 2136-2930
SV40 early polyadenylation signal: bases 3104-3234
pUC origin: bases 3617-4287 (complementary strand)
Ampicillin resistance gene (*bla*): bases 4432-5428 (complementary strand)
ORF: bases 4432-5292 (complementary strand)
Ribosome binding site: bases 5300-5304 (complementary strand)
bla promoter (P3): bases 5327-5333 (complementary strand)

Figure 32 - **pcDNA 3.1 plasmid map**

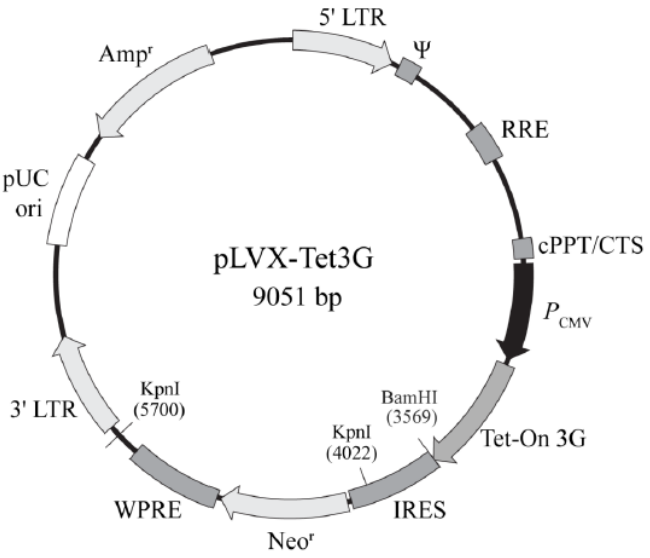

Figure 33 - **pLVX-Tet3G vector map**

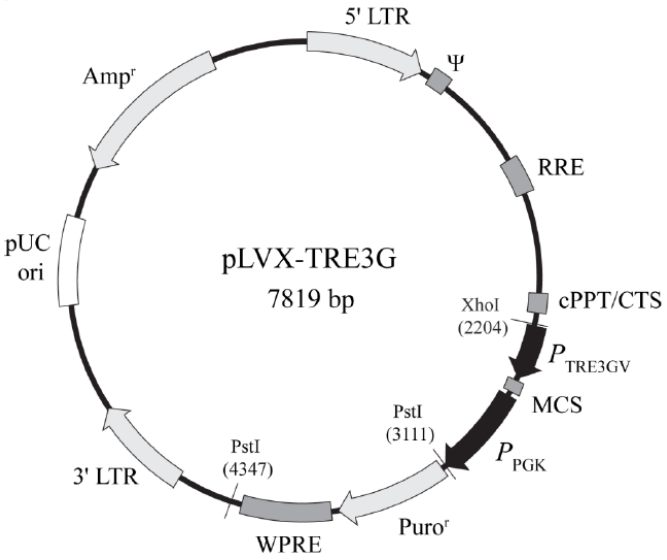

Figure 34 - **pLVX-TRE3G vector map**

```
                                                SmaI
          BamHI      ApaI          NotI         XmaI        MluI       NdeI        EcoRI
2556  GGATCCGGGC CCGCGGCCGC CCCGGGACGC GTCATATGGA ATTC
      CCTAGGCCCG GGCGCCGGCG GGGCCCTGCG CAGTATACCT TAAG
```

Figure 35 - **pLVX-TRE3G multiple cloning site**

7.2) Appendix 2 – Results from DNA sequencing

7.2.1) Primers used for sequencing

Table 1 - **Primers used for DNA sequencing. All primers are forward.**

Anoctamin	Primer sequence
Ano6	5’ – GGATCAACAGAC – 3’
	5’ – GGCTCTCGGTGTTC – 3’
	5’ – GAGCATGGCAGCCC – 3’
	5’ – CATGAGAATCACC – 3’
Ano9	5’ – CTGAGCGGATTCTC – 3’
	5’ – GAGTGCCACGCCAG – 3’
	5’ – GGTTCTGGAGGTG – 3’
Ano10	5’ – GGGAAGACTATGAC – 3’
	5’ – CAAGTCATCCTGG – 3’
	5’ – GAGGCACTCAAGCAG – 3’

7.2.2) Sequencing results – 3-HA tag insertion

A)

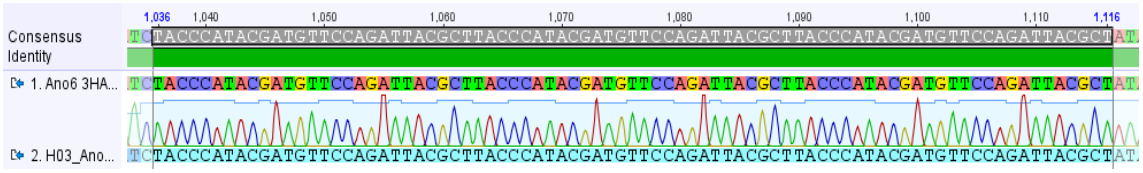

B)

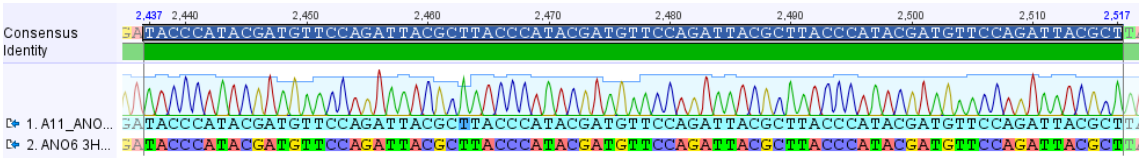

C)

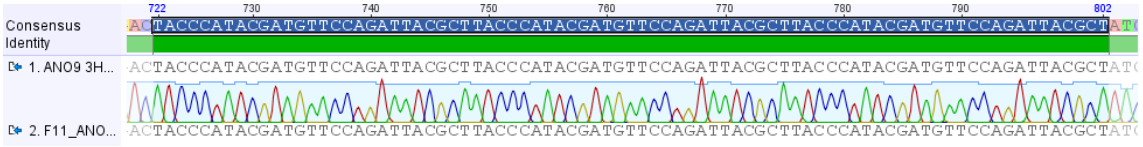

D)

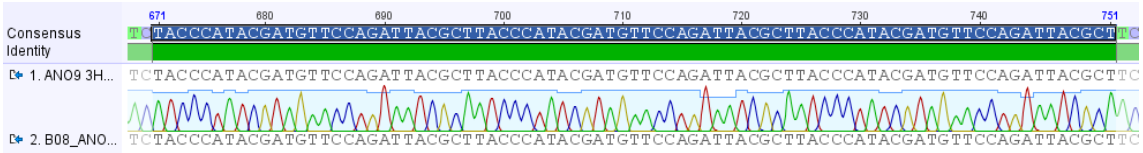

E)

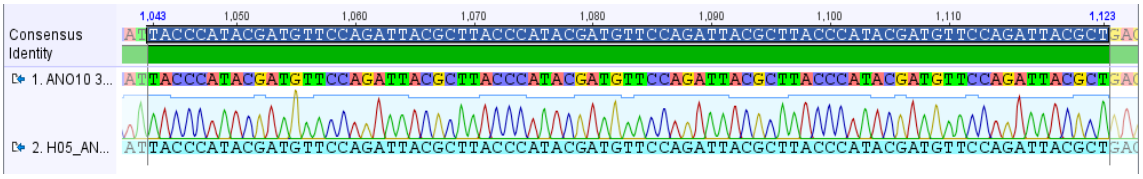

F)

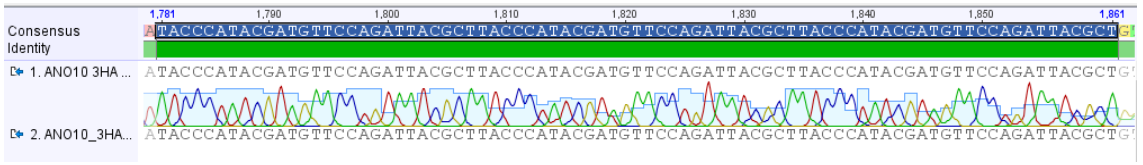

Figure 36 - **Sequencing of 3-HA tag cloned into Anoctamin plasmids. A) and B) Sequencing of the first and second mutagenesis (respectively) of pcDNA 3.1 Ano6 3-HA GFP. C) and D) Sequencing of the first and second mutagenesis of pcDNA 3.1 Ano9 3-HA GFP. E) and F) Sequencing of the first and second mutagenesis of pcDNA 3.1 Ano10 3-HA GFP.**

7.3) Appendix 3 – Primers and PCR conditions used

Table 2 - **Primers for mutagenesis reactions. The table presents only the forward primers. For each, a complementary reverse primer was also used. The 3-HA tag insertion is represented in bold.**

Name	Sequence
Ano6_mut_1	5' – CTGATATTGGTGGCAAGATC**TACCCATACGATGTTCCAGATTACGGCTTACCCATACGA TGTTCCAGATTACGCTTACCCATACGATGTTCCAGATTACGCT**ATAATGTGTCCTCAGTGTG – 3'
Ano6_mut_2	5' – GCAGGTATCGTGATTTCCGA**TACCCATACGATGTTCCAGATTACGCTTACCCATACGATGTTC CAGATTACGCTTACCCATACGATGTTCCAGATTACGCT**TACCCACCTGGACACCCCC – 3'
Ano9_mut_1	5' – GGAGATCTGTGAGGCCCACGAC**TACCCATACGATGTTCCAGATTACGCTTACCCATACGATGT TCCAGATTACGCTTACCCATACGATGTTCCAGATTACGCT**ATCCTCATGTGTCCCCTCGGCG – 3'
Ano9_mut_2	5' – TAGTCTTTCTGAGCGGATTC**TACCCATACGATGTTCCAGATTACGCTTACCCATACGAT GTTCCAGATTACGCTTACCCATACGATGTTCCAGATTACGCT**TCGCTGTTTGAGGCCAGCC – 3'
Ano10_mut_1	5' – GGCCTTGGGTCTACAT**TACCCATACGATGTTCCAGATTACGCTTACCCATACGA TGTTCCAGATTACGCTTACCCATACGATGTTCCAGATTACGCT**GAGAACAGCGGGTCTG – 3'
Ano10_mut_2	5' – TGTCACCACAAGTGAATGCA**TACCCATACGATGTTCCAGATTACGCTTACCCATACGATGTT CCAGATTACGCTTACCCATACGATGTTCCAGATTACGCTGTC**TTTCCAGAATCAAAAG – 3'

Table 3 - **PCR programs used for the mutagenesis reactions of each anoctamin. Mutagenesis 1 corresponds to the first mutagenesis attempt in which the 3-HA tag was not in a correct place. Mutagenesis 2 was the second mutagenesis attempt for each anoctamin.**

Programs used for:	Temperature	Time	Number of cycles
Mutagenesis of Ano6_1	95ºC 95ºC 48ºC 70ºC	2 min 20 s 10 s 4 min 30 s	25
Mutagenesis of Ano6_2	95ºC 95ºC 57ºC 70ºC	2 min 20 s 10 s 4 min 30 s	25
Mutagenesis of Ano9_1	95ºC 95ºC 60ºC 70ºC	2 min 20 s 10 s 4 min 30 s	25
Mutagenesis of Ano9_2	95ºC 95ºC 56ºC 70ºC	2 min 20 s 10 s 4 min 30 s	25
Mutagenesis of Ano10_1	95ºC 95ºC 53ºC 70ºC	2 min 20 s 10 s 4 min 30 s	25
Mutagenesis of Ano10_2	95ºC 95ºC 53ºC 70ºC	2 min 20 s 10 s 4 min 30 s	25

Table 4 - **Primers for colony PCR reactions.**

Name	Sequence
Ano6_1	**Forward:** 5' – GTTGTAGGAGTGGCTTGC – 3'
	Reverse: 5' – CAAAACTGTCGAAGATGCAC – 3'
Ano6_2	**Forward:** 5' – CCACACTTCCTACACCAT – 3'
	Reverse: 5' – GCGTTTTGATACATCGGG – 3'
Ano9_1 and 2	**Forward:** 5' – GCAGCCAGTTGATGAAATC – 3'
	Reverse: 5' – CAAAGAGGTGGGTGAGCT – 3'
Ano10_1	**Forward:** 5' – CATGGTGTCTTGGGTATC – 3'
	Reverse: 5' – GCACATACAACAGGACAC – 3'
Ano10_2	**Forward:** 5' – CAAGTCATCCTGG – 3'
	Reverse: 5' – TTTCATCTGGATATGCCG – 3'

Table 5 - **PCR programs used for the colony PCR reactions of each anoctamin.**

Programs used for:	Temperature	Time	Number of cycles
Ano6_1	94ºC	5 min	35
	94ºC	30 s	
	57ºC	30 s	
	72ºC	1 min	
	72ºC	6 min	
Ano6_2	94ºC	5 min	35
	94ºC	30 s	
	51ºC	30 s	
	72ºC	1 min	
	72ºC	6 min	
Ano9_1 and 2	94ºC	5 min	35
	94ºC	30 s	
	56ºC	30 s	
	72ºC	1 min	
	72ºC	6 min	
Ano10_1	94ºC	5 min	35
	94ºC	30 s	
	54ºC	30 s	
	72ºC	1 min	
	72ºC	6 min	
Ano10_2	94ºC	5 min	35
	94ºC	30 s	
	46ºC	30 s	
	72ºC	1 min	
	72ºC	6 min	

Table 6 – **Primers (forward and reverse) for the PCR reaction of the insertion of 16 bp extensions (extensions in bold).**

Name	Sequence
Ano6	**Forward:** 5' – **TCTTATACTTGGATCC**ATGAAAAAGATGAGCAGGAATGTT – 3'
	Reverse: 5' – **ATTCCATATGACGCGT**TTACTTGTACAGCTCGTCCATGCC – 3'
Ano9	**Forward:** 5' – **TCTTATACTTGGATCC**ATGCAGGGCGAAGAGAGCCTCCGG – 3'
	Reverse: 5' – **ATTCCATATGACGCGT**TTACTTGTACAGCTCGTCCATGCC – 3'
Ano10	**Forward:** 5' – **TCTTATACTTGGATCC**ATGAAAGTGACCTTATCAGCTTTG – 3'
	Reverse: 5' – **ATTCCATATGACGCGT**TTACTTGTACAGCTCGTCCATGCC – 3'

Table 7 - **PCR program used for the insertion of the 16 bp extensions in each anoctamin necessary for cloning into pLVX-TRE3G lentiviral vector.**

Program used for:	Temperature	Time	Number of cycles
Insertion of 16 bp extensions in Ano6, Ano9 and Ano10	95ºC	3 min	35
	95ºC	20 s	
	60ºC	10 s	
	70ºC	5 min	

7.4) Appendix 4 – Structural models of anoctamins with tags and HA immunostaining with and without cell permeabilization

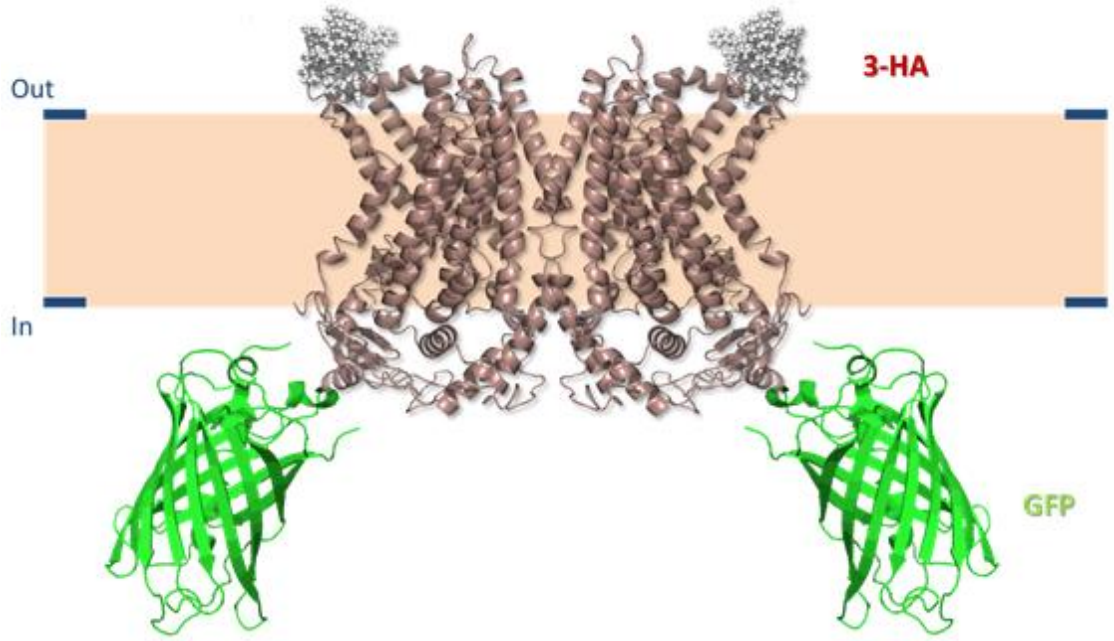

Figure 37 - **Schematic representation of an anoctamin double-tagged construct (3-HA – Triple hemagglutinin tag; GFP – Green Fluorescent Protein) located at the plasma membrane. The predicted dimer structure was obtained using the I-TASSER server (in this case the protein is Ano10 3-HA GFP).**

7.4.1) Anoctamin 6

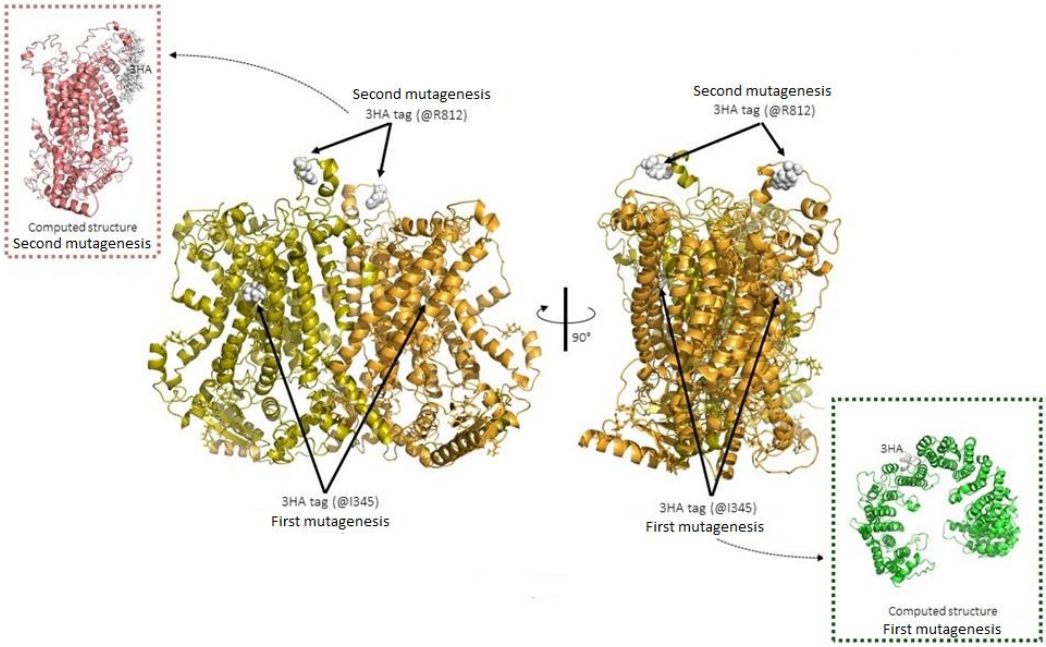

Figure 38 - **Localizations of the 3-HA tag in the two mutagenesis performed for Ano6. Predicted structure of the first and second constructs. (Protein model and image generated by Hugo Botelho, reproduced with permission).**

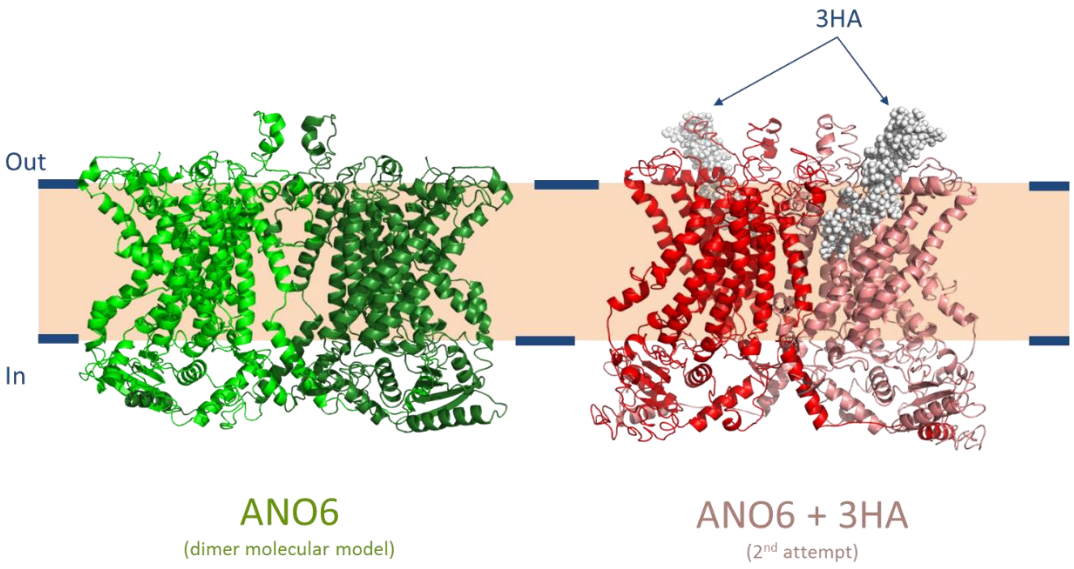

Figure 39 - **Predicted structures of the Ano6 dimer and the Ano6 dimer with the 3-HA tag inserted. (Protein model and image generated by Hugo Botelho, reproduced with permission).**

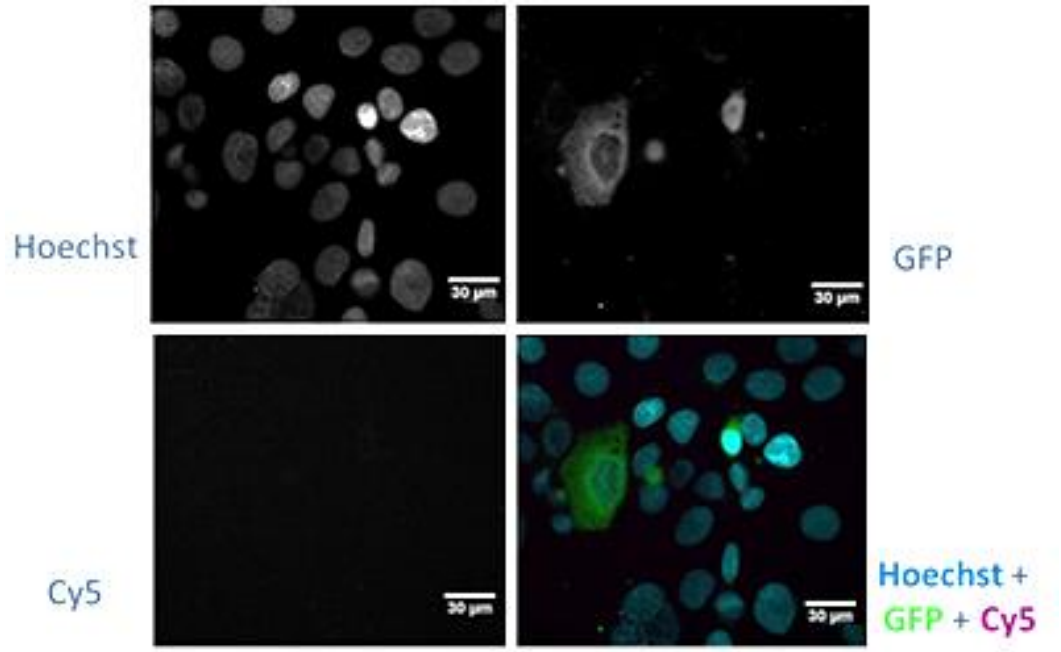

Figure 40 - **Immunofluorescence results of CFBE cells transiently transfected with the first double-tagged Ano6 construct. The plasma membrane was not permeabilized and images were acquired with the 20x objective. In the Hoechst channel (upper left) it is possible to see the nuclei, in the GFP channel (upper right) it is possible to see Ano6 (since it has a GFP-tag in the cytoplasmic C-terminal) and in the Cy5 channel (lower left) it should be seen the membrane staining of Ano6 in case the 3-HA tag was exposed to the outside of the cell (Primary antibody – anti-HA; secondary antibody – Cy5). Scale bar represents 30 µm.**

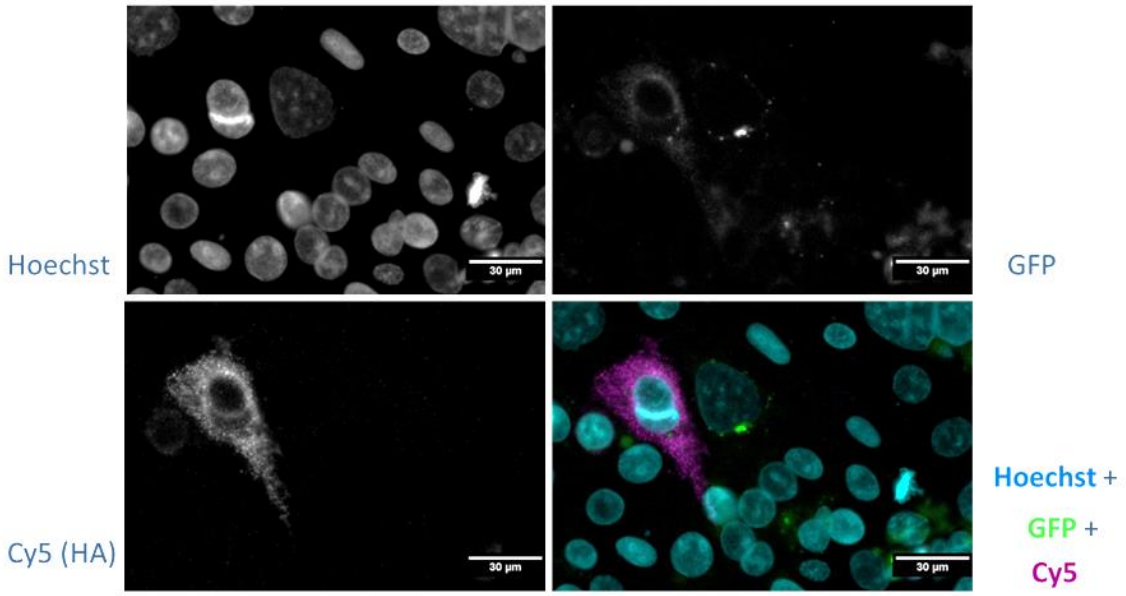

Figure 41 - **Immunofluorescence results of CFBE cells transiently transfected with the first double-tagged Ano6 construct (40x objective). Conditions as above, except that here the plasma membrane was permeabilized. In contrast to non-permeabilized cells (Fig.40), the HA antibody now detects Ano6, indicating that the 3-HA tag is present but intracellularly localized. Hoechst – Nuclei; GFP – Ano6; Cy5 – HA staining. Scale bar represents 30 µm.**

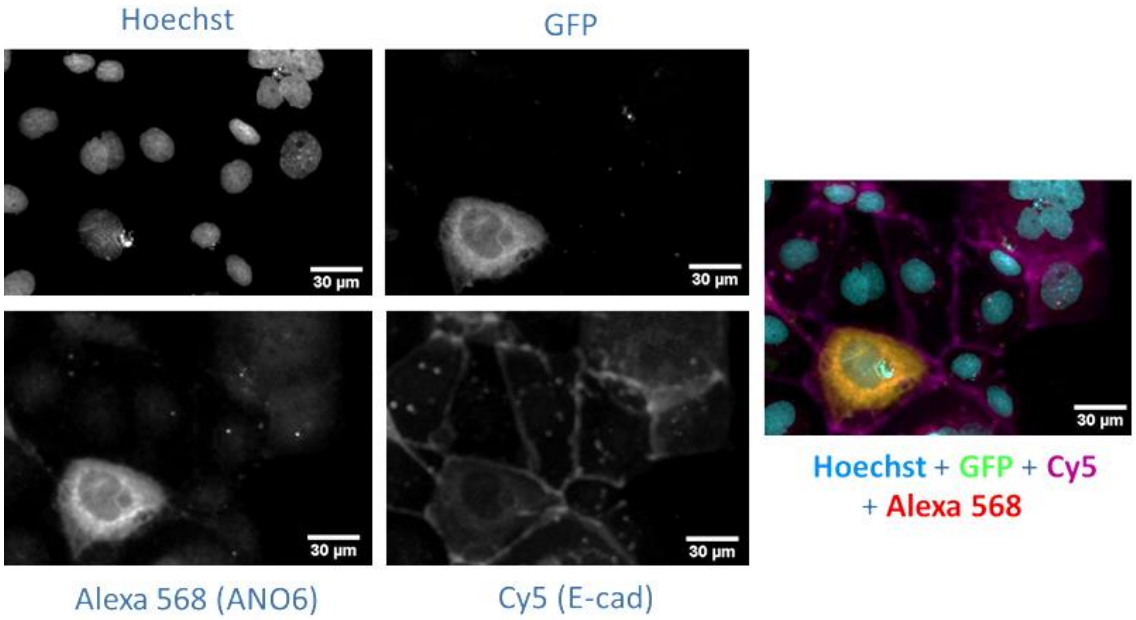

Figure 42 - **Immunofluorescence results of CFBE cells transiently transfected with the first double-tagged Ano6 construct. The plasma membrane was permeabilized and the 20x objective was used. Hoechst – Nuclei; GFP – Ano6; Alexa 568 – Ano6 staining; Cy5 – E-cadherin staining. No overlap is detected between Ano6 and E-cadherin (epithelial cell plasma membrane marker) stainings, meaning that this double-tagged construct of Ano6 is not localized at the plasma membrane. Scale bar represents 30 µm.**

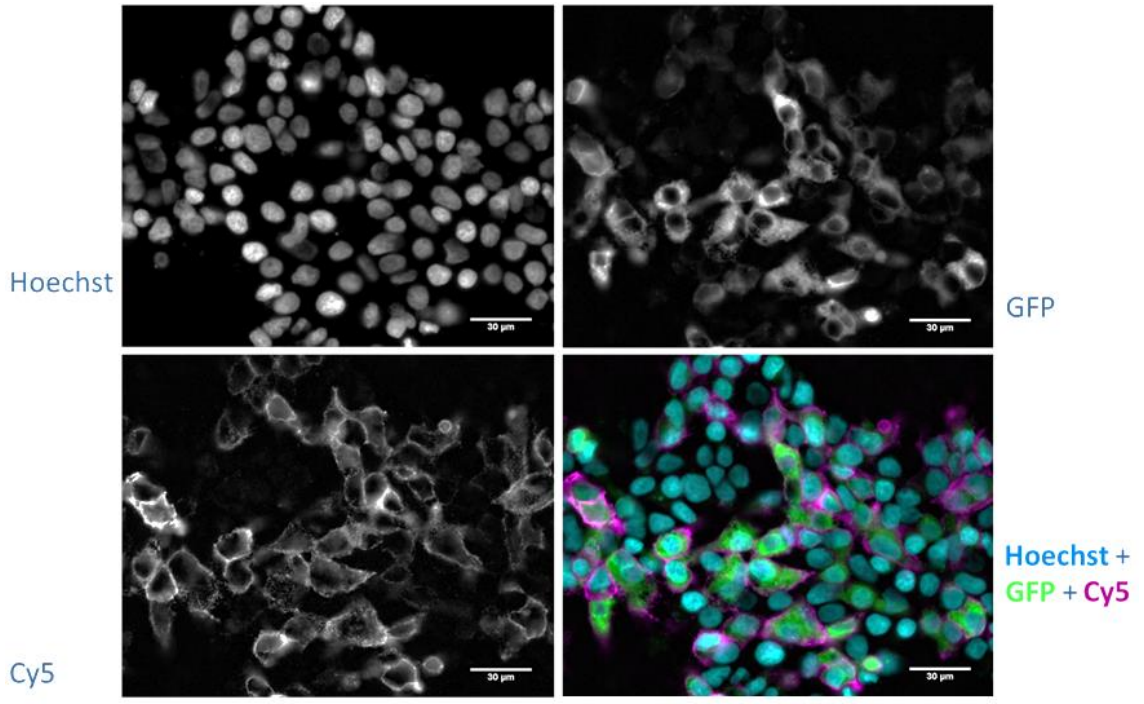

Figure 43 - **Immunofluorescence results of HEK 293T cells transiently transfected with the second double-tagged construct of Ano6. The plasma membrane was not permeabilized and the 40x objective was used. Hoechst – Nuclei; GFP – Ano6; Cy5 – HA staining. HEK 293T cells transfected with this double-tagged Ano6 show a strong staining of the HA antibody without plasma membrane permeabilization, meaning that this protein is localized at the plasma membrane, and that the 3-HA tag is correctly inserted in an extracellular loop of the protein. Scale bar represents 30 µm.**

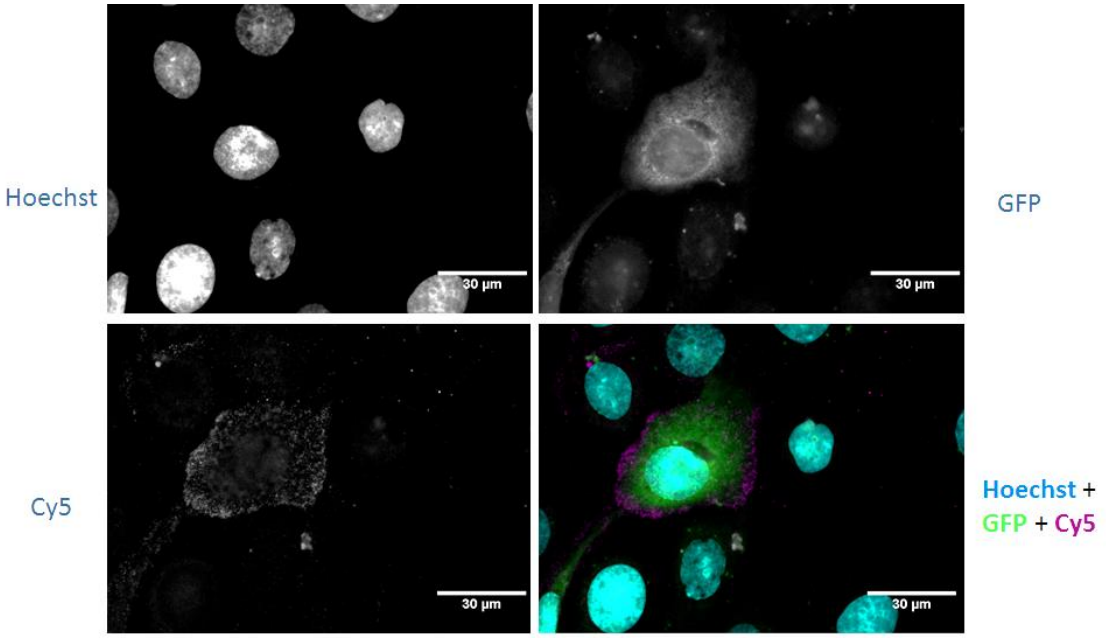

Figure 44 - **Immunofluorescence results of CFBE cells transiently transfected with the second double-tagged construct of Ano6. The plasma membrane was not permeabilized and the 40x objective was used. Hoechst – Nuclei; GFP – Ano6; Cy5 – HA staining. Similarly to what is observed in Fig.43, these results indicate that this second Ano6 construct is localized at the plasma membrane and that the 3-HA tag is correctly inserted in an extracellular loop of the protein. Scale bar represents 30 µm.**

7.4.2) Anoctamin 9

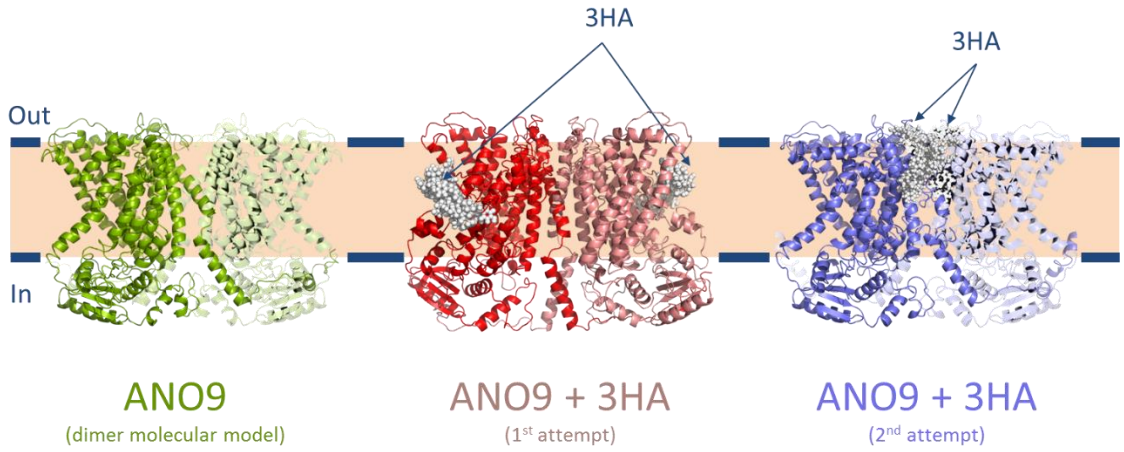

Figure 45 - **Predicted structures of the Ano9 dimer and the Ano9 dimer with the 3-HA tags inserted – First and second mutagenesis. (Protein model and image generated by Hugo Botelho, reproduced with permission).**

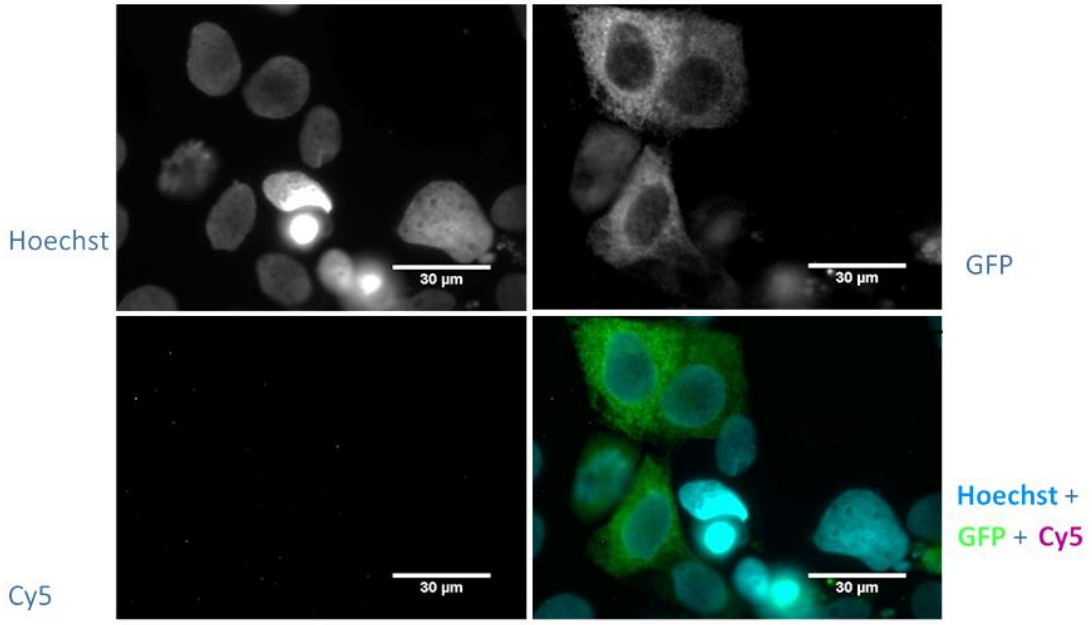

Figure 46 - **Immunofluorescence results of CFBE cells transiently transfected with the first double-tagged Ano9 construct. The plasma membrane was not permeabilized and the 40x objective was used. Hoechst – Nuclei; GFP – Ano6; Cy5 – HA staining. No membrane staining was detected, indicating that either this double-tagged Ano9 is not localized at the plasma membrane or that the 3-HA tag is not inserted in an extracellular loop of the protein. Scale bar represents 30 µm.**

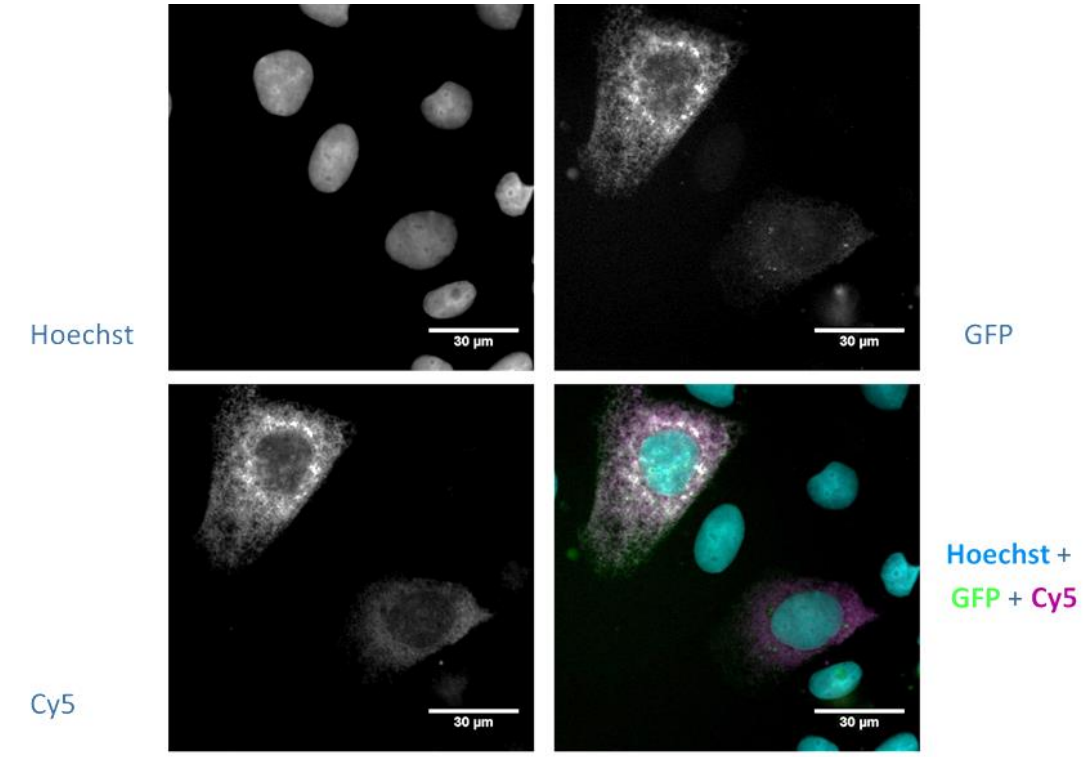

Figure 47 - **Immunofluorescence results of CFBE cells transiently transfected with the first double-tagged Ano9 construct. Conditions as above, except that here the plasma membrane was permeabilized. In contrast to non-permeabilized cells (Fig.46), the HA antibody now detects Ano9, indicating that the 3-HA is present but intracellularly localized. Hoechst – Nuclei; GFP – Ano6; Cy5 – HA staining. Scale bar represents 30 µm.**

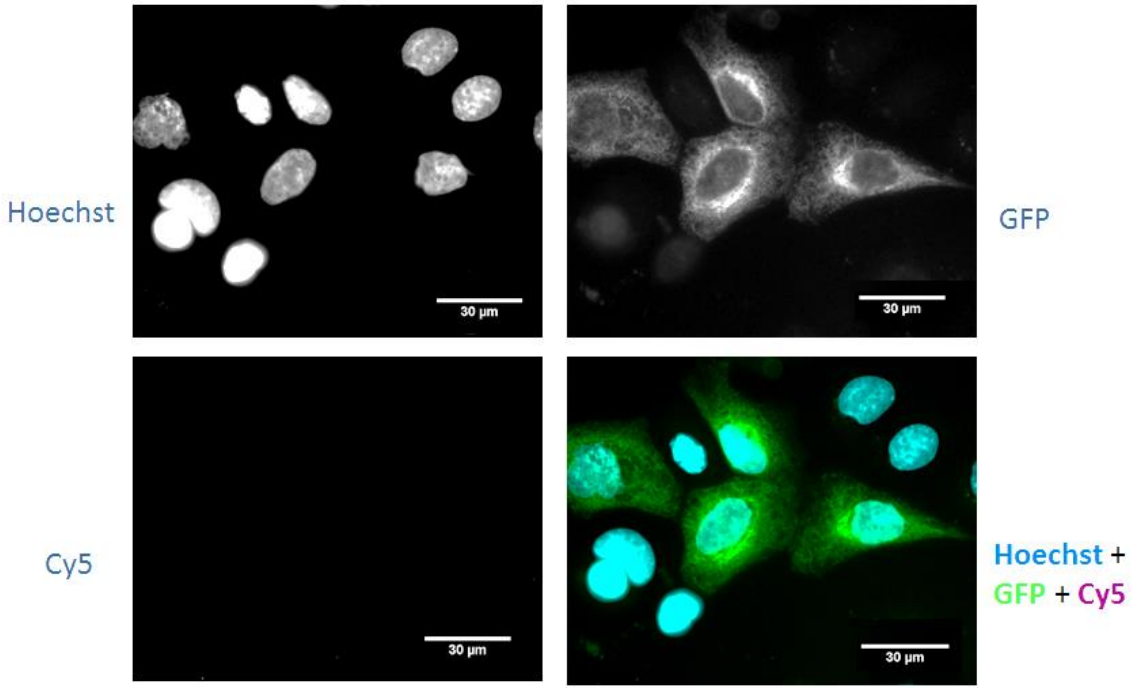

Figure 48 - **Immunofluorescence results of CFBE cells transiently transfected with the second double-tagged Ano9 construct. The plasma membrane was not permeabilized and the 40x objective was used. Hoechst – Nuclei; GFP – Ano6; Cy5 – HA staining. No membrane staining was detected, indicating that either this double-tagged Ano9 is not localized at the plasma membrane or that the 3-HA tag is not inserted in an extracellular loop of the protein. Nevertheless, this construct of Ano9 was used for further experiments. Scale bar represents 30 µm.**

7.4.3) Anoctamin 10

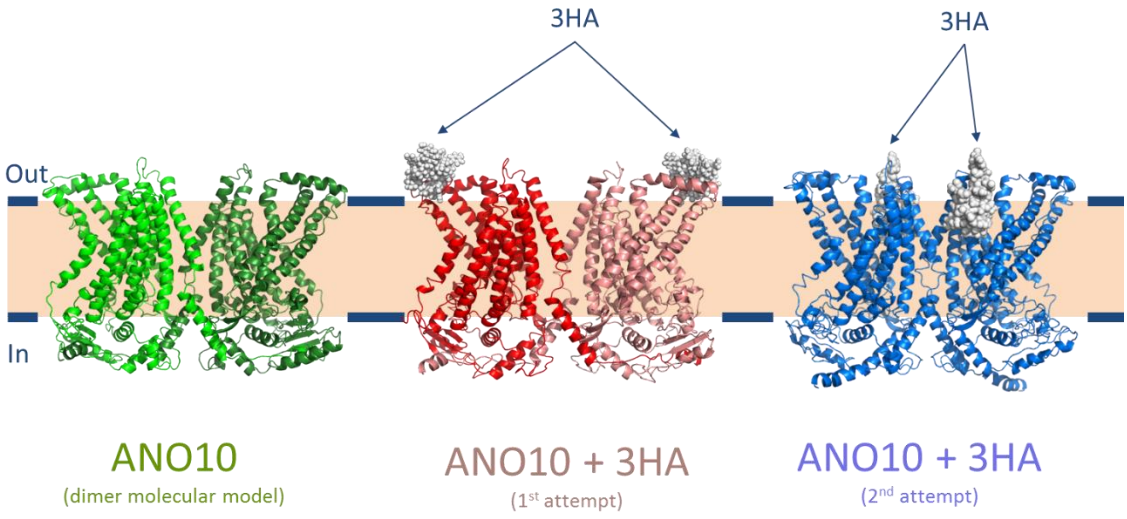

Figure 49 - **Predicted structures of the Ano10 dimer and the Ano10 dimer with the 3-HA tags inserted – First and second mutagenesis. (Protein model and image generated by Hugo Botelho, reproduced with permission).**

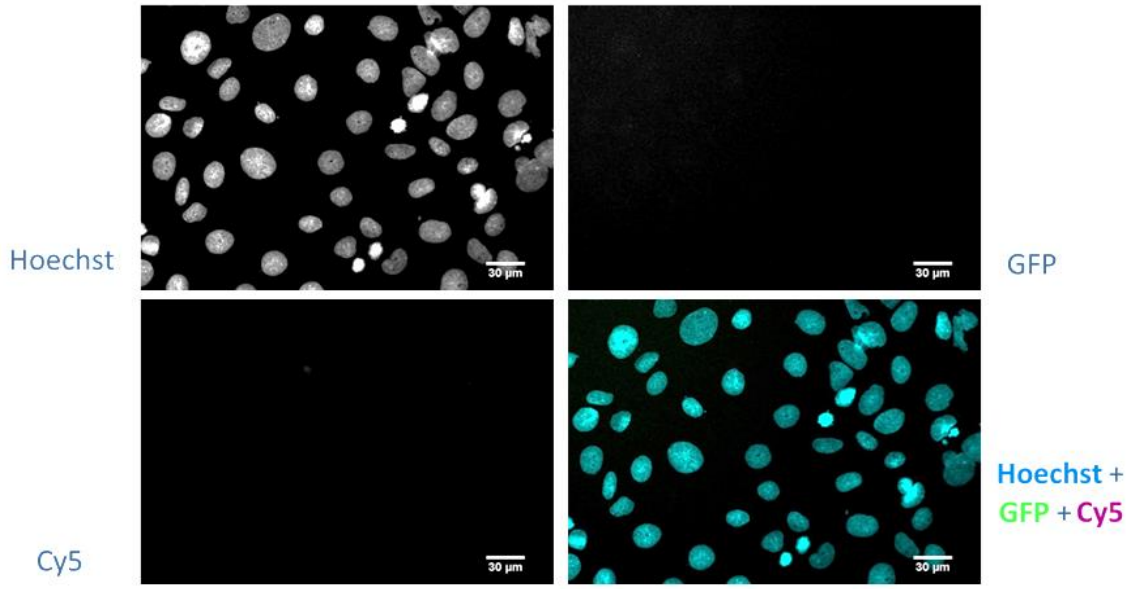

Figure 50 - **Immunofluorescence results of CFBE cells transiently transfected with the first double-tagged Ano10 construct. The membrane was not permeabilized and the 20x objective was used. Hoechst – Nuclei; GFP – Ano6; Cy5 – HA staining. No GFP signal nor HA staining was detected. Scale bar represents 30 µm.**

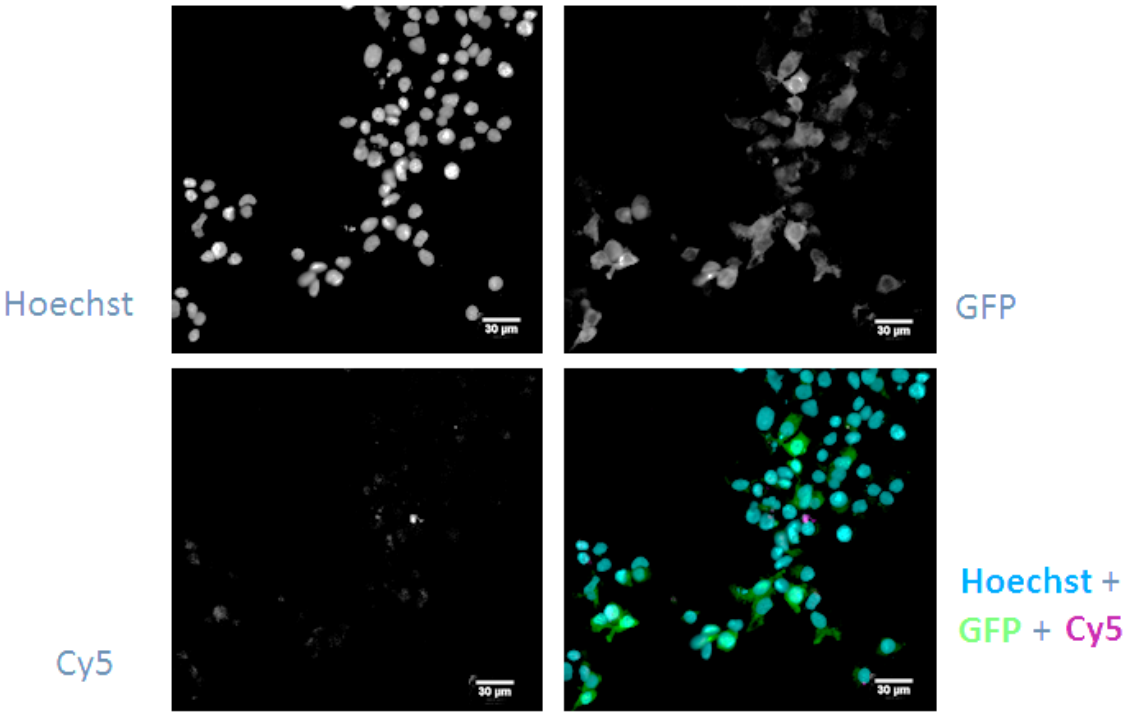

Figure 51 - **Immunofluorescence results of HEK 293T cells transiently transfected with the second double-tagged Ano10 construct. The plasma membrane was not permeabilized and the 20x objective was used. Hoechst – Nuclei; GFP – Ano6; Cy5 – HA staining. With this construct the cells were transfected, but the plasma membrane staining was not conclusive, being only detected for some of the transfected cells. Nevertheless, this construct of Ano10 was used for further experiments. Scale bar represents 30 µm.**

7.5) Appendix 5 – Results from cloning and lentiviral production and transduction

Table 8 - **Cloning reaction using the In-Fusion HD cloning kit.**

Anoctamin cDNA with primer extensions	200 ng
Linearized vector	50 ng
In-Fusion HD Enzyme Premix	2 µL
H_2O	To 10 µL

Table 9 - **In-Fusion HD Cloning Kit positive and negative controls.**

	In-Fusion Cloning reaction					Transformation	Competent cells		Results
	2kb Control Insert	pUC19 control vector	In-Fusion HD Enzyme Premix	H_2O	Incubation	Volume added to competent cells	Competent cells	Transformation efficiency	Number of colonies
Positive control	2 µL	1 µL	2 µL	5 µL	15 min @ 50 ^{0}C	5 µL	XL1-B	>1 x 10^8 cfu/µg	≈ 1200
Negative control	-	1 µL	2 µL	7 µL	15 min @ 50 ^{0}C	5 µL	XL1-B	>1 x 10^8 cfu/µg	3

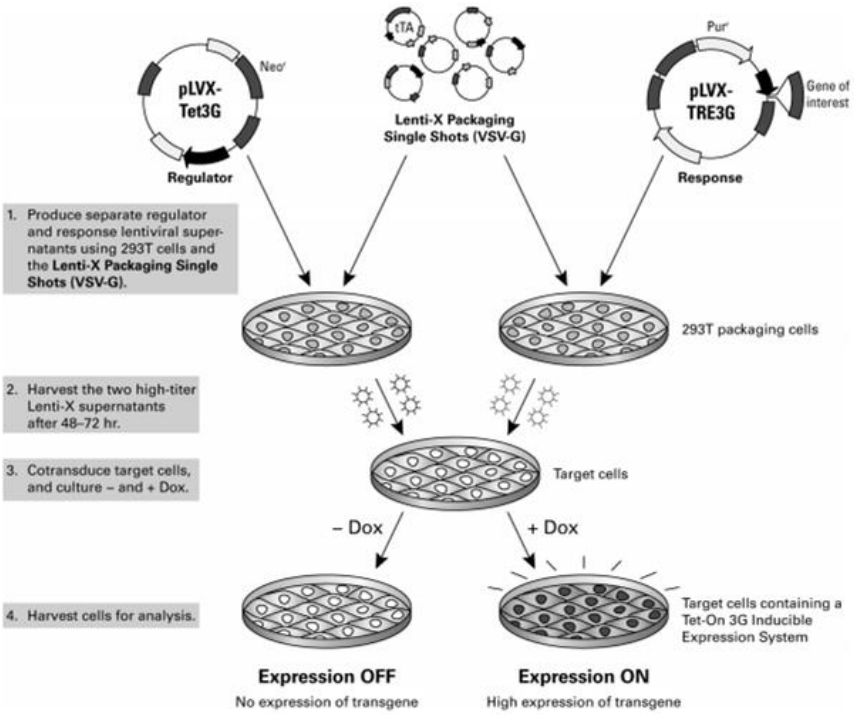

Figure 52 - **Inducible expression of transgene by doxycycline (Dox) in stably transduced cells.**

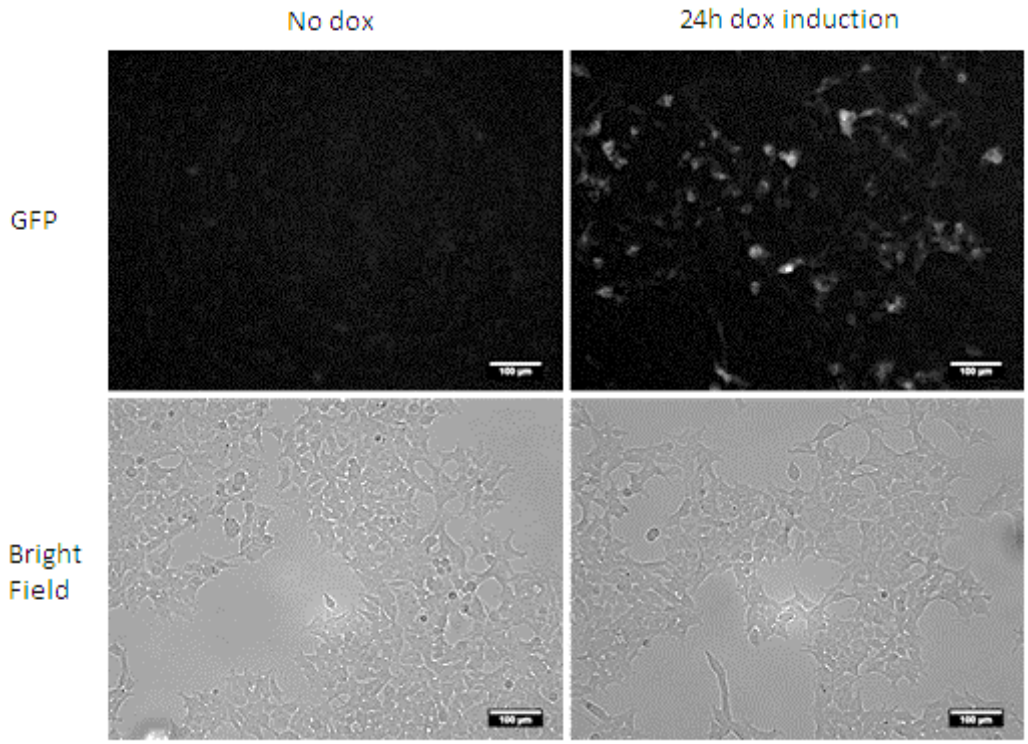

Figure 53 - **HEK 293T cells transiently transduced with lentiviral vectors (pLVX-TRE3G-Ano6 3-HA GFP and pLVX-Tet3G). On the left are represented cells without doxycycline induction, while on the right are represented transfected cells 24h after doxycycline induction, where is possible to observe Ano6 (GFP) expression. The images were acquired with the 10x objective. Scale bar represents 100 µm.**

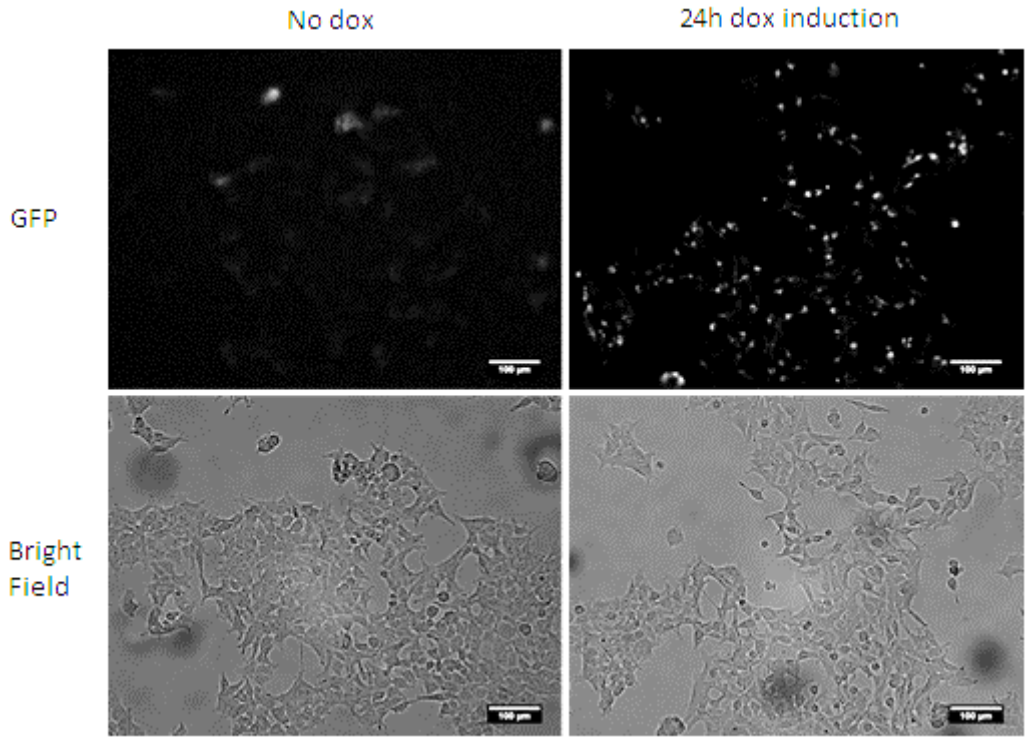

Figure 54 - **HEK 293T cells transiently transduced with lentiviral vectors (pLVX-TRE3G-Ano9 3-HA GFP and pLVX-Tet3G). On the left are represented cells without doxycycline induction, while on the right are represented transfected cells 24h after doxycycline induction, where is possible to observe Ano9 (GFP) expression. The images were acquired with the 10x objective. Scale bar represents 100 µm.**

7.6) Appendix 6 – Antibiotic dose-dependent survival curves for CFBE parental cells

An antibiotic dose-dependent survival curve is a dose response experiment which tests the maximum concentration of antibiotic that a cell line tolerates (before dying) by testing incremental doses. With these experiments, performed by a co-worker (Joana Lérias), it was possible to determine the minimum antibiotic concentration of puromycin, G418 and hygromycin required to kill all CFBE41o- cells.

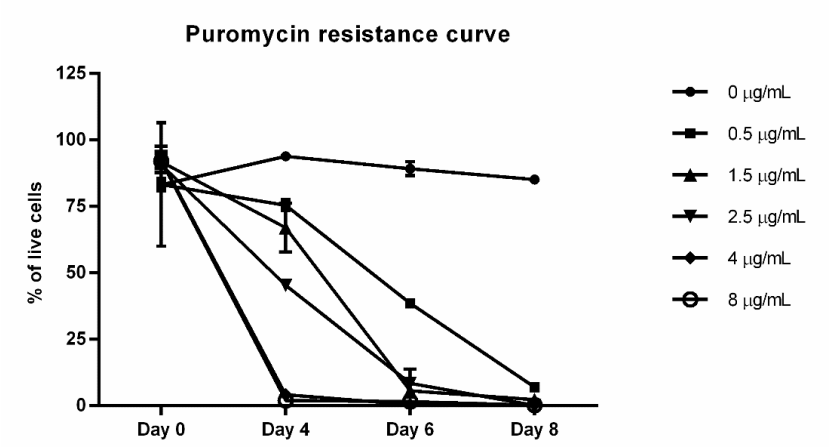

Figure 55 - **Puromycin resistance curve using CFBE41o- cells. 2 µg/mL of puromycin was the concentration used for further experiments since it was between the two lower concentrations that killed all cells in 8 days. (Results obtained by Joana Lérias, reproduced with permission).**

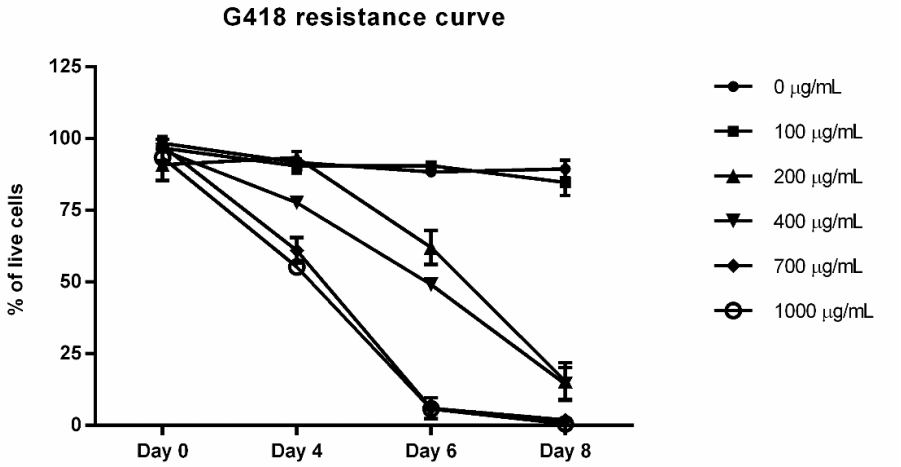

Figure 56 - **G418 resistance curve using CFBE41o- cells. 400 µg/mL of G418 was the concentration used for further experiments since it was the lowest concentration that killed almost all cells in 8 days. (Results obtained by Joana Lérias, reproduced with permission).**

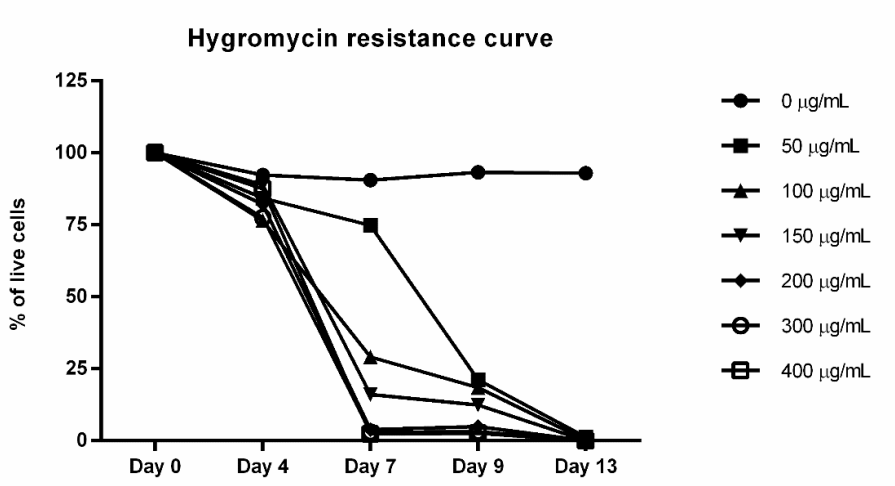

Figure 57 - **Hygromycin resistance curve using CFBE41o- cells. 200 µg/mL of hygromycin was the concentration used for further experiments since it was the lowest concentration that killed all cells in 7 days. (Results obtained by Joana Lérias, reproduced with permission).**

According to the results observed in Fig. 55-57, the final concentrations of antibiotics used for the experiments were the following:

Table 10 - **Concentrations of antibiotics used for the experiments.**

	Puromycin	G418	Hygromycin
Concentration (µg/mL)	2	400	200

7.7) Appendix 7 – Results from Flow cytometry: cell sorting

7.7.1) CFBE Ano6 3-HA GFP

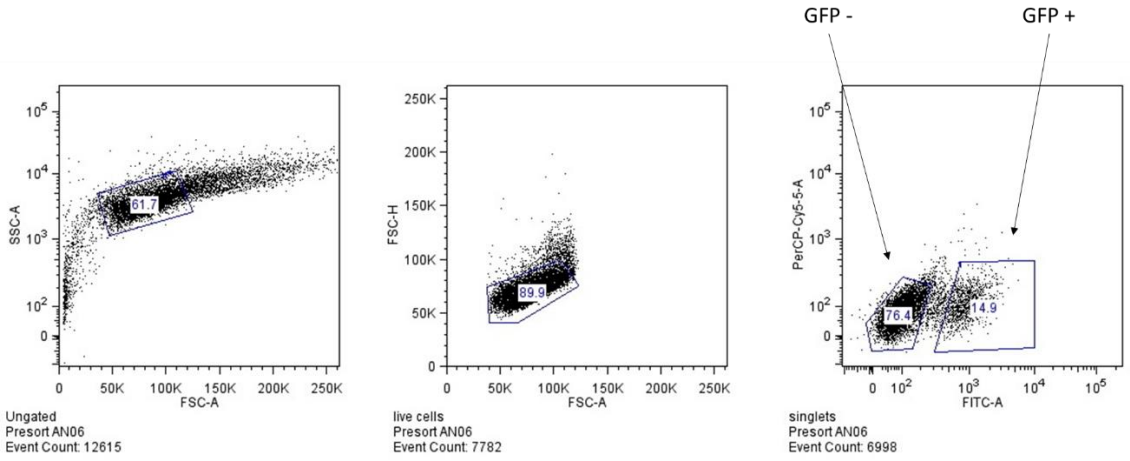

Figure 58 - **Sorting of CFBE Ano6 3-HA GFP cells. The living cells were first selected, followed by a selection of single cells. Finally, the GFP emission intensity was measured and the cells were sorted according to it.**

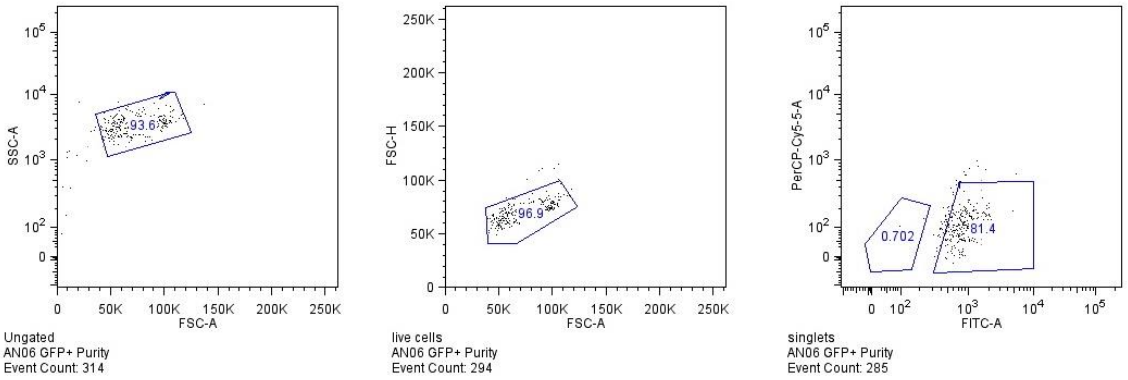

Figure 59 – **GFP positive cells selected from the CFBE Ano6 3-HA GFP heterogeneous population.**

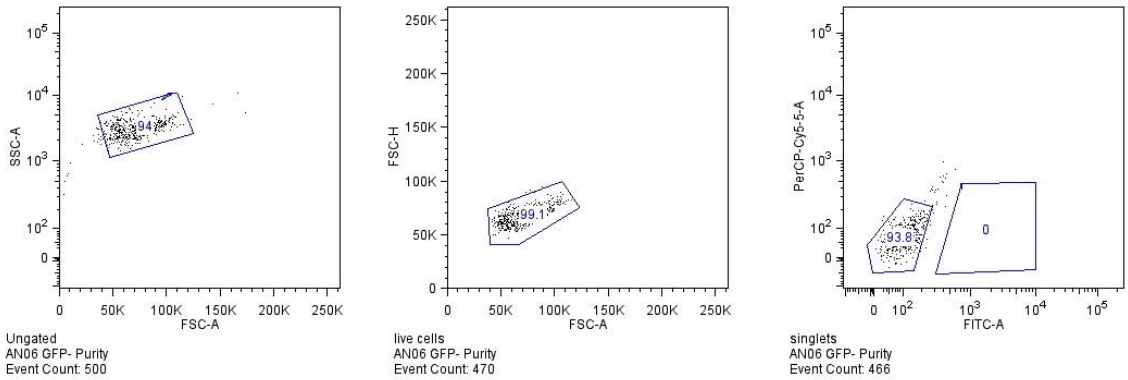

Figure 60 - **GFP negative cells selected from the CFBE Ano6 3-HA GFP heterogeneous population.**

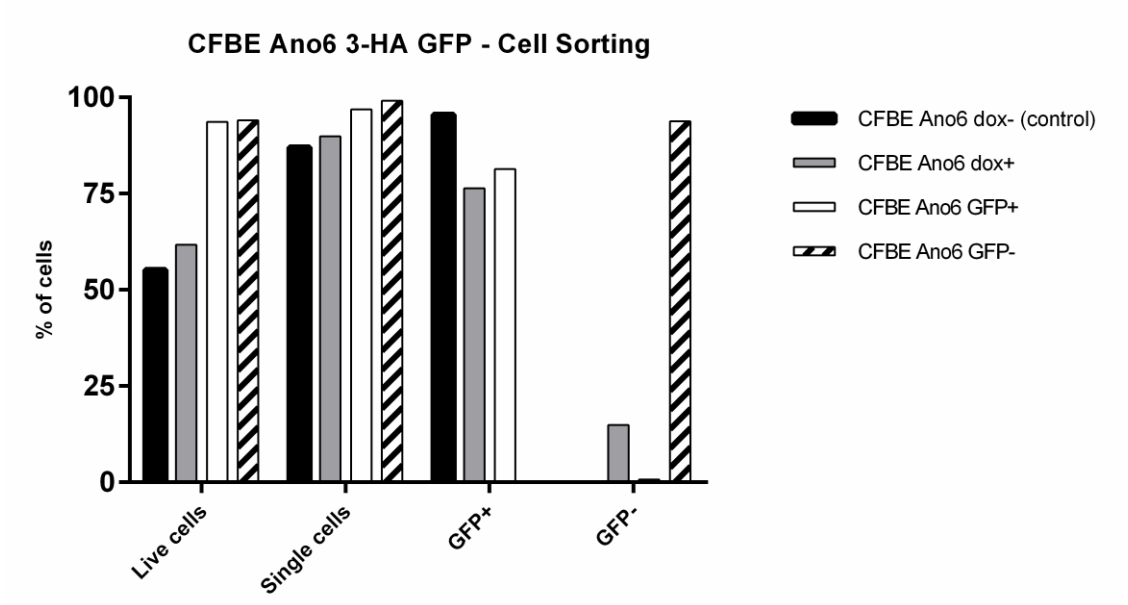

Figure 61 - **CFBE Ano6 3-HA sorting statistics. With these results it is possible to conclude that the GFP (Ano6) positive cells were accurately sorted, since no GFP negative cells were detected in the GFP positive population.**

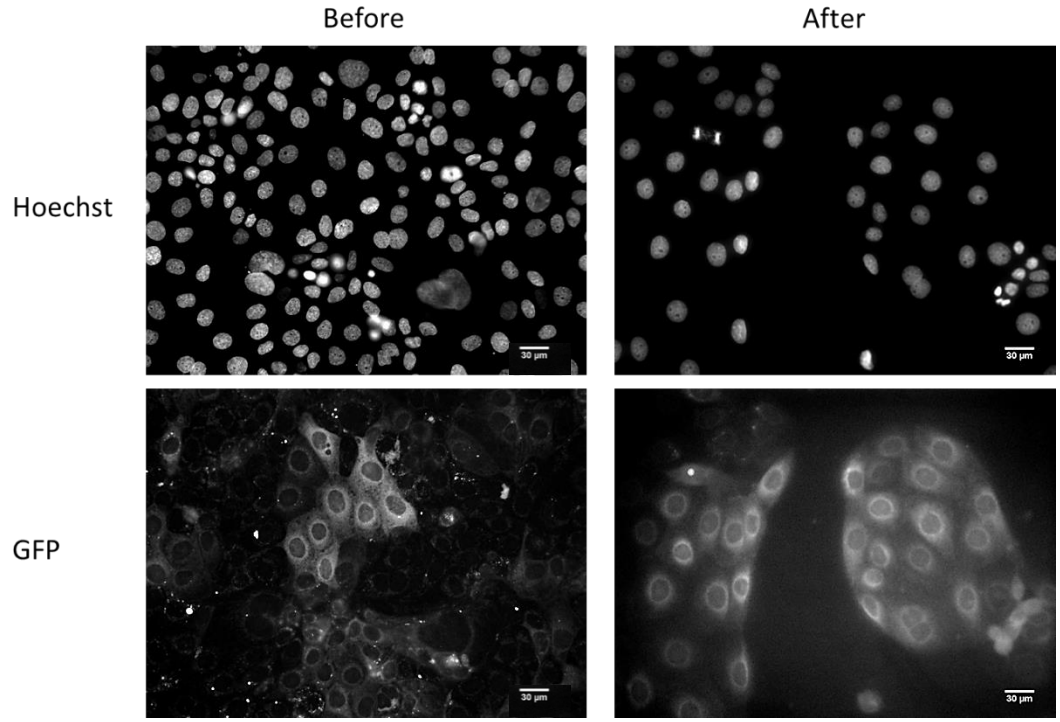

Figure 62 - **CFBE Ano6 3-HA GFP cells, before (left) and after (right) sorting. Images were acquired with the 20x objective. With these results it was possible to observe a cellular population with a more homogeneous GFP (Ano6) expression, confirming the results shown in Fig.61. Scale bar represents 30 µm.**

7.7.2) CFBE Ano9 3-HA GFP

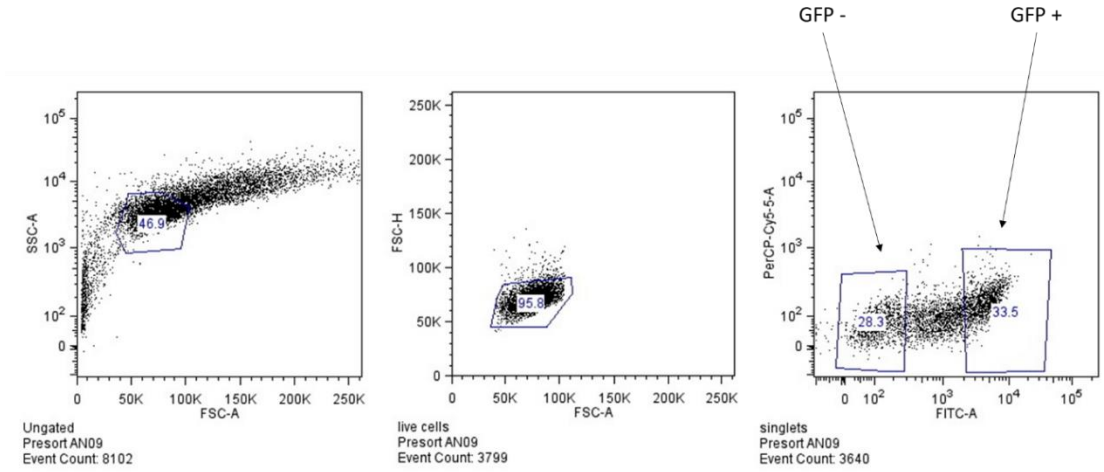

Figure 63 - **Sorting of CFBE Ano9 3-HA GFP cells. The living cells were first selected, followed by a selection of single cells. Finally, the GFP emission intensity was measured and the cells were sorted according to it.**

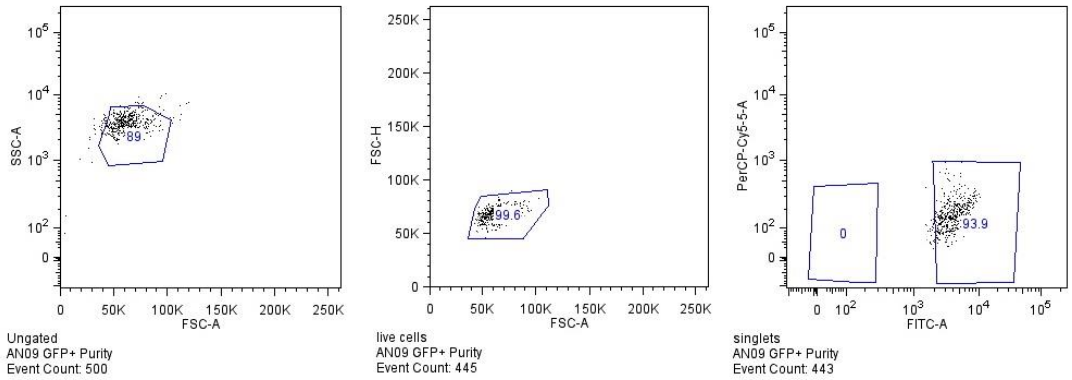

Figure 64 - **GFP positive cells selected from the CFBE Ano9 3-HA GFP heterogeneous population.**

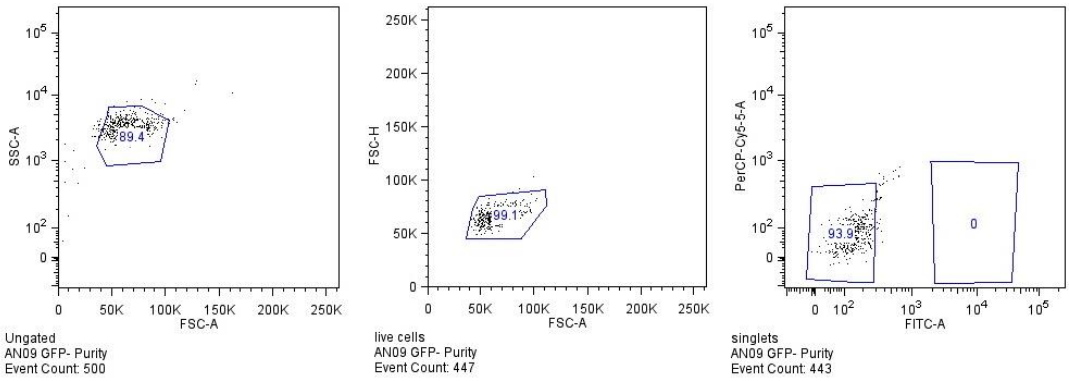

Figure 65 - **GFP negative cells selected from the CFBE Ano9 3-HA GFP heterogeneous population.**

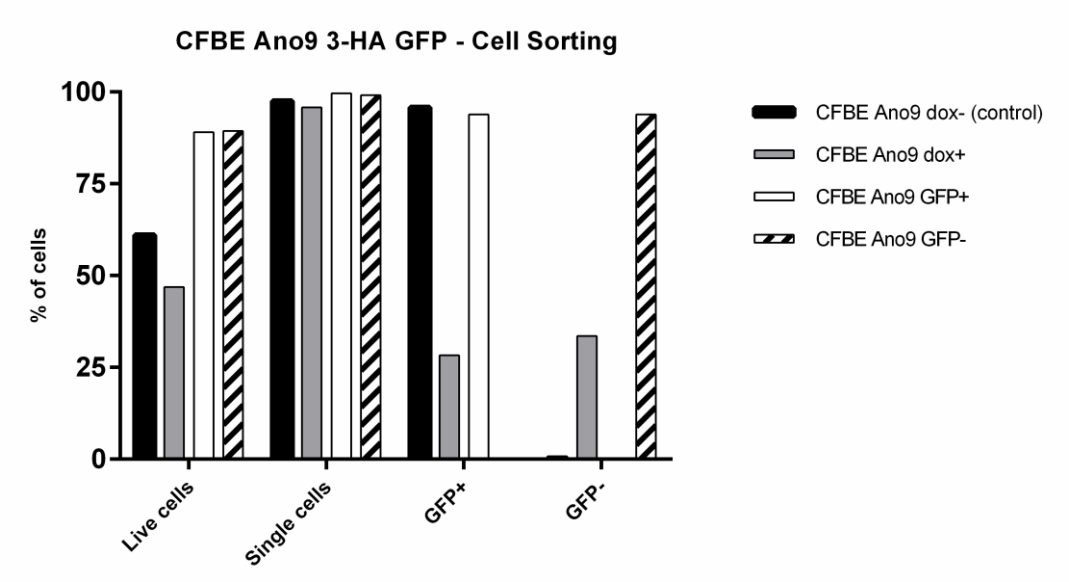

Figure 66 - **CFBE Ano9 3-HA sorting statistics. With these results it is possible to conclude that the GFP (Ano9) positive cells were accurately sorted, since no GFP negative cells were detected in the GFP positive population.**

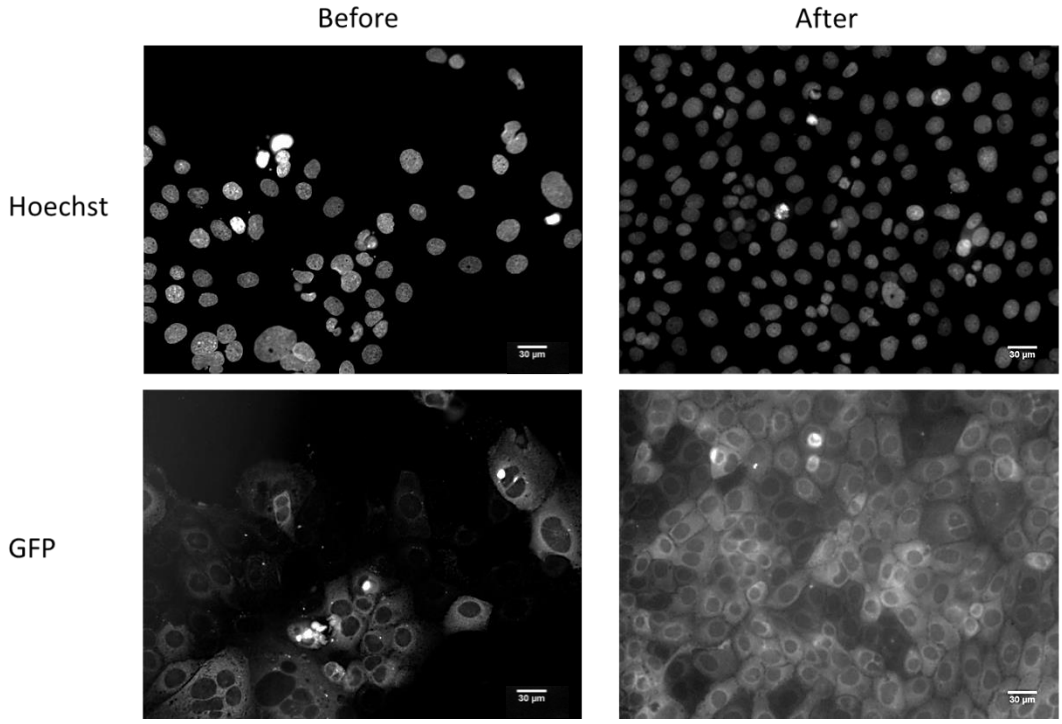

Figure 67 - **CFBE Ano9 3-HA GFP cells, before (left) and after (right) sorting. Images were acquired with the 20x objective. With these results it was possible to observe a cellular population with a more homogeneous GFP (Ano9) expression, confirming the results shown in Fig.66. Scale bar represents 30 µm.**

7.7.3) CFBE mCherry wt-CFTR Ano6 3-HA GFP

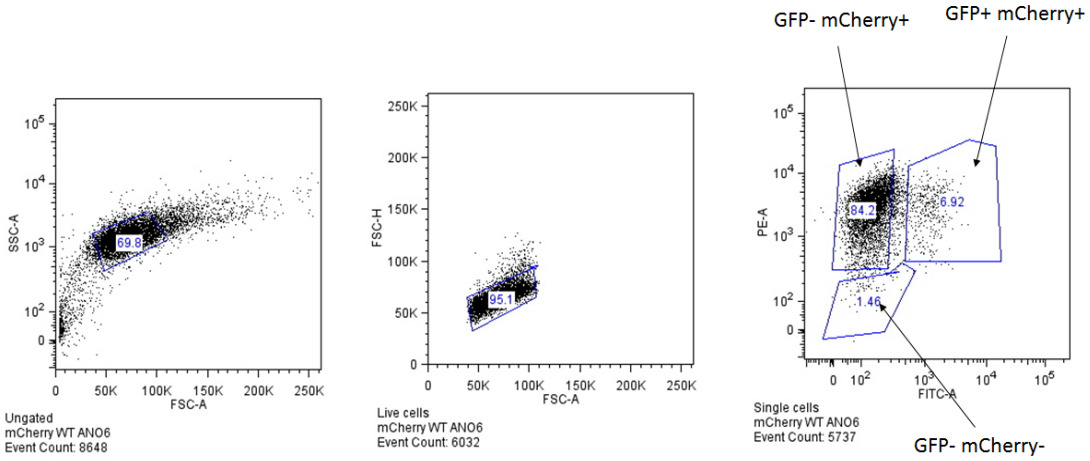

Figure 68 - **Sorting of CFBE mCherry wt-CFTR Ano6 3-HA GFP cells. The living cells were first selected, followed by a selection of single cells. Finally, the GFP and mCherry emission intensities were measured and the cells were sorted accordingly.**

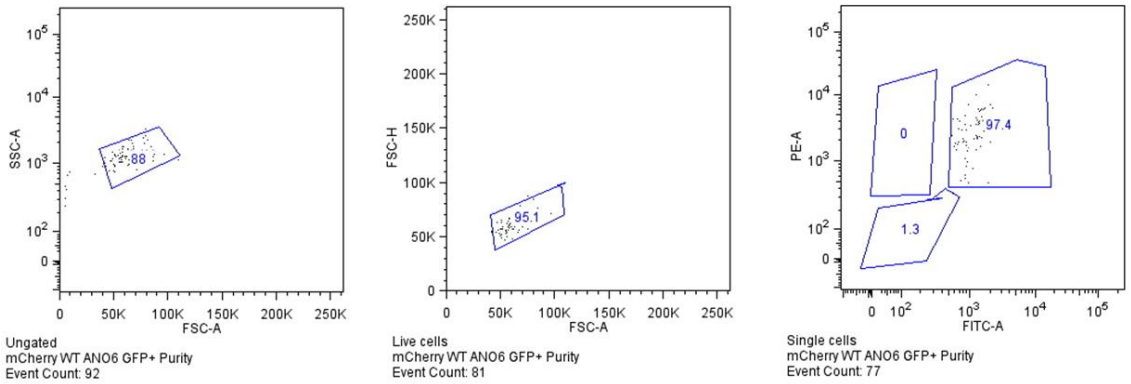

Figure 69 – **GFP and mCherry positive cells selected from the CFBE mCherry wt-CFTR Ano6 3-HA GFP heterogeneous population.**

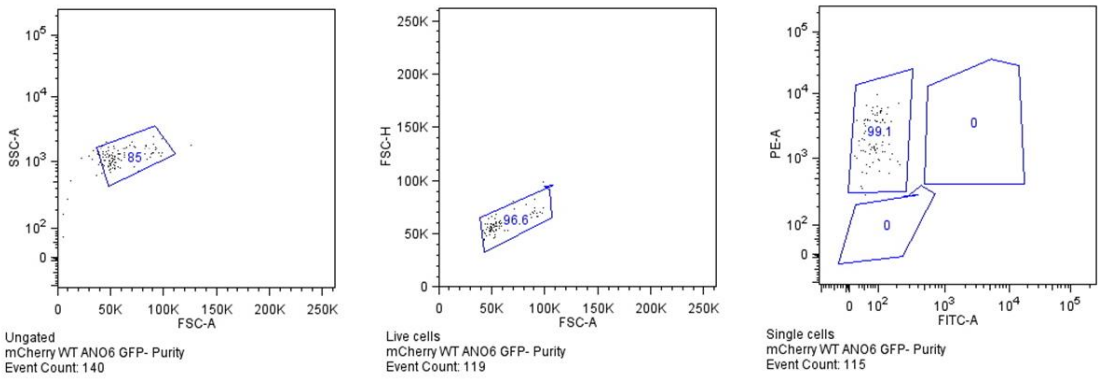

Figure 70 - **GFP negative and mCherry positive cells selected from the CFBE mCherry wt-CFTR Ano6 3-HA GFP heterogeneous population.**

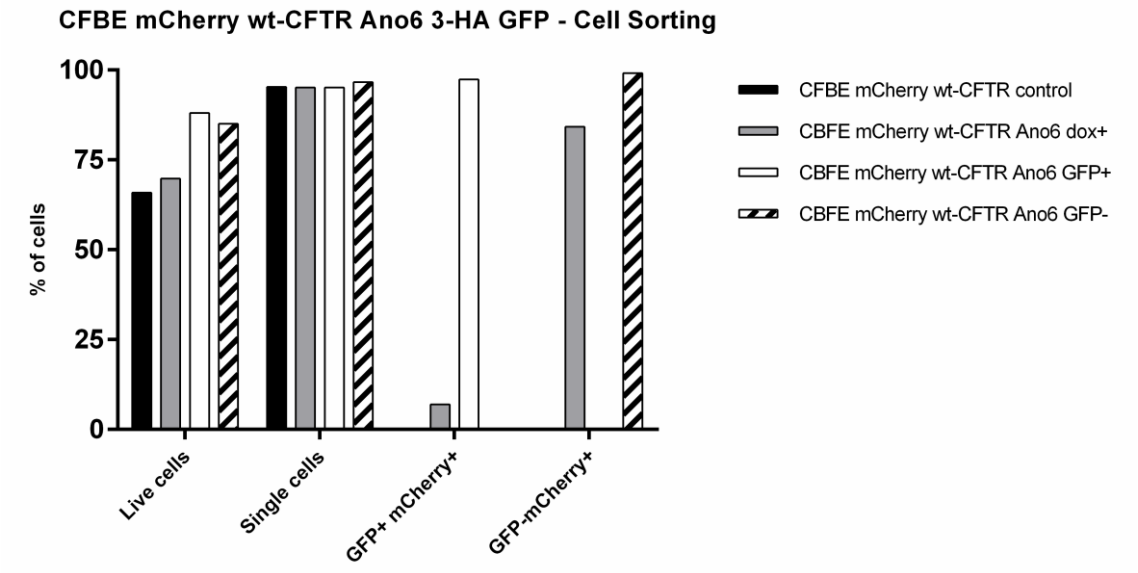

Figure 71 - **CFBE mCherry wt-CFTR Ano6 3-HA GFP sorting statistics. With these results it is possible to conclude that the GFP (Ano6) positive cells were accurately sorted, since no GFP negative cells were detected in the GFP positive population.**

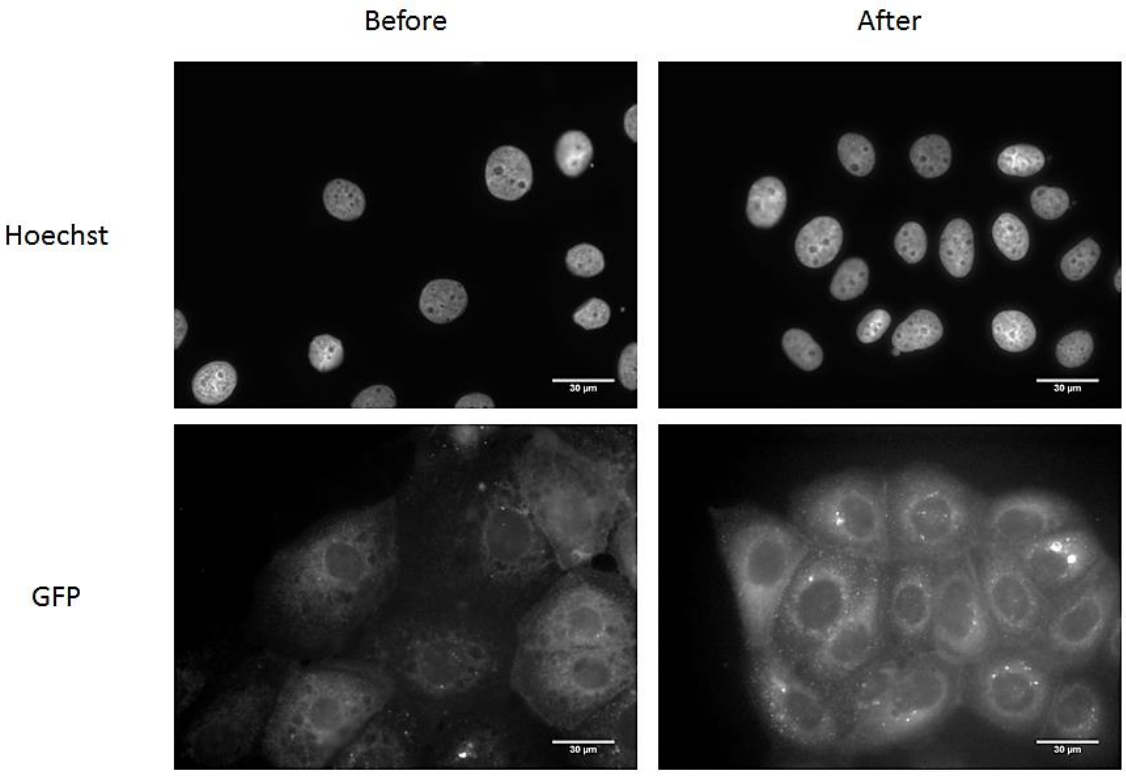

Figure 72 - **CFBE mCherry wt-CFTR Ano6 3-HA GFP before (left) and after (right) sorting. Images were acquired with the 40x objective. With these results it was possible to observe a cellular population with a more homogeneous GFP (Ano6) expression, confirming the results shown in Fig.71. Scale bar represents 30 µm.**

7.7.4) CFBE mCherry F508del-CFTR Ano6 3-HA GFP

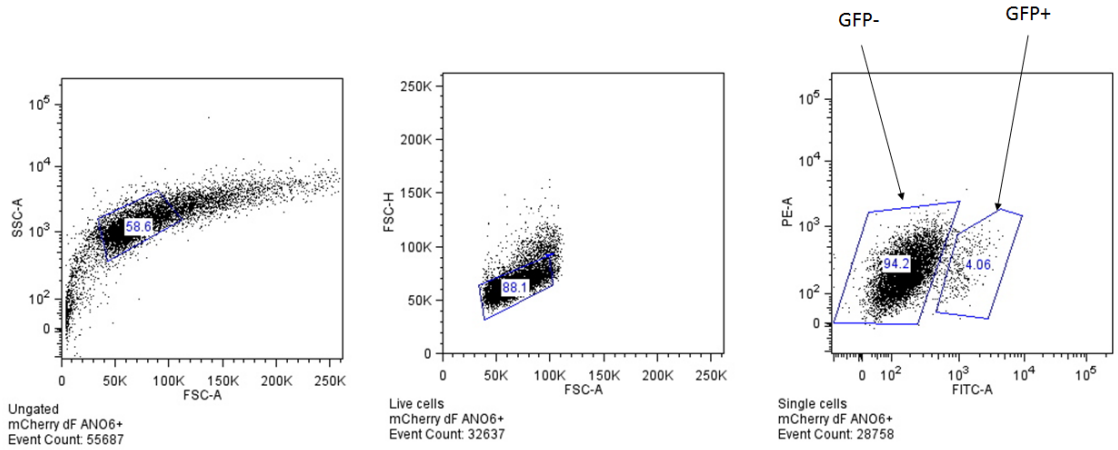

Figure 73 - **Sorting of CFBE mCherry F508del-CFTR Ano6 3-HA GFP cells. The living cells were first selected, followed by a selection of single cells. Finally, the GFP and mCherry emission intensities were measured and the cells were sorted accordingly.**

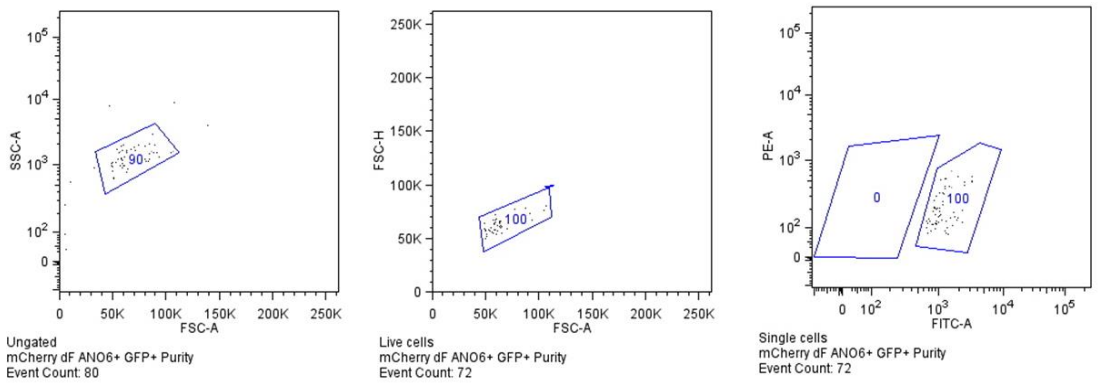

Figure 74 - **GFP positive cells selected from the CFBE mCherry F508del-CFTR Ano6 3-HA GFP heterogeneous population.**

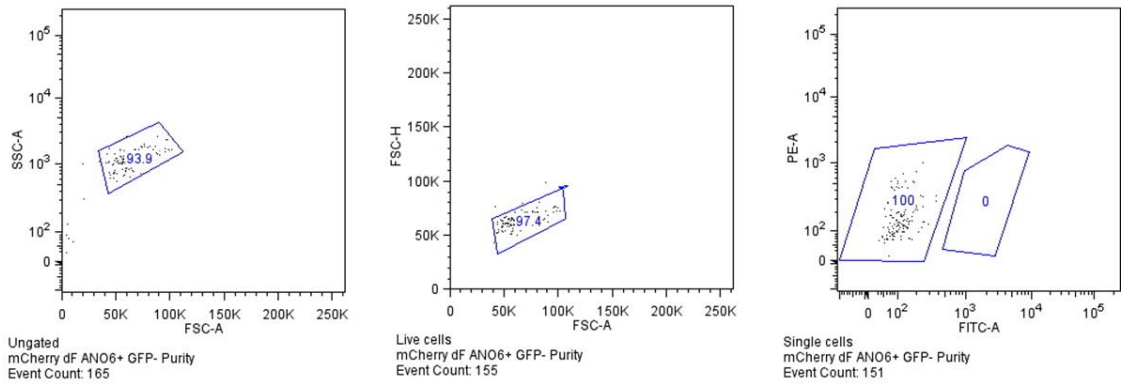

Figure 75 - **GFP negative cells selected from the CFBE mCherry F508del-CFTR Ano6 3-HA GFP heterogeneous population.**

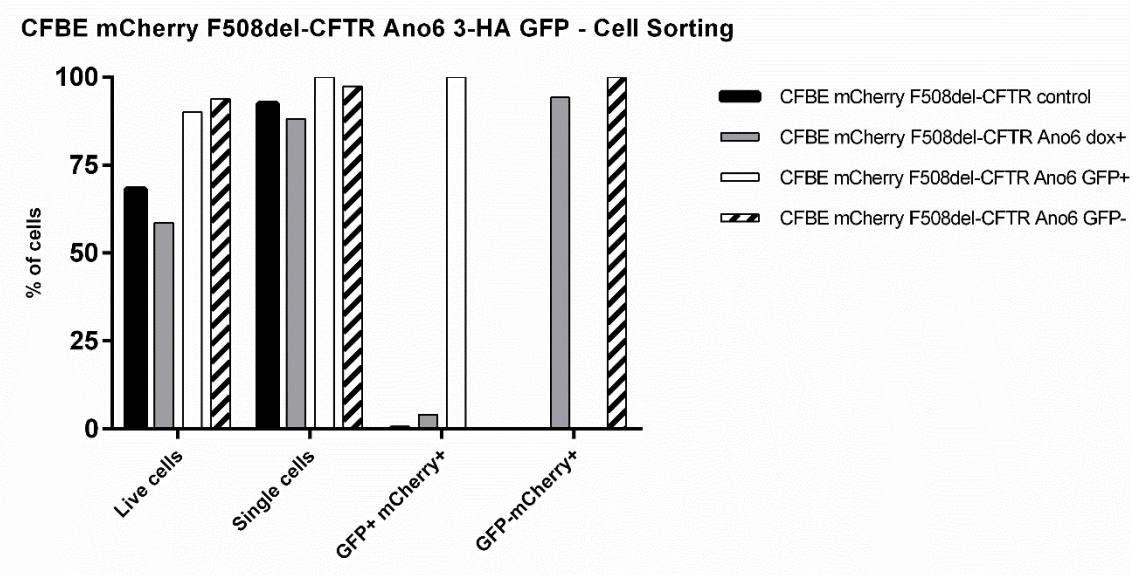

Figure 76 - **CFBE mCherry F508del-CFTR Ano6 3-HA GFP sorting statistics. With these results it is possible to conclude that the GFP (Ano6) positive cells were accurately sorted, since no GFP negative cells were detected in the GFP positive population.**

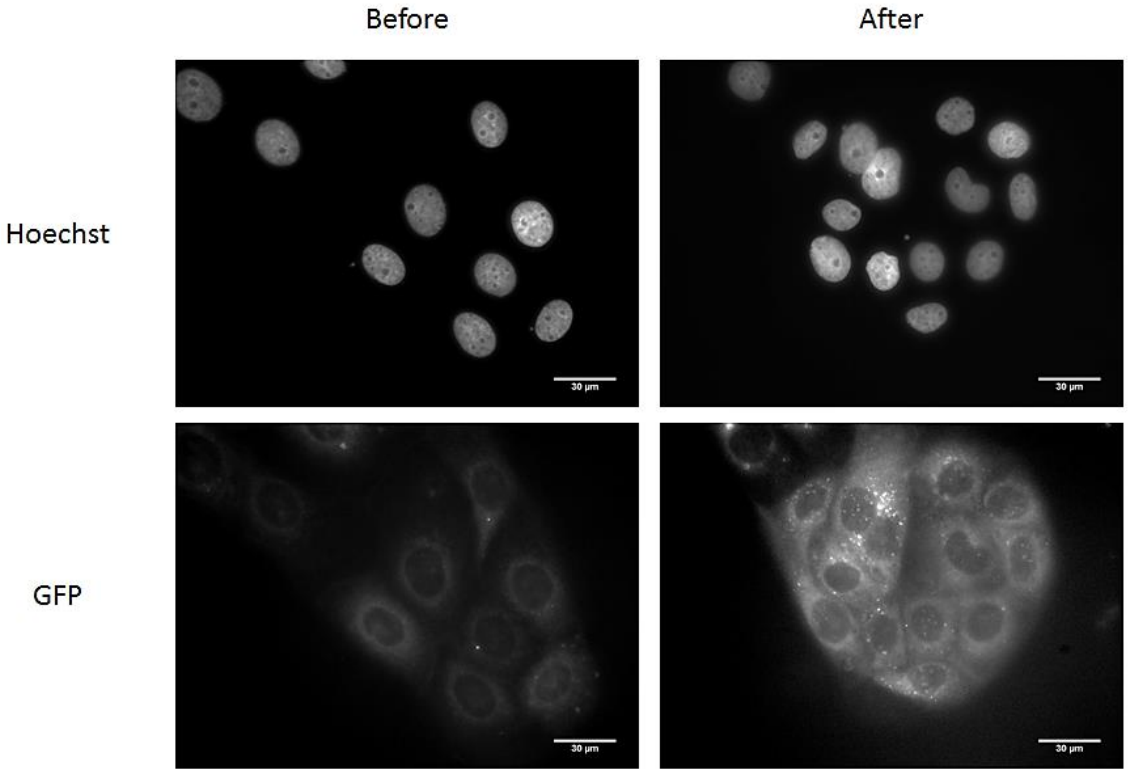

Figure 77 - **CFBE mCherry F508del-CFTR Ano6 3-HA GFP before (left) and after (right) sorting. Images were acquired with the 40x objective. With these results it was possible to observe a cellular population with a more homogeneous GFP (Ano6) expression, confirming the results shown in Fig.76. Scale bar represents 30 µm.**

7.7.5) CFBE mCherry wt-CFTR Ano9 3-HA GFP

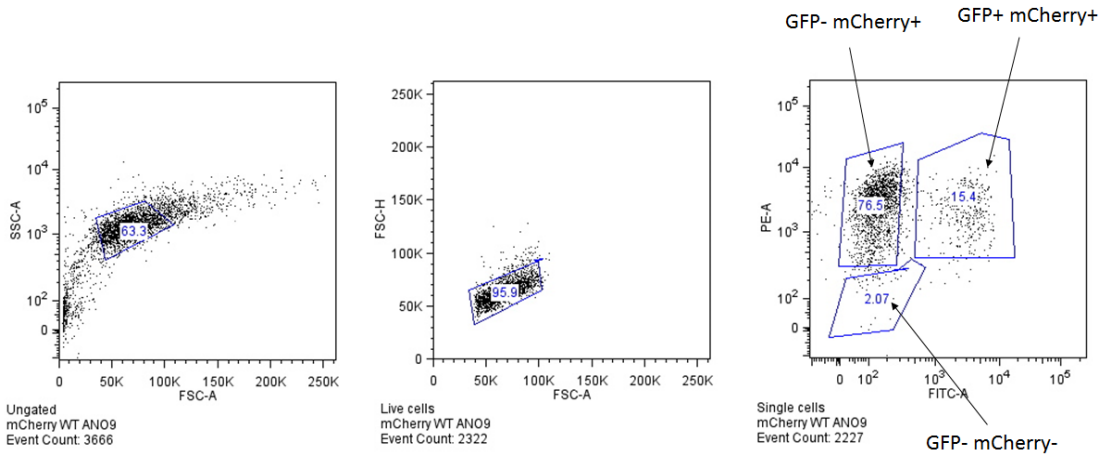

Figure 78 - **Sorting of CFBE mCherry wt-CFTR Ano9 3-HA GFP cells. The living cells were first selected, followed by a selection of single cells. Finally, the GFP and mCherry emission intensities were measured and the cells were sorted accordingly.**

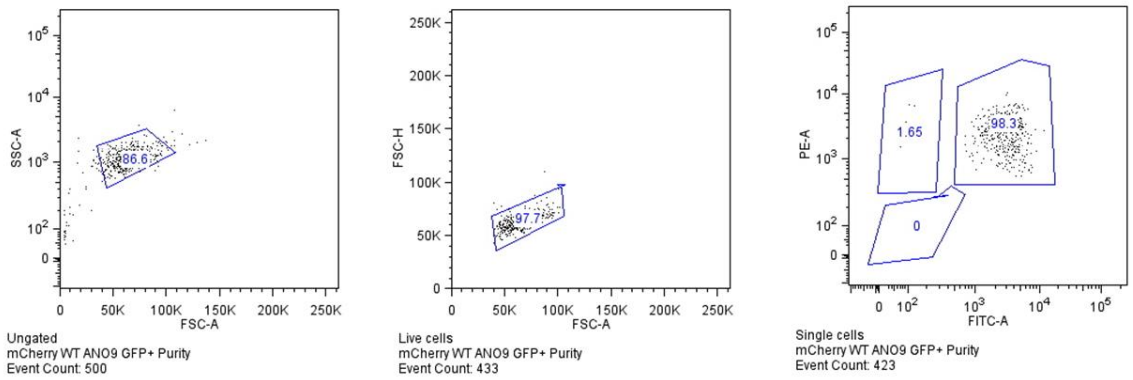

Figure 79 – **GFP and mCherry positive cells selected from the CFBE mCherry wt-CFTR Ano9 3-HA GFP heterogeneous population.**

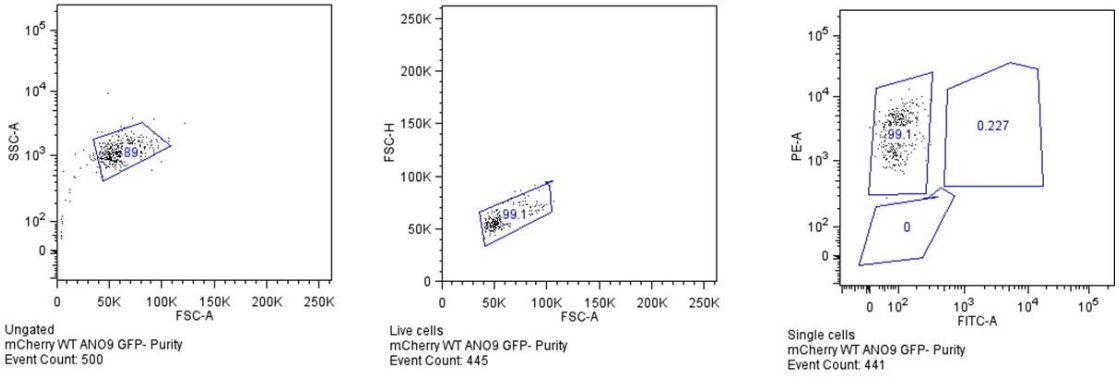

Figure 80 - **GFP negative and mCherry positive cells selected from the CFBE mCherry wt-CFTR Ano9 3-HA GFP heterogeneous population.**

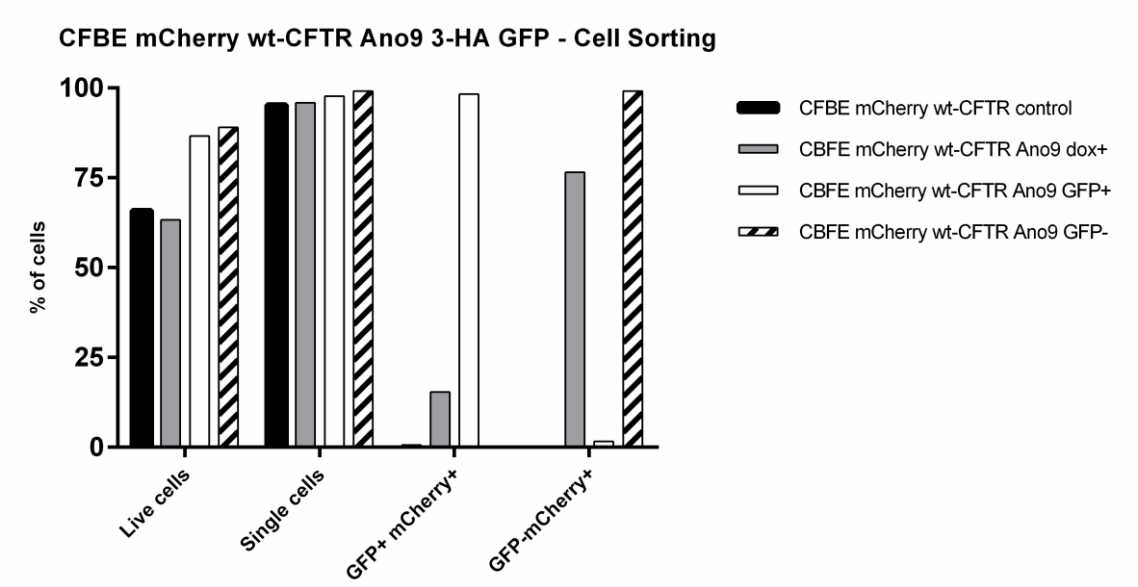

Figure 81 - **CFBE mCherry wt-CFTR Ano9 3-HA GFP sorting statistics. With these results it is possible to conclude that the GFP (Ano9) positive cells were accurately sorted, since no GFP negative cells were detected in the GFP positive population.**

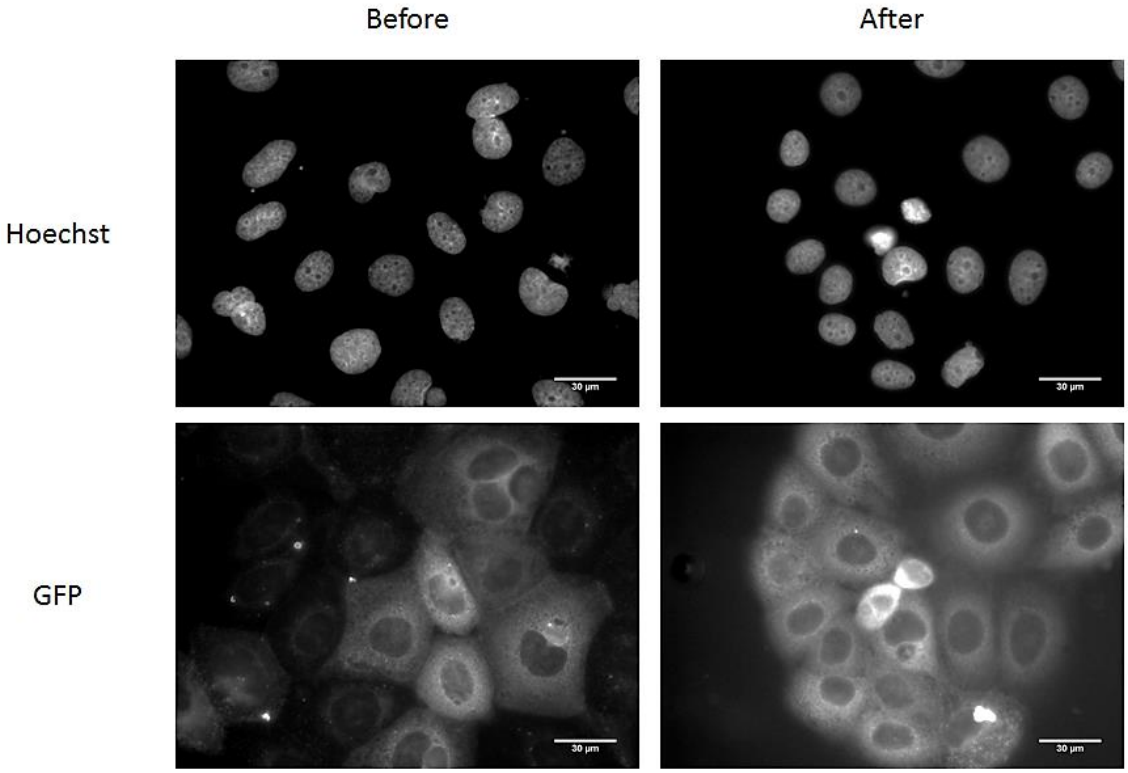

Figure 82 - **CFBE mCherry wt-CFTR Ano9 3-HA GFP before (left) and after (right) sorting. Images were acquired with the 40x objective. With these results it was possible to observe a cellular population with a more homogeneous GFP (Ano9) expression, confirming the results shown in Fig.81. Scale bar represents 30 µm.**

7.7.6) CFBE mCherry F508del-CFTR Ano9 3-HA GFP

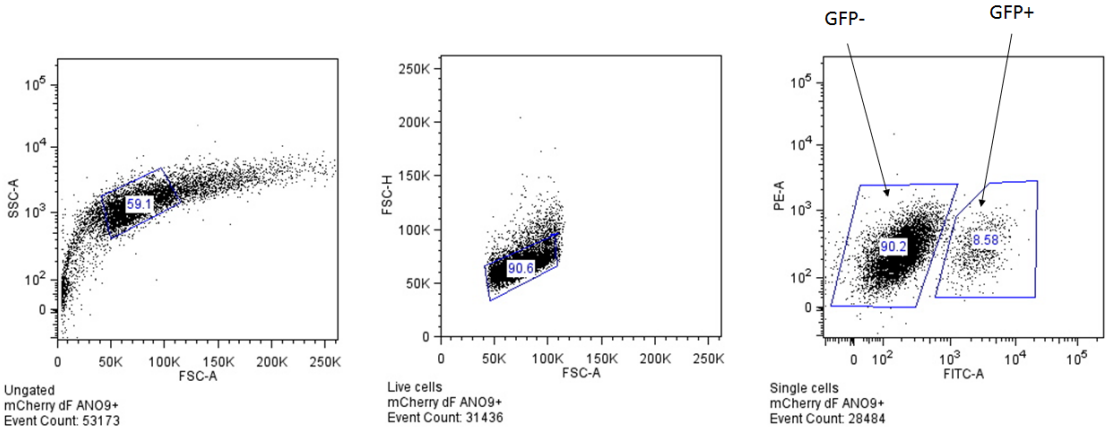

Figure 83 - **Sorting of CFBE mCherry F508del-CFTR Ano9 3-HA GFP cells. The living cells were first selected, followed by a selection of single cells. Finally, the GFP and mCherry emission intensities were measured and the cells were sorted accordingly.**

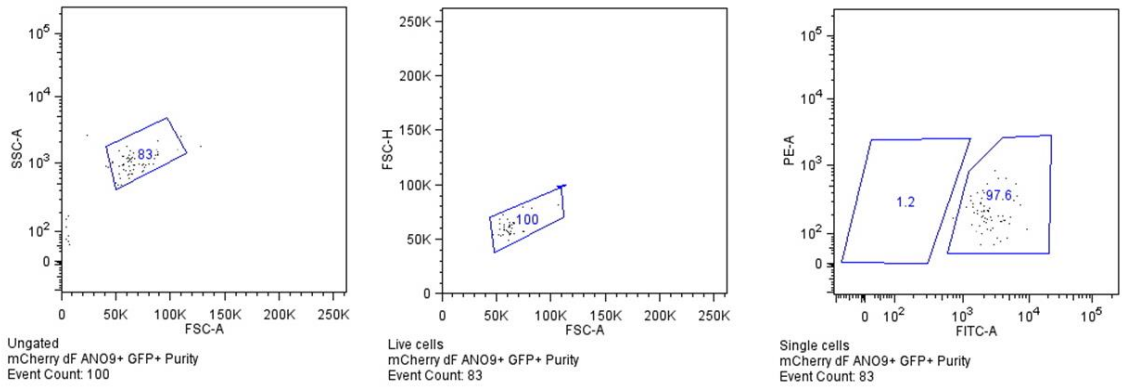

Figure 84 - **GFP positive cells selected from the CFBE mCherry F508del-CFTR Ano9 3-HA GFP heterogeneous population.**

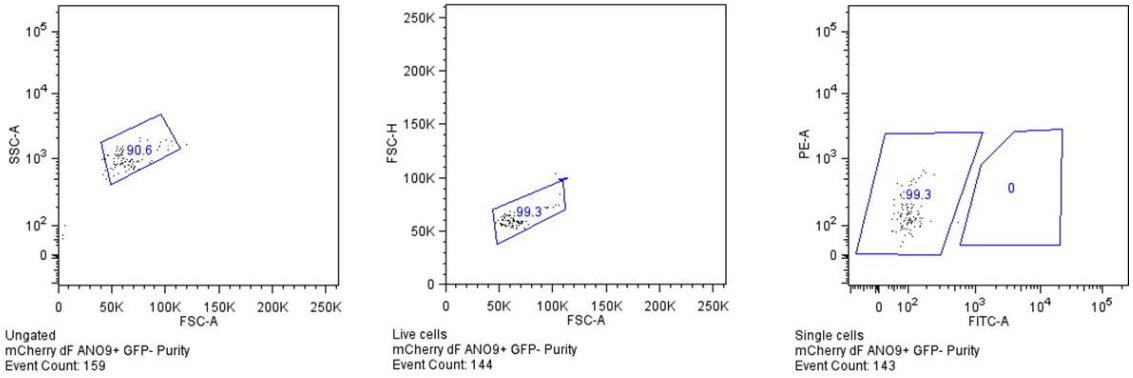

Figure 85 - **GFP negative cells selected from the CFBE mCherry F508del-CFTR Ano9 3-HA GFP heterogeneous population.**

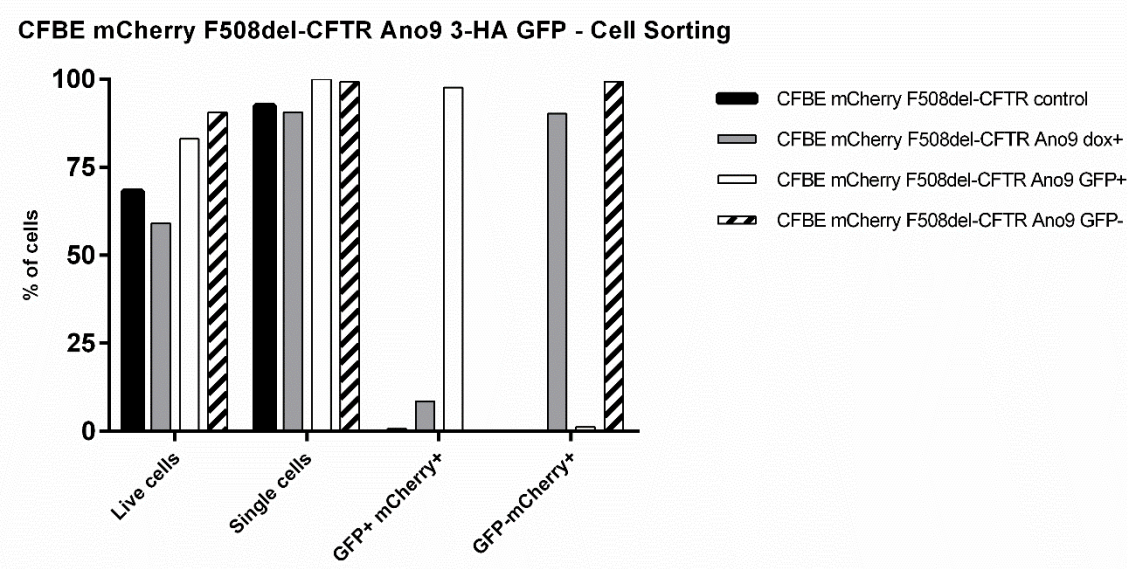

Figure 86 - **CFBE mCherry F508del-CFTR Ano9 3-HA GFP sorting statistics. With these results it is possible to conclude that the GFP (Ano9) positive cells were accurately sorted, since no GFP negative cells were detected in the GFP positive population.**

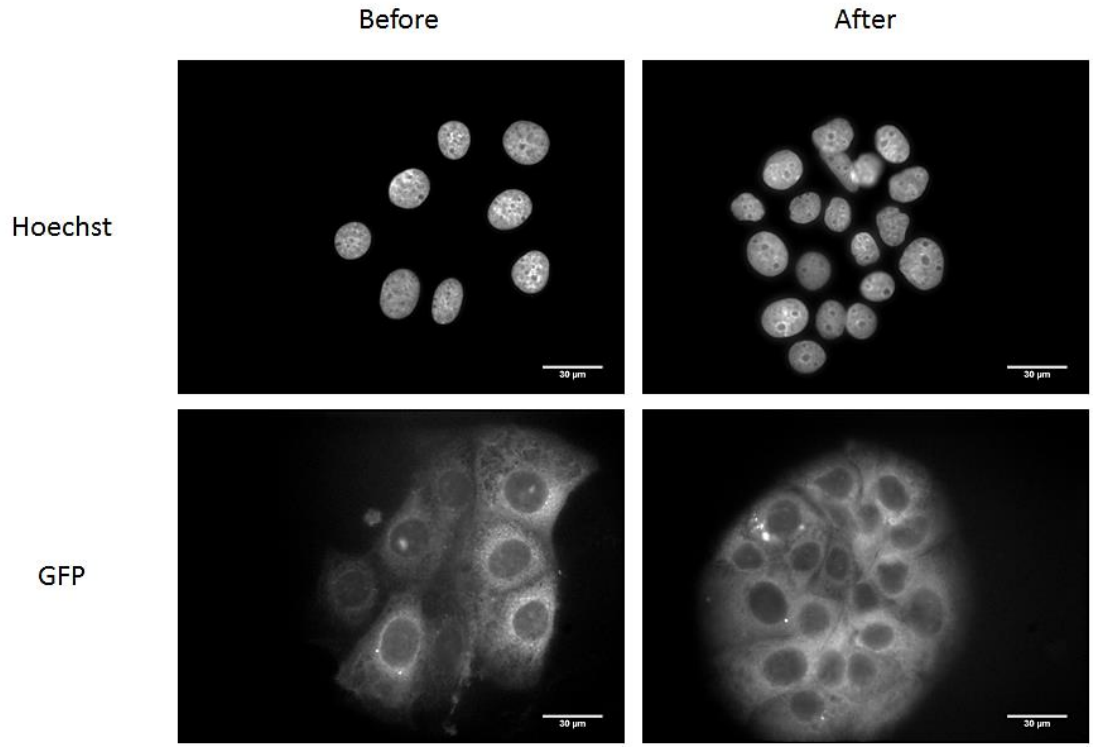

Figure 87 - **CFBE mCherry F508del-CFTR Ano9 3-HA GFP before (left) and after (right) sorting. Images were acquired with the 40x objective. With these results it was possible to observe a cellular population with a more homogeneous GFP (Ano9) expression, confirming the results shown in Fig.86. Scale bar represents 30 µm.**

7.8) Appendix 8 – Structure of the CFTR construct

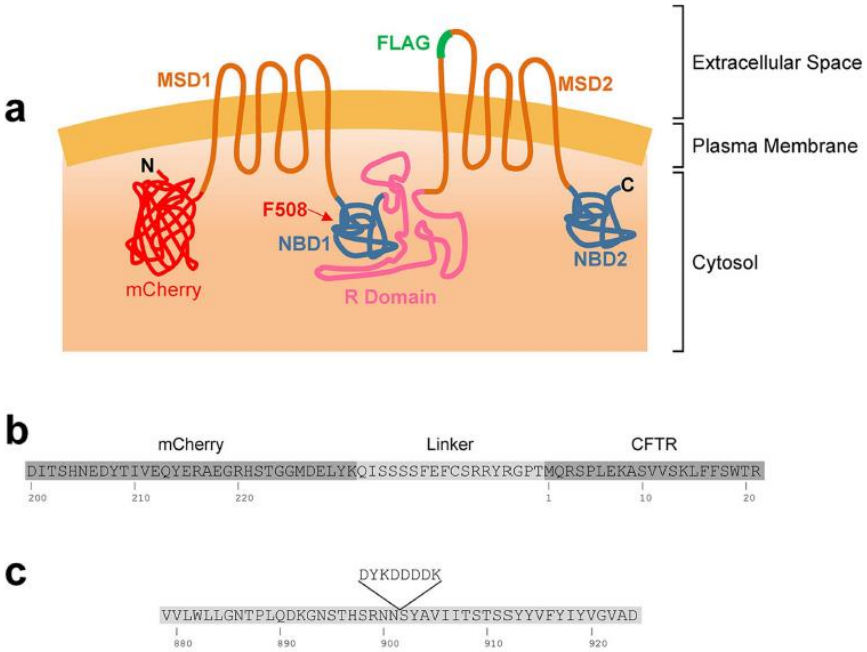

Figure 88 - **Schematic representation of the CFTR traffic reporter construct[145]. A) Topology of the CFTR molecule. mCherry was fused to the N-terminus of CFTR and the Flag-tag was introduced in the fourth extracellular loop. Both wt and F508del variants were generated. B) Amino acid sequence showing the linker that connects mCherry to CFTR. C) Amino acid sequence of CFTR showing the insertion of the Flag tag between Asn901 and Ser902. Adapted from [145].**

7.9) Appendix 9 – CRISPR/Cas9 system

7.9.1) Transfection

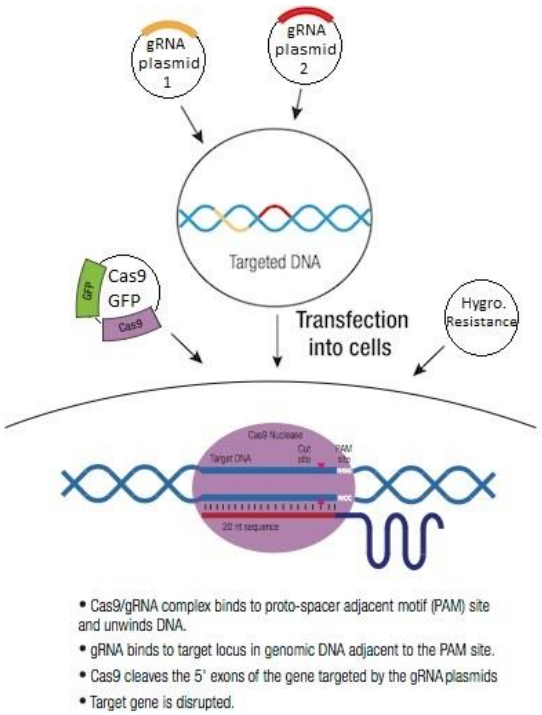

Figure 89 - **CRISPR/Cas9 system used in this project. Adapted from [163].**

7.9.2) gRNA design for Ano6 knockout

gRNA 1 (represented in bold):

5'- TGTACAAAAAAGCAGGCTTTAAAGGAACCAATTCAGTCGACTGGATCCGGTACCAAGGTCGGGCAG
GAAGAGGGCCTATTTCCCATGATTCCTTCATATTTGCATATACGATACAAGGCTGTTAGAGAGATAATT
AAGAATTAATTTGACTGTAAACACAAAGATATTAGTACAAAATACGTGACGTAGAAAGTAATAATTTCT
TGGGTAGTTTGCAGTTTTAAAATTATGTTTTAAAATGGACTATCATATGCTTACCGTAACTTGAAAGTAT
TTCGATTTCTTGGCTTTATATATCTTGTGGAAAGGACGAAACACC**GACGACGACGATGGGGATAT**G
TTTTAGAGCTAGAAATAGCAAGTTAAAATAAGGCTAGTCCGTTATCAACTTGAAAAAGTGGCACCGAGT
CGGTGCTTTTTTTCTAGACCCAGCTTTCTTGTACAAAGTTGGCATTA -3'

gRNA 2 (represented in bold):

5'-TGTACAAAAAAGCAGGCTTTAAAGGAACCAATTCAGTCGACTGGATCCGGTACCAAGGTCGGGCAG
GAAGAGGGCCTATTTCCCATGATTCCTTCATATTTGCATATACGATACAAGGCTGTTAGAGAGATAATT
AGAATTAATTTGACTGTAAACACAAAGATATTAGTACAAAATACGTGACGTAGAAAGTAATAATTTCTT
GGGTAGTTTGCAGTTTTAAAATTATGTTTTAAAATGGACTATCATATGCTTACCGTAACTTGAAAGTATT
TCGATTTCTTGGCTTTATATATCTTGTGGAAAGGACGAAACACC**ACAGACAATTGTCCCCGATT**GTTT
TAGAGCTAGAAATAGCAAGTTAAAATAAGGCTAGTCCGTTATCAACTTGAAAAAGTGGCACCGAGTCG
GTGCTTTTTTTCTAGACCCAGCTTTCTTGTACAAAGTTGGCATTA -3'

7.10) Appendix 10 – Antibodies used

Table 11 - **List of primary and secondary antibodies used for immunofluorescence.**

	Antigen	Host	Cat.No. (Brand)	Application (Dilution)
Primary antibodies	Ano6	Rabbit	Gift from Karl's Lab	IF (1:50)
	HA	Mouse	MMS-101P-200, HA.11 16B12 (Covance)	IF (1:200)
	E-Cadherin	Mouse	610181 (BD Transduction Laboratories)	IF (1:500)
Secondary antibodies	Mouse IgG, Cy5	Goat	A10524 (Invitrogen)	IF (1:500)
	Rabbit IgG, Alexa 568-conjugated	Goat	A11011 (Invitrogen)	IF (1:500)

Table 12 - **List of primary and secondary antibodies used for Western Blot.**

	Antigen	Host	Cat.No. (Brand)	Application (Dilution)
Primary antibodies	GFP	Mouse	11814460001 (Roche)	WB (1:1000)
	α-tubulin	Mouse	T5168 (Sigma-Aldrich)	WB (1:3000)
Secondary antibodies	Anti-mouse IgG – HRP conjugated	Goat	170-6516 (Bio-Rad)	WB (1:3000)

7.11) Appendix 11 – siRNA pilot screen

Table 13 – **List of siRNAs that enhance Ano6 traffic to the plasma membrane. Data include the ratiometric traffic score, the deviation score for the plasma membrane on Ano6 as well as the effects of these genes on wt- and F508del-CFTR traffic. The green arrows mean that siRNAs enhanced CFTR traffic, while the red arrows mean that siRNAs inhibited CFTR traffic. When "-" is shown, the siRNAs did not have an effect of CFTR traffic (in a validation screen).**

siRNA	Score Ratio	Score PM	Gene name	Effect on wt-CFTR A549	Effect on wt-CFTR CFBE	Effect on F508del-CFTR CFBE
FZD10	4.495	-0.400	Frizzled class receptor 10	-	-	-
TMOD3	3.391	4.247	Tropomodulin-3	↑	-	-
PMS1	2.716	1.225	PMS1 homolog 1, mismatch repair system component	-	-	-
PSMB10	2.188	1.393	Proteasome subunit beta 10	-	-	-
OR51E2	2.165	0.345	Olfactory receptor, family 51, subfamily E, member 2	-	-	-
LRP5	1.997	4.434	Low density lipoprotein receptor-related protein 5	-	↓	-
MMP7	1.864	3.613	Matrix metallopeptidase 7	-	-	-
TRPM7	1.845	-1.601	Transient receptor potential cation channel, subfamily M, member 7	-	-	↓
SAR1B	1.801	-0.667	Secretion associated, Ras related GTPase 1B	-	-	-
GRIN1	1.751	3.857	Glutamate receptor, ionotropic, NMDA1 (zeta 1)	-	-	-
CCR5	1.723	-0.788	Chemokine (C-C motif) receptor 5	-	-	-
KIR2DL2	1.705	3.169	Killer cell immunoglobulin-like receptor, two domains, long cytoplasmic tail, 2	-	-	-
CXCR5	1.705	-0.113	Chemokine (C-X-C motif) receptor 5	-	-	-
ARF1	1.662	1.486	ADP-ribosylation factor 1	↓	-	-
PPFIA1	1.632	1.423	Protein tyrosine phosphatase, receptor type, f polypeptide (PTPRF), interacting protein (liprin), alpha 1	-	-	-
KDELR2	1.614	2.597	KDEL (Lys-Asp-Glu-Leu) endoplasmic reticulum protein retention receptor 2	-	-	-
TUBA3C	1.584	0.318	Tubulin, alpha 3c	-	-	-
OR4D1	1.570	0.893	Olfactory receptor, family 4, subfamily D, member 1	-	-	-
ANO1	1.527	0.155	Anoctamin 1, calcium activated chloride channel	-	-	-
MC4R	1.507	4.023	Melanocortin 4 receptor	↑	-	-
ITPR2	1.443	3.074	Inositol 1,4,5-trisphosphate receptor, type 2	-	↓	-
SSTR3	1.429	2.028	Somatostatin receptor 3	↑	-	-
PMF1	1.429	-2.444	Polyamine-modulated factor 1	-	-	-
SCNN1A	1.422	1.753	Sodium channel, non-voltage gated 1 alpha subunit (ENaCa)	-	-	-
PTGER4	1.384	1.771	Prostaglandin E receptor 4 (subtype EP4)	-	-	-
ADC	1.365	1.558	Acetoacetate decarboxylase	-	-	-
APOBEC1	1.300	1.972	Apolipoprotein B mRNA editing enzyme, catalytic polypeptide 1	-	-	-
PIK3R1	1.208	1.600	Phosphoinositide-3-kinase, regulatory subunit 1 (alpha)	-	-	-
PRKAA1	1.187	2.150	Protein kinase, AMP-activated, alpha 1 catalytic subunit	-	-	-
PPP2R1B	1.141	2.413	Protein phosphatase 2, regulatory subunit A, beta	-	-	-
PINK1	1.091	4.798	PTEN induced putative kinase 1	-	-	-
NDUFS5	1.038	2.823	NADH dehydrogenase (ubiquinone) Fe-S protein 5, 15kDa (NADH-coenzyme Q reductase)	-	-	-
PMPCB	1.018	2.373	Peptidase (mitochondrial processing) beta	-	-	-
PPM1A	1.017	1.479	Protein phosphatase, Mg2+/Mn2+ dependent, 1A	-	-	-

Table 14 - **List of siRNAs that inhibit Ano6 traffic to the plasma membrane. Data include the ratiometric traffic score, the deviation score for the plasma membrane on Ano6 as well as the effects of these genes on wt- and F508del-CFTR traffic. The green arrows mean that siRNAs enhanced CFTR traffic, while the red arrows mean that siRNAs inhibited CFTR traffic. When "-" is shown, the siRNAs did not have an effect of CFTR traffic (in a validation screen).**

siRNA	Score Ratio	Score PM	Gene name	Effect on wt-CFTR A549	Effect on wt-CFTR CFBE	Effect on F508del-CFTR CFBE
OR1C1	-1.056	-0.052	Olfactory receptor, family 1, subfamily C, member 1	-	-	-
GPR97	-1.066	-1.432	Adhesion G protein-coupled receptor G3	-	-	-
SEC61A2	-1.117	-3.139	Sec61 translocon alpha 2 subunit	-	-	-
MTNR1A	-1.138	-1.571	Melatonin receptor 1A	-	-	-
HTR7	-1.152	-2.430	5-hydroxytryptamine (serotonin) receptor 7, adenylate cyclase-coupled	-	-	-
PPFIA3	-1.195	-1.039	Protein tyrosine phosphatase, receptor type, f polypeptide (PTPRF), interacting protein (liprin), alpha 3	-	-	-
NEO1	-1.329	-2.675	Neogenin 1	-	-	-
FUZ	-1.337	-1.643	Fuzzy planar cell polarity protein	-	-	-
DHRS4L2	-1.338	-3.642	Dehydrogenase/reductase (SDR family) member 4 like 2	-	-	-
AASDH	-1.342	-1.431	Aminoadipate-semialdehyde dehydrogenase	-	-	-
USP18	-1.483	-1.344	Ubiquitin specific peptidase 18	-	-	-
TACR3	-1.513	-1.785	Tachykinin receptor 3	-	-	-
TMEM11	-1.567	-1.648	Transmembrane protein 11	-	-	-
HSD17B10	-1.611	-2.483	Hydroxysteroid (17-beta) dehydrogenase 10	-	-	-
GABRG2	-1.613	-1.987	Gamma-aminobutyric acid (GABA) A receptor, gamma 2	-	-	-
EIF6	-1.631	-2.872	Eukaryotic translation initiation factor 6	-	-	-
CHN2	-1.657	-1.632	Chimerin 2	-	-	-
GRPR	-1.678	-2.210	Gastrin-releasing peptide receptor	-	-	-
PIM2	-1.714	-3.610	Pim-2 proto-oncogene, serine/threonine kinase	-	-	-
OTUD7A	-1.806	-1.931	OTU deubiquitinase 7A	-	-	-
CA14	-1.817	-2.326	Carbonic anhydrase XIV	-	-	-
TAS1R3	-1.882	-1.964	Taste receptor, type 1, member 3	-	-	-
AHSA1	-1.910	-2.320	AHA1, activator of heat shock 90kDa protein ATPase homolog 1	-	-	-
ADRA2C	-1.924	-2.080	Adrenoceptor alpha 2C	-	-	-
NOD2	-1.936	-3.082	Nucleotide-binding oligomerization domain containing 2	-	-	-
PDE1C	-1.963	-3.918	Phosphodiesterase 1C, calmodulin-dependent 70kDa	-	-	-
CDK19	-2.113	-2.864	Cyclin-dependent kinase 19	-	-	↑
COPZ2	-2.239	-2.450	Coatomer protein complex, subunit zeta 2	-	-	-
HSPA14	-2.303	-3.144	Heat shock 70kDa protein 14	-	-	-
PDE8B	-2.505	-3.363	Phosphodiesterase 8B	-	-	-
APLNR	-2.745	-3.674	Apelin receptor	-	-	-
PDE10A	-2.965	-0.073	Phosphodiesterase 10A	-	-	-
SLC9A3R1	-3.014	-4.229	Solute carrier family 9, subfamily A (NHE3, cation proton antiporter 3), member 3 regulator 1	-	-	-
GPR101	-3.158	-4.275	G protein-coupled receptor 101	-	-	-
OR2B3	-3.581	-4.720	Olfactory receptor, family 2, subfamily B, member 3	-	-	-
AVEN	-3.607	-4.561	Apoptosis, caspase activation inhibitor	-	-	-
FLNB	-3.653	-4.700	Filamin B, beta	-	-	-